

# RE-EVALUATION OF THE LOWER SAN FERNANDO DAM

Report 1

AN INVESTIGATION OF THE FEBRUARY 9, 1971 SLIDE  
VOLUME I: TEXT

by

Gonzalo Castro, Thomas O. Keller, Stephen S. Boynton

GEI Consultants, Inc.  
Winchester, Massachusetts 01890-1943



September 1989

Report 1 of a Series

Approved For Public Release; Distribution Unlimited

RESEARCH LIBRARY  
US ARMY ENGINEER WATERWAYS  
EXPERIMENT STATION  
VICKSBURG, MISSISSIPPI

Prepared for DEPARTMENT OF THE ARMY  
US Army Corps of Engineers  
Washington, DC 20314-1000

Under Contract No. DACW39-85-C-0058

Monitored by Geotechnical Laboratory  
US Army Engineer Waterways Experiment Station  
3909 Halls Ferry Road, Vicksburg, Mississippi 39180-6199

TA7  
W34c  
no. GL-89-  
2  
rept. 1  
v. 1  
c. 3  
Army Corps  
Engineers



20641722

TAF  
W34c  
no. GL-89-2  
rept. 1  
v. 1  
c. 3

Unclassified  
SECURITY CLASSIFICATION OF THIS PAGE

REPORT DOCUMENTATION PAGE				Form Approved OMB No. 0704-0188	
1a. REPORT SECURITY CLASSIFICATION Unclassified		1b. RESTRICTIVE MARKINGS			
2a. SECURITY CLASSIFICATION AUTHORITY		3. DISTRIBUTION / AVAILABILITY OF REPORT Approved for public release; distribution unlimited			
2b. DECLASSIFICATION / DOWNGRADING SCHEDULE					
4. PERFORMING ORGANIZATION REPORT NUMBER(S)		5. MONITORING ORGANIZATION REPORT NUMBER(S)  Contract Report GL-89-2			
6a. NAME OF PERFORMING ORGANIZATION  GEI Consultants, Inc.		6b. OFFICE SYMBOL (if applicable)	7a. NAME OF MONITORING ORGANIZATION USAEWES Geotechnical Laboratory		
6c. ADDRESS (City, State, and ZIP Code)  Winchester, MA 01890-1943		7b. ADDRESS (City, State, and ZIP Code)  3909 Halls Ferry Road Vicksburg, MS 39180-6199			
8a. NAME OF FUNDING / SPONSORING ORGANIZATION US Army Engineer District, Kansas City		8b. OFFICE SYMBOL (if applicable)	9. PROCUREMENT INSTRUMENT IDENTIFICATION NUMBER  DACW39-85-C-0058		
8c. ADDRESS (City, State, and ZIP Code)  Kansas City, KS 64106-2896		10. SOURCE OF FUNDING NUMBERS			
		PROGRAM ELEMENT NO.	PROJECT NO.	TASK NO.	WORK UNIT ACCESSION NO.
11. TITLE (Include Security Classification) Re-Evaluation of the Lower San Fernando Dam, Report 1, An Investigation of the February 9, 1971 Slide, Volume I: Text; Volume II: Appendixes A-F					
12. PERSONAL AUTHOR(S) Castro, Gonzalo; Keller, Thomas O.; Boynton, Stephen S.					
13a. TYPE OF REPORT Report 1 of a series in 2 volumes		13b. TIME COVERED FROM _____ TO _____		14. DATE OF REPORT (Year, Month, Day) September 1989	15. PAGE COUNT 439
16. SUPPLEMENTARY NOTATION Available from National Technical Information Service, 5285 Port Royal Road, Springfield, VA 22161					
17. COSATI CODES			18. SUBJECT TERMS (Continue on reverse if necessary and identify by block number)		
FIELD	GROUP	SUB-GROUP	Earthquakes	Soil liquefaction	
			Embankment dams	Steady-state strength	
19. ABSTRACT (Continue on reverse if necessary and identify by block number)  The lower San Fernando Dam in California developed a major slide in the upstream slope and crest as a result of the 1971 San Fernando earthquake. The purpose of the investigation presented in this report was to test the validity of using steady state concepts and methodology to perform liquefaction analyses of the dam and to further investigate some aspects of the physical mechanism of the slide.  The results of the steady state analyses were consistent with the observed behavior, i.e., (a) the dam was susceptible to a liquefaction failure in the upstream direction, (b) the dam was not susceptible to a liquefaction failure in the downstream direction once the upstream slope had failed, and (c) the strains that accumulated during the 1971 earthquake were sufficient to trigger the upstream liquefaction failure.					
20. DISTRIBUTION / AVAILABILITY OF ABSTRACT <input checked="" type="checkbox"/> UNCLASSIFIED/UNLIMITED <input type="checkbox"/> SAME AS RPT. <input type="checkbox"/> DTIC USERS			21. ABSTRACT SECURITY CLASSIFICATION Unclassified		
22a. NAME OF RESPONSIBLE INDIVIDUAL			22b. TELEPHONE (Include Area Code)		22c. OFFICE SYMBOL

## PREFACE

This study was a part of an investigation of the strength of soils that have been weakened by earthquake shaking, and the stability of embankment dams containing or founded on susceptible soils. This report is one of a series which document the investigation. The project was carried out jointly by Geotechnical Engineers, Inc. (GEI), H. Bolton Seed, Inc., Rensselaer Polytechnic Institute (RPI), and the US Army Engineer Waterways Experiment Station (WES). Principal Investigators were Dr. Gonzalo Castro for GEI, Professor H. Bolton Seed, Professor Ricardo Dobry for RPI, and Dr. A. G. Franklin for WES. Mr. Edward Pritchett, Office of the Chief of Engineers, Washington, DC, was responsible for recognizing the importance and timeliness of this research to the Corps of Engineers, and for generating Corps support for the project. Funding was provided through the US Army Engineer District, Kansas City, for whom oversight was provided by Mr. Francke Walberg.

Essential to the overall investigation was an exploration and records review effort at the Lower San Fernando Dam, in order to obtain crucial data and soil samples for laboratory testing. This effort included an extensive drilling and penetration testing program, excavation of a large diameter shaft, in situ testing, collection of samples, and review of historical records. The Los Angeles Department of Water and Power, owner of the Lower San Fernando Dam, provided access to the site and to the historical records, and other assistance. The California Department of Water Resources provided information from their files.

Drilling, Standard Penetration Testing, and undisturbed sampling from borings were performed by WES, under the supervision of Mr. Joseph Gatz. Cone Penetration Test soundings were performed by Earth Technology Corporation (ERTEC). Excavation of the exploratory shaft was done by Zamborelli Drilling Company, under the direction of GEI. Investigations and sampling in the shaft, and the review of historical records, were done by and under the supervision of Mr. Tom Keller of GEI.

The work presented in this report was done by GEI, under WES Contract No. DACW39-85-C-0058.

The technical monitor and Contracting Officer's Representative at WES was Dr. A. G. Franklin, Chief of the Earthquake Engineering and Geosciences Division, Geotechnical Laboratory. The primary WES reviewer was Dr. Paul F. Hadala, Assistant Chief of the Geotechnical Laboratory. Chief of the Geotechnical Laboratory was Dr. William F. Marcuson III.

Commander and Director of WES during the preparation of this report was COL Larry B. Fulton, EN. Dr. Robert W. Whalin was Technical Director.

## EXECUTIVE SUMMARY

The Lower San Fernando Dam in California developed a major slide in the upstream slope and crest as a result of the 1971 San Fernando earthquake. The liquefaction slide nearly caused a major uncontrolled release of the reservoir. Because of the magnitude of the slide and strong interest of the engineering profession in the evaluation of the seismic stability of earth dams, the Lower San Fernando Dam slide has received considerable attention beginning with detailed studies immediately following the slide (Seed et al, 1973). The purpose of our re-evaluation was to test the validity of using steady state concepts and methodology to perform liquefaction analyses of the dam and to further investigate some aspects of the physical mechanism of the slide. This work was sponsored by the Army Corps of Engineers Waterways Experiment Station (WES).

The results of the steady state analyses were consistent with the observed behavior, i.e., a) the dam was susceptible to a liquefaction failure in the upstream direction, b) the dam was not susceptible to a liquefaction failure in the downstream direction once the upstream slope had failed, and c) the strains that accumulated during the 1971 earthquake were sufficient to trigger the upstream liquefaction failure.

A field exploration program was conducted in 1985 at the damsite as part of this investigation. The main purpose of the exploration program was to characterize and obtain undisturbed samples of the intact downstream section of the dam so that analyses of the failed upstream section could be made. Sampling was concentrated in those areas of the downstream shell which were symmetrically opposite to the areas of the upstream shell which failed in 1971.

The exploration program consisted of six standard penetration test borings, twelve cone penetration test soundings, six undisturbed sample borings, and one 6-foot-diameter/85-foot deep exploration shaft to obtain undisturbed samples, perform in situ density tests, and map the sidewalls of the shaft. Undisturbed samples were distributed among GEI, WES, and H. B. Seed.

A prefailure cross section of the dam is shown in Fig. 2, and a cross section of the dam during the 1985 exploration program is shown in Fig. 4.

The exploration program on the downstream side revealed a relatively loose very silty fine sand layer about 15 feet thick at the base of the hydraulic fill shell. This finding

is consistent with field observations in trenches and borings made on the upstream side of the dam soon after the 1971 failure (Seed, 1973) which showed that the slide occurred through a zone of soil at the base of the upstream hydraulic fill shell. Observations in 1971 indicated that very large strains occurred in this zone.

Construction records of the dam indicate that the same borrow areas and similar construction methods were used for both the upstream and downstream shells, and, therefore, we assumed in our analyses that the upstream and downstream hydraulic fill shells were similar in composition. The 15-foot-thick layer of soil found at the base of the downstream shell is the critical layer of the dam from a liquefaction standpoint, and our liquefaction analyses focused on this layer.

Our liquefaction analyses were divided into an evaluation of the liquefaction susceptibility of the upstream and downstream slopes of the dam and an evaluation of the potential for earthquake loading to trigger a liquefaction failure (flow slide).

#### Liquefaction Susceptibility

The void ratio of the critical layer in the downstream shell was measured using three methods: fixed piston sampling in boreholes, hand carved "tripod" tube sampling in a deep exploration shaft, and field density testing using sand cone techniques in the exploration shaft. All three methods resulted in similar measurements of in situ void ratio within the normal scatter expected for a hydraulic fill. Therefore, both the fixed piston samples from boreholes and the tripod tube samples from the exploration shaft were found to be appropriate for measuring in situ void ratio for the liquefaction analyses as well as for performing laboratory tests to obtain undrained steady state strengths.

The steady state line of a batch mix of the critical layer soil was determined using various testing methods and by four separate laboratories. The various testing methods confirmed that the steady state line is not a function of the following:

- ° initial structure, i.e., method of sample preparation.
- ° initial state, i.e., consolidation stress
- ° stress path, i.e., test type

In general, the steady state lines determined by each of the four laboratories were in remarkable agreement.

The in situ steady state strengths of samples from the downstream critical layer prior to the 1971 failure were estimated on the basis of measured values of  $S_{us}$  in the laboratory and, using the steady state line, corrections for void ratio changes which took place between 1971 and the time of laboratory testing. In situ void ratio changes which took place between 1971 and 1985 were estimated using lateral movement and settlement measurements of the downstream slope made by the Los Angeles Department of Water and Power (LADWP). Void ratio changes which took place between the time of 1985 sampling and laboratory testing were based on direct measurements of sample volume changes.

The in situ steady state strength of the upstream critical layer was determined on the basis of estimated void ratio differences between the upstream and downstream layers. These differences were due to prolonged submergence of the upstream slope and additional load on the downstream slope from berms.

Based on the results of 23 tests performed on undisturbed samples by GEI and Stanford University laboratories, a representative value of the undrained steady state strength of the upstream critical layer was estimated to be about 0.26 tsf just prior to the 1971 failure. The representative strength was selected to be the highest value that is lower than two-thirds of the measured values (approximately equal to the average minus one-half of the standard deviation). Other reasonable selections of a representative strength would indicate values of  $0.26 \pm 0.05$ . The static driving shear stress prior to the failure in the critical layer on the upstream side of the dam was computed to be about 0.48 tsf. Therefore, the factor of safety of the upstream slope against liquefaction susceptibility was about 0.54. Thus, even though the upstream slope was stable under drained conditions, the 1971 earthquake caused sufficient strains to trigger an undrained liquefaction (flow) slide.

The in situ steady state strength of the downstream critical layer was estimated to be about 0.33 tsf just prior to the 1971 failure. The static driving shear stress in the critical layer on the downstream side of the dam was computed to be about 0.33 tsf prior to the upstream slide and about 0.22 tsf immediately after the slide. Therefore, the factor of safety of the downstream slope against liquefaction susceptibility was about 1.0 and 1.5 prior to and immediately after the upstream slide, respectively. The 1971 earthquake caused high pore pressures and slight deformations in the downstream

slope, but the earthquake did not cause the slope to undergo a flow slide.

### Triggering of Liquefaction

The triggering analysis for the Lower San Fernando Dam included three steps, namely, a) determination of the triggering strain for the critical soil layer, b) estimation of the strains induced by the 1971 earthquake and other previous earthquakes, and c) comparison of the strains in a) and b) to determine whether the results are consistent with the observed behavior.

An accumulated undrained shear strain of about 1.5% in the critical layer of the upstream slope is sufficient to lower the shear resistance of the layer to the driving shear stress and trigger the flow slide. If a smaller shear strain of about 0.5% is reached, the soil creeps under the driving shear stress until the failure is triggered at a strain of about 1.5%.

Based on our triggering analysis, an earthquake with a maximum base rock acceleration of about 0.15 g and time record similar to the 1971 earthquake would be sufficient to trigger a liquefaction flow slide of the upstream slope. The maximum base rock acceleration at the damsite during the 1971 earthquake was about 0.55 to 0.6 g. Therefore, the 1971 earthquake was much larger than necessary to trigger the failure.

Based on our analyses of the earthquake history of the damsite, earthquake shaking at the damsite from events prior to the 1971 earthquake did not exceed peak accelerations of about 0.1 g, and thus could not trigger a flow slide of the upstream slope of the dam.

Deformation measurements of the surface of the downstream slope made by the LADWP after the 1971 earthquake indicate that shear strains in the critical layer of the downstream hydraulic fill shell were about 2 to 3%, and thus the shear resistance of the critical layer was probably reduced to values close to the undrained steady state strength. However, creep leading to failure of the downstream slope did not occur. This is consistent with the fact that the downstream slope was not susceptible to a liquefaction failure once the upstream slope had failed. However, limited shear deformations and volume changes did develop which were reflected in lateral and vertical movements of the surface of the downstream slope of the dam.

The contrasting behavior between the upstream and downstream sections of the dam clearly illustrates the importance



of the relationship between driving shear stress  $\tau_d$  and undrained steady state strength  $S_{us}$ . If  $\tau_d$  exceeds  $S_{us}$  as in the upstream slope, a major flow (liquefaction) slide can occur. If  $\tau_d$  is lower than  $S_{us}$  as in the downstream slope, the earthquake can produce increases in pore pressures and limited deformations, but a flow slide cannot occur regardless of the intensity of shaking.

## CONTENTS

VOLUME 1	<u>Page</u>
PREFACE	i
EXECUTIVE SUMMARY	iii
LIST OF TABLES	x
LIST OF FIGURES	xi
LIST OF APPENDIXES	xiii
CONVERSION FACTORS, NON-SI TO SI (METRIC) UNITS OF MEASUREMENT	xiv
1. Introduction	1
1.1 Purpose	1
1.2 Scope of Work	1
1.3 Authorization	2
1.4 Project Personnel	3
1.5 Acknowledgments	3
2. Historical Background	4
2.1 Construction of Dam	4
2.2 Slide in 1971	5
2.3 Reconstruction of the Dam	6
3. SUBSURFACE CONDITIONS IN 1985	7
3.1 General	7
3.2 Blowcount Profiles	7
3.3 Hydraulic Fill Shell	9
4. Susceptibility of Dam to Liquefaction Flow Slide	13
4.1 Analytical Approach	13
4.2 Determination of In situ Void Ratios of Critical Layer	15
4.2.1 In Situ Void Ratios of Critical Layer in 1985	15
4.2.2 In Situ Void Ratios of Critical Layer Prior to Failure	18
4.3 Determination of Slope of Steady State Line	18
4.4 Determination of $S_{US}$ for Undisturbed Specimens of Critical Layer	21
4.5 Correction of Measured $S_{US}$ to 1971 In Situ Void Ratio	22

## CONTENTS (Contd.)

	<u>Page</u>
4.5.1 Correction Method	22
4.5.2 Selection of $S_{us}$ for Analysis	22
4.6 Calculation of In Situ Driving Shear Stress and the Factor of Safety	25
4.6.1 In Situ Driving Shear Stress	25
4.6.2 Factor of Safety Against Liquefaction	26
4.7 Liquefaction Susceptibility Through Upper Zones of the Hydraulic Fill	27
4.8 Conclusions	28
5. Earthquake Required to Trigger Liquefaction Failure	30
5.1 Introduction	30
5.2 Strain Required to Trigger Flow Slide	30
5.2.1 Monotonic Tests	31
5.2.2 Cyclic Load/Creep Tests	33
5.3 In situ Strains Induced by Earthquake Loading	33
5.4 Determination of Yield Acceleration, $k_y$	34
5.5 Analyses to Define Time Histories of Acceleration	35
5.6 Critical Layer Strains During Earthquake Loading	35
5.7 Failure Mechanism--1971 Flow Slide	36
5.8 Earthquake History of the Dam	40
5.9 Comments on Methodology for Triggering Analysis	41
6. CONCLUSIONS	43
REFERENCES	47
NOTATIONS	51
TABLES	
FIGURES	
VOLUME 2	
APPENDIXES A THROUGH F	

## LIST OF TABLES

- 1 - Summary of Void Ratio and Steady State Strength Data -  
Samples from Zone 5 of Hydraulic Fill - GEI Test Data
- 2 - Summary of Void Ratio and Steady State Strength Data  
Samples from Zone 5 of Hydraulic Fill  
Stanford University Test Data
- 3 - Void Ratio Corrections Applied to Critical Layer Tube  
Samples
- 4 - Number of Tests Performed to Define Steady State Line of  
Critical Layer Soil
- 5 - Summary of Liquefaction Susceptibility Analyses of  
Hydraulic Fill Zones 2 and 3
- 6 - Summary of Most Significant Earthquakes in the  
San Fernando Valley Area

## LIST OF FIGURES

- 1 - Site Location Map
- 2 - Cross Section Through Lower San Fernando Dam - Prefailure Geometry
- 3 - Cross Section After 1971 Earthquake & Reconstructed Cross Section
- 4 - Cross Section Through Lower San Fernando Dam - 1985 Geometry
- 5 - 1985 Boring Location Plan
- 6 - Cross Section at Station 16+40 Showing N-values
- 7 - Cross Section at Station 9+35 Showing N-values
- 8 - Cross Section at Station 5+85 Showing N-values
- 9 - Hydraulic Fill Zones at Location 111
- 10 - Hydraulic Fill Zones at Location 103
- 11 - Grain Size Curves - Hydraulic Fill Zone 5 Samples
- 12 - Flow Chart for Evaluating Liquefaction Susceptibility of Critical Layer
- 13 - Coefficient of Swelling Vs. Initial Void Ratio
- 14 - 1985 In situ Void Ratios of Critical Layer Vs. Depth
- 15 - Steady State Line - Batch Mix 7 - GEI Test Results
- 16 - Steady State Line - Batch Mix 7 - Test Results from Four Laboratories
- 17 - Steady State Diagram - Critical Layer Soils
- 18 - 1971 In situ Steady State Strengths of Upstream Critical Layer Soils Vs. Elevation
- 19 - 1971 In situ Steady State Strength of Downstream Critical Layer Soils Vs. Elevation
- 20 - Schematic Stress Strain Curve for Liquefaction Failure

LIST OF FIGURES  
(concluded)

- 21 - Flow Chart for Evaluating Potential to Trigger Liquefaction Failure
- 22 - Stress Strain Curves of Anisotropically Consolidated Samples of Batch Mix 7
- 23 - Stress Paths of Critical Layer Soils
- 24 - Creep Rate Vs. Cumulative Axial Strain - Batch Mix 7
- 25 - Computed Shear Strains in Critical Layer Vs. Maximum Base Rock Acceleration
- 26 - Qualitative Driving & Resisting Forces at Initiation of Slide
- 27 - Ranges of Maximum Accelerations in Rock

LIST OF APPENDIXES

- A - Subsurface Exploration Program
- B - Exploration Shaft
- C - In situ Void Ratio Changes of Critical Layer
- D - Static and Pseudostatic Stability Analyses
- E - Shake Analyses
- F - Laboratory Testing Program

## CONVERSION FACTORS, NON-SI TO SI (METRIC) UNITS OF MEASUREMENT

Non-SI units of measurement used in this report may be converted to metric (SI) units as follows:

<u>Multiply</u>	<u>By</u>	<u>To Obtain</u>
cubic feet	0.02831685	cubic metres
inches	2.54	centimetres
pounds (force)	4.448222	newtons
pounds (force) per square inch	6.894757	kilopascals
square inches	6.4516	square centimetres



## 1. INTRODUCTION

### 1.1 Purpose

The Lower San Fernando Dam in California developed a major slide in the upstream slope and crest as a result of the 1971 San Fernando earthquake. The liquefaction slide nearly caused a major uncontrolled release of the reservoir. Because of the magnitude of the slide and strong interest of the engineering profession in the evaluation of the seismic stability of earth dams, the Lower San Fernando Dam slide has received considerable attention beginning with detailed studies immediately following the slide (Seed et al, 1973). The purpose of our re-evaluation was to test the validity of using steady state concepts and methodology to perform liquefaction analyses of the dam and to further investigate some aspects of the physical mechanism of the slide that had not been explained by the results of prior investigations (Castro et al, 1985). This work was sponsored by the Army Corps of Engineers Waterways Experiment Station (WES).

### 1.2 Scope of Work

The scope of work included the following:

1. Review available historical records and past reports about the dam that are pertinent to understanding the slide.
2. Perform a field exploration program at the dam, including:
  - a. One deep exploration shaft, 6 feet in diameter and 85 feet deep, to obtain undisturbed samples, measure in situ density, and map sidewalls of the excavation.
  - b. Six standard penetration test borings.
  - c. Twelve cone penetration test soundings.
  - d. Six fixed-piston undisturbed sample borings.
  - e. Two groundwater observation wells.
3. Perform a laboratory testing program on samples obtained from the dam, including:

- a. Index tests:
    - 7 specific gravity
    - 7 compaction
    - 1 Atterberg Limit
    - 1 mineralogic analyses
    - 38 gradation
  - b. Triaxial tests on undisturbed samples:
    - 20 monotonically loaded
    - 5 cyclically loaded
  - c. Triaxial tests on remolded samples:
    - 21 monotonically loaded
    - 11 cyclically loaded
  - d. Vane shear test on one clay sample.
4. Perform analyses of the dam using steady state strength concepts to determine its susceptibility to a liquefaction flow slide and to determine the earthquake shaking required to trigger a liquefaction failure.
  5. Attend meetings to discuss our findings and those of other investigators.
  6. Prepare this report.

### 1.3 Authorization

This work was authorized by the U.S. Army Corps of Engineers Waterways Experiment Station, Corps of Engineers Contract No. DACW39-85-C-0058, effective May 13, 1985. Dr. A. G. Franklin of WES was the technical contact for the GEI contract. WES also contracted with Professors H. B. Seed and R. Dobry to carry out investigations of the Lower San Fernando Dam slide. Samples obtained by GEI were provided to WES and Professors Seed and Dobry for their investigations. Meetings were held during the course of the work to exchange results obtained by the various organizations. This report contains only the results of GEI investigations unless noted otherwise.

#### 1.4 Project Personnel

The following key personnel at GEI were responsible for carrying out the work on this project:

Principal-in-Charge:	Gonzalo Castro
Project Manager:	Thomas O. Keller
Project Engineers:	Stephen S. Boynton Jay R. Perkins Kathryn D. Ayan R. Lee Wooten Paul G. Costello
In-House Consultant:	Steve J. Poulos

#### 1.5 Acknowledgments

The borings were performed by WES personnel and equipment, and the cone soundings were performed by the Earth Technology Corporation. Joseph Gatz coordinated the drilling program for WES and Frank Stewart performed the drilling and sampling. Zamborelli Drilling advanced the exploration shaft. The field work was performed under the technical direction of GEI.

The State of California Department of Water Resources provided information on the dam from their files. The Los Angeles Department of Water and Power (LADWP) provided support to conduct the field work and extensive data on the construction and past performance of the dam. The willingness of Messrs. S. Matsuda, W. Wu, R. Bruce, A. Rudisill, Ms. C. Trehuba and others of LADWP to assist in the investigation and their responses to our numerous requests for information is greatly appreciated.

## 2. HISTORICAL BACKGROUND

### 2.1 Construction of Dam

The Lower San Fernando Dam is located in San Fernando, California (Fig. 1). A cross section through the Lower San Fernando Dam showing the major sections of the embankment prior to the 1971 failure is shown in Fig. 2. All elevations in this report refer to National Geodetic Vertical Datum (NGVD). A general description of the dam construction is presented by Seed et al (1973) and a brief overview is given below.

Embankment construction was started in 1912. The embankment was founded on an alluvium foundation consisting primarily of stiff clay with lenses of sand and gravel. Old drawings of the dam show three, clay-filled cutoff trenches extending through the alluvium to bedrock.

The majority of the embankment consists of hydraulic fill placed between 1912 and 1915. This material was sluiced from the floor of the reservoir and discharged from starter dikes on the upstream and downstream edges of the embankment. The actual dimensions of the starter dikes are unknown, and therefore, the dimensions shown in Fig. 2 are estimates based on typical hydraulic fill construction practice. The hydraulic fill process resulted in upstream and downstream shells consisting of sands and silts and a central core consisting of clayey soil.

Construction photos of the hydraulic fill placement contained in historical records and past reports indicate that the upstream and downstream sections were raised symmetrically and constructed in a similar manner. Therefore, it is reasonable to assume that the general layering of the upstream hydraulic fill shell is similar to that of the downstream hydraulic fill shell.

A 10- to 15-foot-thick hydraulic fill layer consisting of "ground-up" shale from the left abutment was placed in 1916 over the hydraulic fill described above. Records indicate that the maximum size of the ground shale was about 3 inches. Limited 1985 sampling of the ground shale zone disclosed a widely graded sand and silty sand.

The embankment was raised a number of times between 1916 and 1930 by placement of rolled fills. The maximum height of the embankment of about 135 feet was reached in 1930. A thin blanket was placed on the lower part of the downstream slope

in 1929 and 1930 apparently for seepage control and to provide additional stability due to the raising of the crest. The composition of the blanket was described in a post-construction report as a mixture of shale and gravelly material placed in 12-inch layers and compacted by trucks.

The final addition to the dam was a 4.5H:1V berm placed on the downstream slope in 1940. Construction records related to the composition of the berm could not be found, but it has been described in a previous report (Baumann et al, 1966) as a rolled fill. A photograph of the construction operation shows a roller traveling on the fill.

## 2.2 Slide in 1971

A major slide of the upstream slope and crest of the Lower San Fernando Dam occurred within about a minute after the February 9, 1971 San Fernando earthquake. An investigation of the slide was performed and reported by Seed et al, 1973, Seed et al, 1975a; Seed et al, 1975b; and Lee et al, 1975. The field investigation showed that the liquefaction slide occurred through the lower part of the upstream hydraulic fill shell. Seed et al, 1973 presented three reconstructed cross sections of failed portions of the dam based on the results of a trench made through the slide area, boring data, and surficial mapping. All three cross sections indicated that the "liquefied" zone was a triangular area with its base at or near the bottom of the hydraulic fill. One of these reconstructed cross sections is presented in Fig. 3. The upper part of Fig. 3 shows that large blocks of essentially intact soil from the upstream section of the dam moved into the reservoir, riding over the liquefied soil. After movement stopped, the liquefied soil was found to have extruded upwards, between the intact blocks, and to have flowed as far as 250 feet from the toe of the dam. The block of soil which contained the toe of the dam moved about 150 feet into the reservoir.

Seismoscopes located on the bedrock abutment and crest of the dam were analyzed to determine earthquake motions at the site. Earthquake motions recorded in the abutment seismoscope had a peak acceleration of about 0.55 to 0.6 g (Seed et al, 1973). Interpretation of the seismoscope on the crest indicated peak accelerations of the crest of about 0.55 g (Seed et al, 1973). The seismoscope record from the crest was analyzed (Seed, 1979) to obtain the following time history of the embankment motion:

Time

0	Start of main shock of earthquake
~14 sec	Strong motion of earthquake completed - slight tilting of dam crest
~40 sec	Start of slide movement at crest of dam
~90 sec	End of main slide movement

The slide movements of the crest started about 26 seconds after the earthquake shaking stopped and the slide duration was about 50 seconds. Thus the large slide movements developed in the absence of earthquake loads and were driven only by the static stresses from the weight of the materials in the embankment.

The downstream shell of the embankment developed settlements and horizontal displacements of up to about one foot but remained essentially intact after the earthquake.

### 2.3 Reconstruction of the Dam

The dam was reconstructed in 1975 to act as a backup dam to a new dam constructed in the reservoir area. Water has not been impounded behind the Lower San Fernando Dam since the 1971 failure.

A cross section of the embankment in its 1985 configuration is shown in Fig. 4. A large excavation on the upstream side of the dam was made in 1974-1975 to replace a portion of the slide debris with compacted earth backfill. The new crest was placed at a lower elevation, and the center of the new crest is downstream of the original centerline of the dam.

A plan view of the dam showing its 1985 geometry is shown in Fig. 5. The portion of the upstream slope involved in the most catastrophic sliding was located approximately between Stations 2+00 and 14+00.

### 3. SUBSURFACE CONDITIONS IN 1985

#### 3.1 General

A field exploration program was conducted at the dam site between September 9 and December 20, 1985. The main purpose of the exploration program was to characterize and obtain undisturbed samples of the intact downstream section of the dam. The test results for the downstream section were used for analysis of the failed upstream section. Sampling was concentrated in those areas of the downstream shell that were symmetrically opposite to the areas of the upstream shell which failed in 1971.

The exploration program consisted of the following:

- a. Six standard penetration test (SPT) borings and 12 cone penetration test (CPT) soundings along four cross sections to define the character of the materials in the dam.
- b. Undisturbed sample borings adjacent to five selected SPT/CPT locations.
- c. One deep exploration shaft located adjacent to an SPT/CPT location to obtain undisturbed samples, perform in situ density tests, and map the sidewalls of the shaft.

A plan view showing SPT, CPT, and exploration shaft locations is presented in Fig. 5. Explorations were conducted at 12 locations at the dam site. The borings and soundings were numbered according to the location numbers shown in Fig. 5. The exploration shaft was performed at Location 111.

Details of the borings and exploration shaft are presented in Appendices A and B, respectively. Details of cone penetration test soundings are presented in a report by Earth Technology Corporation (1985).

#### 3.2 Blowcount Profiles

SPT borings were performed at six locations as shown in Fig. 5. Borings S103 and S111 were located at the approximate center of the downstream hydraulic fill shell. Boring S105 was located near the center of the clayey core and Borings S101 and S104 were located in a transition zone between the core and the shell. Boring S102 was performed just upstream of the clayey core in a location where upstream slide movements in 1971 were limited.

Cross sections of the dam showing standard penetration test values (N-values) from the 1985 borings are presented in Figs. 6, 7, and 8. These cross sections also show the approximate limits of the zones of the dam depicted in Fig. 4. Groundwater levels in 1985 were located just above the base of the hydraulic fill as shown in Figs. 7 and 8.

The "dense fill" shown in the SPT cross sections represents the rolled fill and ground shale hydraulic fill layer. These layers could not be differentiated on the basis of soil description, SPT, or CPT data. The best samples of what are presumed to be the ground shale layer (on the basis of construction elevations) were obtained in Boring S102 between Els. 1078 and 1095. Samples of the ground shale in this boring consisted of dense widely graded sand and dense silty sand with N-values ranging from 33 to 60 blows/foot.

Continuous split-spoon samples of the "clayey core" were obtained in Boring S105. The core was predominantly a silty clay; however, about 20% of the core consisted of sandy soils found in layers ranging from about 1 to 30 inches thick. The relatively high N-values in Boring S105 at elevations of about 1026 and 1052 are in sandy zones of the core. Blowcounts in clayey zones were typically 8 blows/foot near the top of the core and increased to about 18 blows/foot near the base of the core.

The transition between the clayey core and the sandy shell is typified by Boring S104. The soil profile in this boring consisted of about 70% sandy layers and 30% clayey layers.

The hydraulic fill at the locations of Borings S103 and S111 consisted of sand and silt with virtually no clay layers. The hydraulic fill at these locations was divided into five zones, as shown in Figs. 7 and 8. These zones are described in Section 3.3.

All SPT borings penetrated the alluvium foundation layer of the dam. The alluvium consisted of stiff clay with lenses of dense sandy material.

Borings were performed through the Lower San Fernando Dam in 1966 (Suzuki, 1966) and 1967 (Mayeda et al, 1969). The 1966 program consisted of three borings performed through the clayey core of the dam. The 1967 program consisted of three borings performed primarily through the clayey core and one boring (CH67-A) performed through the downstream shell. Boring CH67-A was located on the downstream berm road at Station 11+82, 149 feet south of the dam centerline. Six split-spoon samples of the hydraulic fill portion of the dam were obtained in Boring CH67-A.



Nineteen SPT borings were performed by the California Department of Water Resources immediately after the 1971 failure (Seed et al, 1973).

The blowcounts of the sandy shell and core obtained in the 1985 borings are within the scatter of the blowcounts measured in these layers during the 1966, 1967, and 1971 boring investigations.

### 3.3 Hydraulic Fill Shell

The general character of the hydraulic fill as found under the downstream berm road is described in this section. At this location the hydraulic fill represents the mirror image of a section of the upstream hydraulic fill shell which failed in 1971 (see Fig. 3).

#### Location 111

Location 111 is located on the berm road at Sta 5+85. The subsurface explorations at this location were: SPT Boring S111, CPT Sounding C111, Undisturbed Sample Borings U111 and U111A, and the Exploration Shaft. Split-spoon samples were taken continuously through the hydraulic fill in Boring S111.

The hydraulic fill at Location 111 has been divided into five zones on the basis of 1985 N-values and descriptions of split-spoon samples. These zones, together with N-values and CPT tip resistance values, are shown in Fig. 9. This figure also shows the three locations in the exploration shaft where sampling and wall mapping was performed.

The five zones in Fig. 9 were more easily identified by N-values trends than by CPT tip resistance trends. The CPT tip resistance profile (based on average CPT values) generally mirrors the SPT profile but does not provide a good demarcation between zones. Therefore, SPT data and soil descriptions were used as the primary means to identify zonation within the hydraulic fill shell.

Each zone was stratified in "macro" layers with typical thicknesses ranging from about 6 to 15 inches. An example of macro layering is shown in Fig. B5, a photograph of the exploration shaft wall. Undisturbed samples and wall mapping of the exploration shaft revealed that almost all of these

"macro" layers were intensely stratified by "micro" layers. The micro layers varied significantly in thickness but were typically about 0.05 to 0.20 inches thick. An example of micro layering is shown in Fig. B6.

A general description of each zone of the hydraulic fill identified in Fig. 9 is presented below.

Zone 1 - This zone, approximately 20 feet thick, consisted primarily of stratified narrowly graded to widely graded sands and silty sands. Thin clay lenses were found on occasion, but their combined thickness was only about 6 inches. Blowcounts ranged from 14 to 34 blows/foot, with a typical value of 20 blows/foot. Approximately 30 macro layer changes were observed in the continuous split-spoon sample boring indicating an average layer thickness of about 8 inches. CPT tip resistance values in this zone also indicated about 30 macro layer changes based on the number of spikes in the record.

Zone 2 - This zone, approximately 15 feet thick, was characterized by the presence of sandy silt layers in addition to stratified sands and silty sands. Occasional thin clay layers were observed in this zone. Blowcounts ranged from 14 to 21 blows/foot, with a typical value of 17 blows/foot. Approximately 30 macro layer changes were observed in split-spoon samples which was consistent with the number of spikes in the CPT tip resistance record. The average macro layer thickness in this zone was about 6 inches. A photograph of a 3.4-foot thickness of this zone taken in the exploration shaft is shown in Fig. B5 (Appendix B). The soil layering observed in the exploration shaft was consistent with layering shown by SPT borings and CPT soundings.

Zone 3 - This zone, approximately 12 feet thick, consisted primarily of stratified sands and silty sands. On average, the sands in this zone were somewhat cleaner than in zones above. Blowcounts ranged from 22 to 35 blows/foot with a typical value of 28 blows/foot. This zone was somewhat less stratified than the zones above. About six macro layer changes were observed in split-spoon samples and about ten layer changes were indicated by the CPT tip resistance record. The average macro layer thickness in this zone indicated by SPT and CPT data was about 15 inches. A photograph of a 3-foot thickness of this zone is shown in Fig. B6. This photograph clearly shows the intense stratification (micro layers) within each of the macro layers.

Zone 4 - This zone, about 5 feet thick, consisted primarily of dense, widely graded stratified silty sand. Blowcounts in this zone were typically greater than 40 blows/

foot. Macro layer thicknesses in this zone were similar to that of Zone 3.

Zone 5 - This zone, approximately 15 feet thick, consisted primarily of stratified silty fine sands and sandy silts. This zone was critical from the standpoint of the liquefaction failure. Blowcounts in this zone ranged from 11 to 28 blows/foot, with a typical value of 18 blows/foot. Approximately 15 to 20 macro layers were identified in split-spoon samples of this zone, and the CPT tip resistance record indicated a comparable to slightly greater number of macro layers. In general, macro layers in this zone were typically 9 to 12 inches thick.

A photograph of a 2.3-foot thickness of this zone is shown in Fig. B7. Micro layers are extensive in this zone but are not obvious in Fig. B7 because sufficient time was not available for drying of the shaft wall to highlight the stratification. Grain size curves of undisturbed samples from this zone are shown in Fig. 11. The dashed line in Fig. 11 is the gradation of a mixture of bag samples (Batch Mix 7) taken from Zone 5 of the exploration shaft. Batch Mix 7 had a liquid limit of 24 and plasticity index of 4.

Groundwater level was encountered in this zone, at El. 1012.4. Note that no water was impounded behind the dam at the time of the groundwater level reading in October 1985.

#### Location 103

Location 103 is located on the berm road at Sta 9+35 which is 350 feet west of Location 111. The following subsurface explorations were conducted at Location 103: SPT Boring S103, CPT Sounding C103, and Undisturbed Sample Boring U103. Split-spoon samples were taken continuously through the hydraulic fill in Boring S103. The five zones identified at Location 111 also existed at Location 103. The five zones at Location 103, together with N-values and CPT tip resistance values, are shown in Fig. 10. The trends of blowcounts and soil layering are similar in S103 and S111. The CPT tip resistance trends in C103 generally mirror the N-value trends in S103.

Discussion. - The main factors which support our assumption that the upstream and downstream hydraulic fill shells were symmetrical are:

- a. The material source for both shells was the same, i.e., the floor of the reservoir.

- b. Construction photos indicate that the hydraulic fill was raised symmetrically and that placement techniques were similar for both shells.
- c. Two SPT borings performed through the downstream shell (S103 and S111) and located about 350 feet apart indicated similar zonation in the east-west direction of the dam (parallel to dam centerline).
- d. As will be shown in later sections of the report, in situ void ratios and steady state shear strengths of Zone 5 soils at Locations 103 and 111 were similar.

Zone 5 was considered to be the most critical zone of the dam from a liquefaction standpoint for the following reasons:

- a. Zone 5 is located at approximately the same elevation as the zone which experienced large strains during the 1971 failure, i.e., the zone at or near the base of the hydraulic fill shell.
- b. The static shear stresses available to drive a flow slide are greatest at the base of the hydraulic fill compared to upper parts of the hydraulic fill.
- c. N-values in Zone 5 are generally lower than N-values at higher elevations in the hydraulic fill, especially when corrected for overburden pressure. Therefore, Zone 5 would be expected to have somewhat lower strength than the other zones.
- d. Most of the failure surface for the 1971 liquefaction flow slide was within Zone 5.

Consequently, the remainder of our evaluation of the 1971 slide is concentrated on Zone 5. In the following sections of our report, Zone 5 is used synonymously with the phrase "critical layer."

#### 4. SUSCEPTIBILITY OF DAM TO LIQUEFACTION FLOW SLIDE

##### 4.1 Analytical Approach

A procedure for evaluating the susceptibility of an embankment, or any soil mass, to a liquefaction failure is presented by Poulos, Castro, and France (1985). Liquefaction susceptibility is determined by performing a stability analyses which requires that the undrained steady state shear strength and the shear stress in situ be determined. The terms "liquefaction" and "steady state" are defined as follows:

Liquefaction - a phenomenon of instability wherein the shear resistance of a mass of soil decreases and becomes lower than the applied shear stress when subjected to monotonic, cyclic, or dynamic loading at constant volume. The mass undergoes very large unidirectional shear strains - it appears to flow - until the applied shear stresses are as low or lower than the reduced shear resistance.

Steady State - a state of deformation of any mass of particles in which the mass is continuously deforming at a constant volume, constant normal effective stress, constant shear stress, and constant rate of shear strain. The steady state strength is the shear strength of the mass when deforming under steady state conditions.

Note that the definition of liquefaction refers to a stability failure of a soil mass rather than to the behavior of a specific soil element. Liquefaction susceptibility depends on the strength of all soils along the potential failure surface. Zones of loose (contractive) soils are critical to analyzing liquefaction susceptibility because only loose soils can have an undrained strength that is significantly lower than their drained strength. Thus only loose soils have the potential to lose strength when earthquake or other rapid loading changes the condition from drained to undrained. A liquefaction failure can occur if, and only if, the strength loss in the loose zone(s) is large enough to render the mass unstable. When a liquefaction failure occurs, the reduced strength need not be zero, and conversely, even a very low reduced strength may not lead to a liquefaction failure if other zones are strong enough to prevent a loss of stability.

The primary steps in the stability analyses for determining the liquefaction susceptibility of a soil mass are as follows:

1. Determine in situ undrained steady state shear strength.
  - Determine in situ void ratio (prefailure).
  - Determine slope of steady state line from a plot of steady state void ratio vs. effective stress during steady state deformation.
  - Determine undrained steady state strengths for "undisturbed" specimens.
  - Correct measured undrained steady state strengths to in situ void ratio using the slope of the steady state line.
2. Calculate in situ driving shear stress along the failure surface using conventional procedures for stability analysis.
3. Calculate factor of safety against liquefaction susceptibility,  $F_L$  as the ratio of driving shear stress to the undrained steady state shear strength. If the driving shear stress is less than the steady state strength ( $F_L < 1$ ), then the soil mass is susceptible to liquefaction.

The steps in the procedure listed above were followed in our re-evaluation of the Lower San Fernando Dam to determine if the procedure would predict that the upstream slope of the dam was susceptible to a liquefaction flow slide prior to the earthquake that caused the slide. The layer at the base of the hydraulic fill shell of the dam, Zone 5, was judged to be the most critical from a liquefaction standpoint. Therefore, the soils in this critical layer are the focus of our liquefaction evaluation.

A soil mass which is susceptible to liquefaction (unstable) will only experience a liquefaction failure when a sufficiently large triggering event, such as an earthquake, causes the strength of the soil to decrease to its undrained steady state strength. In the case of the Lower San Fernando Dam, the triggering event was an earthquake. A discussion of the earthquake required to trigger the 1971 flow slide of the Lower San Fernando Dam is presented in Section 5.

A flow chart for evaluating the liquefaction susceptibility of the Lower San Fernando Dam is presented in Fig 12. The primary steps in the procedure are shown on the right side of the flow chart, and ancillary steps for this particular project are shown on the left side. In the following sections each step of the procedure is described.

Data from laboratory tests on critical layer soils performed at Stanford University (Seed, R. B. et al, 1987), Corps of Engineers Waterways Experiment Station (WES, 1987), and Rensselaer Polytechnic Institute (Vasquez-Herrera et al, 1988) have been incorporated into this report. Data from these organizations were used to expand the data base for critical layer soils and to allow comparisons to be made between the test results of various organizations.

#### 4.2 Determination of In situ Void Ratios of Critical Layer

The in situ void ratio of the critical layer on the upstream side of the dam just prior to the 1971 failure is required to perform the liquefaction susceptibility analysis. In situ void ratios of the critical layer on the downstream side of the dam were determined from samples and tests performed in 1985 (in situ  $e_{1985}$ ). The in situ void ratios of the downstream critical layer just prior to the 1971 failure (in situ  $e_{1971}$ ) were determined by correcting the 1985 in situ void ratios for volume changes which took place between 1971 and 1985. In situ void ratios of the upstream critical layer were determined on the basis of estimated void ratio differences between the upstream and downstream layers. In the following sections we present our determinations of in situ  $e_{1985}$  and  $e_{1971}$ .

##### 4.2.1 In situ Void Ratios of Critical Layer in 1985

In situ void ratios of the critical layer on the downstream side of the dam were determined using three methods: fixed-piston sampling in boreholes, and "tripod" tube sampling and field density testing in the exploration shaft.

Fixed-Piston Sampling - Undisturbed samples of the critical layer were obtained from borings using a Hvorslev-type fixed-piston sampler. Careful measurements of sampler penetration and soil recovery were made to document soil volume changes which may have occurred during sampling. Fixed-piston sampling procedures are described in Appendix A, Poulos et al, 1985, and Keller, 1981.

Tripod Tube Sampling - Undisturbed samples of the critical layer were obtained from the floor of the exploration shaft using a tripod sampler developed by GEI. The tripod sampling procedure is described in Appendix B and Marcuson et al, 1980. The procedure involves advancing a tube into the soil in increments using hand carving techniques, such that any length changes during carving can be

measured. The tube alignment is maintained vertical by a tripod frame (Fig. B1).

Field Density Testing - Void ratios of the critical layer were determined by field density tests using the sand cone technique (ASTM D1556). These tests were performed at the floor of the exploration shaft, adjacent to the tripod tube sampling locations. Field density test procedures are described in Appendix B.

Appropriate corrections were made to the measured void ratios to obtain 1985 in situ void ratios. Corrections were made for the volume changes ( $\Delta V$ ) which occurred during tube sampling and for swelling of soils prior to sampling caused by unloading at the base of the exploration shaft. The following types of corrections were made for the various void ratio determination methods:

	<u>Void Ratio Correction</u>	
	<u><math>\Delta V</math> During Sampling</u>	<u><math>\Delta V</math> due to Swell During Shaft Excavation</u>
Fixed-Piston Samples	Yes	No
Tripod Tube Samples	Yes	Yes
Field Density Tests	No	Yes

The soil length of fixed-piston and tripod tube samples were measured at GEI's laboratory in Winchester, Massachusetts. No changes in length of these samples took place during transportation or tube cutting, and therefore, no void ratio corrections were necessary for these effects.

A summary of all void ratio measurements in the critical layer soils is presented in Tables 1 and 2. Data used to compute void ratio corrections for volume changes which occurred during tube sampling are presented in Table A2 (Appendix A) and Table B1 (Appendix B). As shown by Tables 1 and 2, a large number of tube samples had only very small void ratio corrections for volume changes during sampling.

Void ratio corrections for swelling at the base of the exploration shaft were estimated using data from triaxial swelling tests performed in the GEI laboratory (Appendix F, Section F.4.7). Five undisturbed samples from the critical layer were consolidated to their 1985



in situ stresses and then unloaded. The void ratios were plotted as a function of effective stress ( $\bar{\sigma}_o$ ) during unloading. The coefficient of swelling,  $\Delta e / \Delta \log \bar{\sigma}_o$ , of each sample is plotted in Fig. 13 as a function of the percent fines of the sample.

The initial effective stress at the base of the exploration shaft was estimated to be two thirds of the vertical effective stress ( $K_o = 0.5$ ). Void ratio measurements in the critical layer were made in saturated soils located 0.5 feet to 1.5 feet above the groundwater level. The effective stress in soils of the critical layer after shaft excavation was estimated to be the suction corresponding to a column of water equal to the distance between the sample and the groundwater level (about 1 foot). The effective stress caused by the self weight of the sample was not significant and therefore was not added to the suction pressure. Void ratio corrections for swelling were made by determining the total change in effective stress of soils at the base of the shaft and the relationship shown in Fig. 13. A summary of void ratio corrections for swelling of critical layer samples is presented in Table 3. Undisturbed exploration shaft samples of the critical layer tested by both GEI and Stanford were corrected for swelling using the same procedure.

A plot of 1985 in situ void ratios of critical layer soils vs. elevation is presented in Fig. 14. A unique relationship between in situ void ratio and depth would not be expected because of the gradation differences among the samples (Fig. 11). However, there is no consistent difference between the void ratios measured using fixed piston samples, tripod tube samples, or field density tests.

Void ratio measurements of the critical layer were made at two locations on the downstream slope. These are Locations 111 and 103, about 350 feet apart (Fig. 5). The data indicate that void ratios of the critical layer are relatively consistent across substantial distances parallel with the dam axis. One void ratio measurement was made by Stanford on a sand sample obtained from the clayey core zone (Location 105) at the same elevation of Zone 5 at Locations 111 and 103. The void ratio of this sand sample was significantly higher than other samples from Zone 5 as shown in Fig. 14.

#### 4.2.2 In situ Void Ratios of Critical Layer Prior to Failure

In situ void ratios of the downstream critical layer at the time of the 1971 dam failure were determined by correcting the measured 1985 in situ void ratios for the compression of the soils that occurred immediately following the 1971 earthquake and also due to the gradual lowering of the groundwater level within the dam as a result of the permanent lowering of the reservoir.

In situ void ratios of the upstream critical layer at the time of the 1971 failure were determined by correcting downstream values for estimated void ratio differences between the upstream and downstream layers. These differences were due to prolonged submergence of the upstream slope (reservoir effect) and additional compression of downstream soils from the weight of the 1930 and 1940 berms.

The Los Angeles Department of Water and Power provided GEI with detailed vertical and horizontal movement survey data of the embankment obtained by their personnel between 1929 and 1985. These data, presented in Appendix C, formed the basis for analyses made to estimate the void ratio changes which occurred in the critical layer between the time of failure in 1971 and the time of sampling in 1985. In addition, the data were used to evaluate void ratio differences between upstream and downstream critical layer soils.

Analyses of void ratio changes induced by the 1971 earthquake and by the subsequent drop in the groundwater level are presented in Appendix C. This appendix also contains our evaluation of the void ratio differences between the upstream and downstream critical layers. The resulting void ratio corrections for the triaxial specimens are listed in Table 3 and the corresponding void ratios are listed in Tables 1 and 2. The same correction procedure was used for samples tested by GEI and Stanford.

#### 4.3 Determination of Slope of Steady State Line

The "steady state line" (SSL) depicts a correlation, unique for a particular soil, between the void ratio and the effective minor principal stress ( $\bar{\sigma}_{3s}$ ) during steady state deformation. The effective minor principal stress could be replaced in the plot by effective stress on the specimen failure plane ( $\bar{\sigma}_{fs}$ ) or by undrained steady state strength ( $S_{us}$ ). Values of  $\bar{\sigma}_{3s}$ ,  $\bar{\sigma}_{fs}$ , and  $S_{us}$  are all related by factors

that are a function of the steady state friction angle,  $\phi_s$ . Refer to Section F.4.4 of Appendix F for the relationships between these parameters.

A representative mixture of soils from the critical layer (Zone 5) was made from eight bag samples obtained from the exploration shaft. This remolded mixture is referred to in this report as Batch Mix 7 (see Appendix F, Section F.2). A grain size curve of Batch Mix 7 is shown in Fig. 11 and compared with grain size curves of undisturbed samples from the critical layer.

Monotonically loaded triaxial shear tests were performed on remolded samples of Batch Mix 7 at various void ratios to define the slope of the steady state line for critical layer soils. A summary of these triaxial tests is presented in Appendix F, Sections F.4.4 and F.4.5.

A variety of test procedures were used to measure the steady state strength of critical layer soils. The parameters varied in this test program were test type, consolidation type, sample preparation procedure, and end platen treatment. A summary of the number of tests performed using each method is shown in Table 4.

Remolded specimens were fabricated using two different methods. Fifteen specimens were prepared in layers of moist soil using a tamper to compact each layer to the desired initial void ratio. Specimens were placed at water contents of typically 3 to 4% (relatively dry) or 7% (relatively moist). Two samples were placed as a slurry after thorough mixing with water. Samples were generally placed at a high void ratio so that they would be contractive during shear. Fifteen tests were performed using lubricated end platens and two tests were performed using conventional end platens.

Fifteen consolidated-undrained ( $\bar{R}$ ) and two consolidated-drained (S) triaxial tests were performed. Ten of the  $\bar{R}$  tests and the two S tests were isotropically consolidated. The remaining five  $\bar{R}$  tests were anisotropically consolidated. Most of the triaxial test specimens were sheared at an axial strain rate of between 0.5 and 2.0% per minute. Two specimens were sheared at faster rates of 48 and 33% per minute ( $\bar{R}202$  and  $\bar{R}207$ ). A typical  $\bar{R}$  test result on a compacted specimen of Batch Mix 7 is shown in Fig. F78.

The steady state line (SSL) for Batch Mix 7 is shown in Fig. 15 as a plot of void ratio versus effective stress on the specimen failure plane during steady state deformation. The initial state for each test is also shown in Fig. 15 as well as the path followed during shear.

The SSL for Batch Mix 7 has a straight line portion up to  $\bar{\sigma}_{fs} = 4$  tsf and is slightly curved at higher effective stresses. The straight line portion has a slope of 0.11 on a semilog plot. The steady state friction angle for Batch Mix 7 is  $34^\circ$ , as shown in Fig. F84.

The various testing methods used to develop the SSL for Batch Mix 7 show that the SSL is not a function of the following:

- initial structure, i.e., method of sample preparation
- initial state, i.e., consolidation stress
- stress path, i.e., test type

Three other laboratories performed triaxial tests on the same critical layer soil (Batch Mix 7) to define its steady state line. These laboratories were Stanford University (Seed, R. B. et al, 1987), Corps of Engineers Waterways Experiment Station (WES, 1987), and Rensselaer Polytechnic Institute (Vasquez-Herrera et al, 1988). Steady state strength data from these laboratories are plotted together with GEI's data in Fig. 16. Data from all laboratories plot very close to the steady state line defined by GEI with the exception of several data points from WES which plot slightly below the line. The WES data were not checked by GEI as of the date of this report and the reason for the slight discrepancy is unknown. In general, the agreement between laboratories is remarkable.

Previous investigations have shown that for a given soil: a) the slope of the steady state line on a semilog plot is affected chiefly by the shape of the grains and b) the vertical position of the steady state line is sensitive to grain size distribution (Castro et al, 1982).

The slope of the SSL defined for the critical layer soils is used to correct the strengths of "undisturbed" specimens, as described in Section 4.5.

#### 4.4 Determination of $S_{us}$ for Undisturbed Specimens of Critical Layer

A total of 16 consolidated-undrained ( $\bar{R}$ ) triaxial tests were performed by GEI on "undisturbed" samples of the critical layer (Zone 5) to define steady state strengths of the samples. These samples were obtained from two locations on the downstream side of the dam: Locations 103 and 111 (see Fig. 5). Two types of samples were obtained at Locations 111: fixed-piston samples from borings and tripod tube samples from the exploration shaft. Fixed-piston samples were obtained at Location 103. The test samples are representative of the Zone 5 soils because they were taken from the full thickness of Zone 5 and from borings located 350 feet apart.

The undisturbed specimens of the critical layer samples were stratified to various degrees. The stratification was highlighted after partial drying of the tested specimens. Grain size analyses of undisturbed samples of the critical layer were performed on a mixture of the layers representative of the failed zone of the specimen.

X-ray photographs of the undisturbed tube samples were examined to select a section of tube for triaxial testing that contained approximately only one soil type. Lubricated ends were used for virtually all tests to allow for the use of shorter samples that facilitated the selection of a relatively uniform triaxial specimen.

The specimens were consolidated to relatively high effective stresses so that the specimens would be contractive after consolidation because the steady state condition is more easily achieved within the strain limits of a triaxial test when specimens are contractive.

The results of  $\bar{R}$  tests performed on undisturbed samples of the critical layer are presented in Appendix F, Section F.4.3. A typical  $\bar{R}$  test result is shown in Fig. F64.

Stanford University (Seed, R. B. et al, 1987) performed seven additional  $\bar{R}$  tests on undisturbed samples from the critical layer. Four tests were performed on fixed-piston samples, three from Location 111 and one from Location 105, and three tests were performed on tripod tube samples from the exploration shaft.

Summaries of laboratory void ratio and shear strength data at steady state for undisturbed samples are presented in Table 1 (GEI data) and Table 2 (Stanford data). Data from GEI's tests are plotted as solid square symbols on the steady state diagram shown in Fig. 17. All of the steady state points for undisturbed samples plot above the SSL for Batch

Mix 7. We believe that this relationship occurs because the batch mix was more widely graded than the soils comprising the thin layers of the undisturbed samples. The undrained steady state shear strengths shown in Fig. 17 were obtained at the void ratio after consolidation in the laboratory, not at the in situ void ratio. Therefore, correction of the results to the in situ void ratio must be made, as described in the next step.

#### 4.5 Correction of Measured $S_{us}$ to 1971 In situ Void Ratio

##### 4.5.1 Correction Method

The steady state strengths of undisturbed samples of the critical layer were determined in the laboratory for void ratios obtained after consolidation (Section 4.4). The void ratios of these samples at the time of the 1971 failure were determined in Section 4.2. The slope of the steady state line for each undisturbed sample of the critical layer is the same as the slope of the SSL for Batch Mix 7 because the average grain shape of both soils is the same.

Steady state lines were drawn parallel to the SSL for Batch Mix 7 through each laboratory data point of  $S_{us}$  and  $e_c$  in Fig. 17 (solid squares). Only GEI laboratory test data are shown in Fig. 17. The estimated 1971 in situ void ratio of each sample,  $e_{1971}$ , was plotted on the SSL for that sample. Solid circles in the plot are based on estimated upstream void ratios, and open circles are based on estimated downstream void ratios. The estimated in situ steady state shear strength of each sample in 1971 was then read directly from the plot; upstream strength from solid circle symbols and downstream strength from open circle symbols.

##### 4.5.2 Selection of $S_{us}$ for Analysis

Upstream  $S_{us}$  - A plot of 1971 in situ values of upstream  $S_{us}$  versus elevation is shown in and Fig. 18. This plot includes data from both GEI and Stanford. The  $S_{us}$  values are scattered, as expected for an in situ hydraulic fill deposit of sand. The scatter reflects the natural variability in soil gradation and placement energy which occurred during the hydraulic filling operation. The final void ratio of a sandy deposit after consolidation under any effective stress is very dependent on its initial void ratio. The steady state strength of a sand is very sensitive to void ratio, and therefore, the scatter in initial

placement void ratio results in scatter in steady state strength.

The data in Fig. 18 show that the strengths obtained from the tripod samples and from the fixed-piston boring samples were similar. This result is consistent with data obtained in another GEI project (GEI, 1985) and lends confidence to the sampling methodology with the fixed-piston sampler. In addition, Fig. 18 shows that the data generated by both GEI and Stanford are similar when the same method is used for making void ratio corrections.

The data in Fig. 18 were evaluated to arrive at a reasonable steady state strength to use in stability analyses. There are three methods one might consider to select a strength for analyses, as explained below:

Average Strength - When the spatial variation of strength is such that the failure surface must pass through all zones, an average strength is appropriate for analyses. The strength in the critical layer of the Lower San Fernando Dam varies apparently at random based on our test results. However, it is reasonable to expect some vertical variation in strength values in the layer due to stratification caused by the hydraulic fill process. Since the failure occurred in Zone 5 mostly as horizontal shear, a strength averaged over height would be too high to use for stability analyses.

Lowest Strength - Failure surfaces seek out planes of weakness in stratified soils, and therefore, the lowest strength, representing the weakest stratum, is often used for analyses in these cases. Some of the strata comprising the critical layer of the Lower San Fernando Dam are probably relatively weaker than others. However, these strata are typically 6 to 12 inches thick, and it is unlikely that a particular weak stratum would exist over great lateral extent. Therefore, the strength of the weakest layer would be too low to use for stability analyses.

"Two-Thirds" Strength - A strength between the two described above would be reasonable to use for stability analysis of the Lower San Fernando Dam. The U.S. Army Corps of Engineers (1970), in their manual for analyzing the stability of earth dams, recommends the following: "For each embankment zone and foundation layer, design shear strengths should be selected such that two thirds of the test values exceed the design values." This method for arriving at a steady state strength for the critical layer of the Lower San Fernando Dam is reasonable considering the nature of the soils comprising the critical layer. The "two-thirds" strength is approximately equal to the average strength minus one half of the standard deviation.

The "two-thirds" and average steady state strengths of the upstream critical layer are shown in Fig. 18. The relatively high value of  $S_{us}$  obtained from Test R12 was not included in the computation of the average, since a localized dense pocket would not significantly influence the overall strength of the critical layer. The "two-thirds" value of steady state strength for the upstream critical layer is 0.26 tsf while the average is 0.31 tsf. The data in Fig. 18 can be interpreted in different ways to arrive at a value of steady state strength to use in the liquefaction susceptibility analysis. A reasonable range for the steady state strength is  $0.26 \pm 0.05$  tsf.

Downstream  $S_{us}$  - A value of  $S_{us}$  for analysis of the downstream critical layer was selected using the same procedure described above for the upstream critical layer. A plot of 1971 in situ values of downstream  $S_{us}$  versus elevation is shown in Fig. 19. The "two-thirds" value of steady state strength for the downstream critical layer is 0.33 tsf. A reasonable range for strength selection from the data in Fig. 19 is  $0.33 \pm 0.05$  tsf.



#### 4.6 Calculation of In situ Driving Shear Stress and the Factor of Safety

##### 4.6.1 In situ Driving Shear Stress

The "driving" shear stresses in the upstream and downstream critical layer were determined by conventional static stability analyses described in Appendix D. The driving shear stress in the critical layer is equal to the minimum shear resistance the layer must have to just maintain stability of the slope, assuming "mobilized" strengths in other layers. The "mobilized" strengths are those that would act while deformations of the slope were occurring and would be available to resist a massive flow slide.

Upstream Slope - The strengths in the clayey core were assumed to be the peak undrained strengths,  $S_{up}$ , using a  $S_{up}/\bar{p}$  ratio ranging from 0.20 to 0.30. Drained strengths were used for the rolled fills and ground shale hydraulic fill. The steady state friction angle,  $\phi_s$ , for these layers was varied between  $30^\circ$  and  $35^\circ$  in the analyses. A slip surface through the upstream slope is shown in Fig. D1. Using average  $S_{up}$  and  $\phi_s$  values as described above, the average driving shear stress,  $\tau_d$ , in the critical layer on the upstream side of the dam is 0.48 tsf. Based on the range of soil strengths used in the stability analysis, a reasonable range for  $\tau_d$  is  $0.48 \pm 0.04$  tsf.

Downstream Slope - Stability analyses of the downstream slope of the dam were performed in the same way as the upstream slope. The berms on the downstream slope were assumed to act in a drained condition with  $\phi_s = 40^\circ$ . A reasonable range for the average driving shear stress in the critical layer on the downstream side of the dam is  $0.33 \pm 0.08$  tsf for the prefailure configuration.

Immediately after the failure of the upstream slope, the average driving shear stress in the critical layer on the downstream side of the dam was reduced to about  $0.22 \pm 0.06$  tsf by the removal of the slide mass on the upstream side.

#### 4.6.2 Factor of Safety Against Liquefaction

The factor of safety against liquefaction susceptibility,  $F_L$ , is:

$$F_L = \frac{\text{Undrained Steady State Shear Strength}}{\text{Driving Shear Stress}}$$

Values of  $S_{us}$  and  $\tau_d$  in the critical layer on the upstream side of the dam were obtained in Sections 4.5 and 4.6.1, respectively. They are shown graphically in Fig. 18. For the upstream slope the best estimate for the factor of safety is:

$$F_L = \frac{S_{us}}{\tau_d} = \frac{0.26 \text{ tsf}}{0.48 \text{ tsf}} = 0.54$$

Therefore, the upstream slope was potentially unstable prior to the 1971 flow slide. The average driving shear stress in the critical layer was greater than the available undrained steady state shear strength.

Note that the steady state strength used to compute  $F_L$  was the "two-thirds" value, i.e., two thirds of the measured strengths of the critical layer were greater than the  $S_{us}$  used to compute  $F_L$ . However, the value of  $F_L$  would still be less than one if the average value of  $S_{us}$  were used.

A  $F_L < 1$  does not necessarily mean that a liquefaction flow slide of the slope will occur. An event, in this case an earthquake, must occur to trigger a failure. The earthquake must be large enough to strain the critical soil to the point where the peak strength is overcome and a reduction in strength to  $S_{us}$  takes place leading to a slide. Triggering of the slide is discussed in Section 5.

The upstream slope was stable under static loading conditions prior to the 1971 earthquake because the available strengths of all layers were their drained strengths. The factor of safety against sliding using drained strengths for all layers was about 2.

The value of  $F_L$  for the downstream slope prior to the failure was computed using the best estimates of  $S_{us}$  and  $\tau_d$  on the downstream side of the dam, as follows:

$$F_L = \frac{S_{us}}{\tau_d} = \frac{0.33 \text{ tsf}}{0.33 \text{ tsf}} = 1.00$$

which is significantly larger than the value of 0.54 for the upstream side.

After the upstream slope failed, the  $F_L$  of the downstream slope increased to about 1.5 due to a reduction in driving shear stress. The downstream slope may have been susceptible to liquefaction before the 1971 failure of the upstream slope ( $F_L \approx 1.0$ ) but was not susceptible to liquefaction after the upstream slope failure ( $F_L \approx 1.5$ ).

#### 4.7 Liquefaction Susceptibility Through Upper Zones of the Hydraulic Fill

In previous sections, the liquefaction susceptibility for a failure through Zone 5, judged to be the critical layer in the hydraulic fill shell, has been addressed. Eight triaxial tests were performed on undisturbed samples from Zones 2 and 3 of the hydraulic fill shell, located above Zone 5.

In situ values of  $S_{us}$  prior to the 1971 failure were estimated for undisturbed samples from Zones 2 and 3 of the upstream shell using the same procedures described previously. Estimated values of  $S_{us}$  for Zones 2 and 3 are presented in Table 5.

Driving shear stresses through upper zones of the hydraulic fill shell on the upstream side of the dam were determined using the same stability analyses procedures described previously. Driving shear stresses in Zones 2 and 3 were typically 0.41 tsf and 0.43 tsf, respectively. As expected, these values of  $\tau_d$  are less than the  $\tau_d$  of 0.48 tsf computed for Zone 5. Computed values of  $F_L$  for failure surfaces through Zones 2 and 3 of the hydraulic fill on the upstream side of the dam are presented in Table 5 for each sample tested. All  $F_L$  values are larger than one, except for one borderline case with  $F_L = 0.83$ . Thus results of our liquefaction susceptibility analyses indicate that a liquefaction failure could not occur through Zones 2 and 3. We believe that liquefaction failures through Zones 1 and 4 were also not possible. Zone 1 had generally higher N-values than Zone 2 and had a slightly lower driving shear stress, indicating that it would be less critical than Zone 2. Zone 4 was a dense widely graded sand that would probably be dilative during undrained shear.

Intact pieces of the upper zones of the shell were found during investigations of slide debris on the upstream side of the dam (Seed et al, 1973). All available evidence indicates that the liquefaction flow slide occurred through the critical layer near the base of the hydraulic fill shell and not through the upper zones of the shell. This is consistent with

the  $F_L$  computed by GEI for Zones 5 and for the upper zones of the hydraulic fill.

#### 4.8 Conclusions

The measured values of undrained steady state strength and driving shear stresses in the upstream slope of the Lower San Fernando Dam are consistent with the fact that the upstream slope was susceptible to a liquefaction flow slide at the time of the 1971 San Fernando earthquake. The data also confirm that the failure would occur through a layer of soil at the base of the hydraulic fill shell and not through the overlying layers in the shell. The measured strengths indicate that the downstream side of the dam may have been susceptible to a liquefaction failure prior to the 1971 upstream slope failure. However, the downstream slope was not susceptible to a liquefaction failure once the upstream slope failed because the driving shear stresses on the downstream side of the dam were significantly reduced by loss of the upstream slope.

It has been suggested (Seed, 1987) that the undrained steady state strength can be correlated with blowcounts and that such a correlation can be used to estimate strengths at any given site. Data obtained at the Lower San Fernando Dam has been used to develop such a correlation. In general, use of blowcounts to estimate steady state strength is believed by the authors to be inappropriate as explained below.

The blowcounts obtained in the critical zone of the Lower San Fernando Dam in the post-earthquake investigations of 1971 and 1985 are on the order of 20 blows/foot. Thus the sampler penetration per blow was on average less than one inch. Densification of the soil within a couple of inches of the spoon tip would occur after each blow, increasing the penetration resistance for the subsequent blow. Thus, even if each penetration occurred under undrained conditions, the resistance to penetration would not reflect the in situ undrained strength but a higher strength value considering the sensitivity of undrained strength to changes in density. Furthermore, it is likely that the soil is drained, at least partially, during each penetration and thus the penetration test reflects at least partly drained rather than undrained conditions. Because of the large difference between drained and undrained strength in loose sands and because of the sensitivity of undrained strength to changes in volume, the blowcounts for different soils with the same value of  $S_{us}$  will vary widely depending on the ability of the soil to drain and to densify during the SPT test. Densification and drainage will depend on soil gradation, stratification, and other factors unrelated to  $S_{us}$ . Thus a correlation between blowcounts and  $S_{us}$  would only be appropriate if the SPT test were

a fully undrained test. This is not likely to be the case for sandy soils. Therefore, blowcounts should not be used for determinations of  $S_{us}$  that are critical to evaluating the safety of a structure. Blowcounts should only be used as a crude guide as to whether the soil is relatively loose or dense, and for identifying those zones of a soil deposit that might be critical for stability.

It has been conjectured (National Research Council, 1985) that in liquefaction slides water redistribution may occur causing a reduction of the undrained strengths below their in situ pre-earthquake values. The analysis of the Lower San Fernando Dam demonstrates that the critical soils through which the failure took place failed at their pre-earthquake void ratios because:

- a. The zone of critical soils that developed extremely large deformations was about 15 feet in thickness, about 200 feet wide, and about 1,000 feet long. Such a large volume of soil could not have changed significantly in density during the 1.5 minutes that elapsed from the beginning of shaking to the end of the slide movements.
- b. The values of  $S_{us}$  that were measured, assuming no water redistribution, agreed well with the observation of a failure in the upstream direction and no failure in the downstream direction.

It is possible that after very large deformations and as the sliding mass moved into the reservoir, water may have been trapped under and between the various sections of the failing mass. Thus the overall resistance to sliding would decrease, leading to the very flat slope of the final configuration of the failure mass. However, the soils within the failure mass deformed under undrained conditions prior to the movement of a substantial part of the sliding mass into the reservoir.

## 5. EARTHQUAKE REQUIRED TO TRIGGER LIQUEFACTION FAILURE

### 5.1 Introduction

When a soil mass is susceptible to liquefaction, the stress strain behavior in critical zones of the soil mass can be shown by the schematic stress strain curve in Fig. 20. The driving shear stress  $\tau_d$  is well below the drained strength, but it is higher than the undrained steady state strength. Undrained straining leads to a massive failure if the strain reaches the triggering strain  $\gamma_{tr}$ , the strain at which the driving shear stress exceeds the available strength. Undrained straining can be caused by a rapid monotonic, cyclic, or transient increase in shear stress. The additional shear stress must be applied rapidly so that it causes undrained behavior. Previous work (Castro et al, 1982; Poulos et al, 1986) has shown that the triggering strain is about the same whether triggering is caused by monotonic or by cyclic loading.

Based on this background, the triggering analysis for the Lower San Fernando Dam included three steps, namely, a) determination of the triggering strain  $\gamma_{tr}$  for the critical soil layer, b) estimation of the strains induced by the 1971 earthquake and other previous earthquakes, and c) comparison of the strains in a) and b) to determine whether the results are consistent with the observed behavior.

The analytical approach used to determine the earthquake magnitude required to trigger a liquefaction flow slide of the upstream slope is shown by the flow chart in Fig. 21. The left side of the flow chart in Fig. 21 shows the general steps used to determine the triggering strain required to reduce soil strengths of the critical layer to steady state values. The right side of the flow chart shows the steps used to determine the amount of strain that various earthquakes would produce in the critical layer. The above steps were combined to arrive at the earthquake magnitude required to trigger a liquefaction failure.

A description of the triggering analysis, an explanation of the delayed failure of the dam, and a summary of the earthquake history of the dam prior to 1971 are presented below.

### 5.2 Strain Required to Trigger Flow Slide

Remolded specimens of Batch Mix 7, which represent the critical layer, were anisotropically consolidated in a tri-axial cell such that the ratio of undrained steady state strength  $S_{us}$  to driving shear stress  $\tau_d$  was about 0.65

( $F_L = 0.65$ ). We desired a laboratory  $S_{us}/\tau_d$  of 0.54, our estimate of the factor of safety against liquefaction susceptibility in the critical layer for an upstream failure. However, we could only achieve values as low as 0.60 and typically 0.65 due to the sample preparation and consolidation procedures used.

In terms of stresses on the  $45^\circ$  plane of the specimen, the ratio  $q_{us}/q_c$  is also 0.65. Values of  $q_{us}$  are only a function of void ratio after consolidation and  $q_c$  is the static shear stress applied to the specimen during consolidation.

### 5.2.1 Monotonic Tests

A series of monotonically loaded triaxial tests with varying strain rates were performed on Batch Mix 7. These tests were done on anisotropically consolidated remolded (compacted) specimens. The results are reported in Appendix F, Section F.4.6. These tests were performed to determine the triggering strains for various strain rates and to estimate the peak strength of critical layer soils prior to the failure.

Several specimens were consolidated such that the ratio of undrained steady state strength,  $S_{us}$ , was about 0.65 times the applied static consolidation shear stress,  $\tau_d$ . Stress-strain curves of two tests consolidated in this way are shown in Fig. 22. The shear stress is plotted in terms of  $q$ , the shear stress on the  $45^\circ$  plane of the specimen.

Stress-strain curve A in Fig. 22 is from Test R209 performed with strain control at a relatively slow rate of 0.9% axial strain per minute. The consolidation shear stress,  $q_c$ , was about 0.50 tsf for this test. The peak shear strength of this specimen was  $q_p = 0.62$  tsf, and it occurred at an axial strain of only 0.13%. The specimen strength was reduced to the consolidation shear stress in about 1.1% axial strain. Continued straining caused further reductions in strength. The undrained steady state strength of the specimen was reached after about 25% axial strain.

A second specimen (Test R203) was set up in the same way as the specimen in Test R209. However, the specimen in Test R203 was sheared at a very fast strain rate of about 4,600%/min as opposed to a slow strain rate of 0.9%/min. The high strain rate was obtained by the sudden application of a large axial load, higher than the peak strength of the specimen. The stress-strain curve of the fast strain rate specimen, monitored with a high

speed strip chart recorder, is shown by Curve B in Fig. 22. The peak strength of the fast strain rate specimen was higher than that of the slow strain rate specimen but occurred at a similarly low axial strain. The loss in strength of the fast strain rate specimen with continued straining was more gradual than for the slow strain rate specimen. The steady state strength of the fast strain rate specimen was not reached within the strain limits of the triaxial test.

Slow strain and fast strain rate laboratory tests were performed at two effective consolidation stresses which bracket the average in situ stresses in the critical layer prior to the 1971 failure. Stress paths for the laboratory tests and those estimated to apply in situ are shown in Fig. 23.

The average in situ static stresses on the failure plane through the upstream hydraulic fill shell of the dam prior to the 1971 failure are plotted in Fig. 23 as point A. Curves e and f in Fig. 23 are estimated stress paths for 1971 in situ conditions for slow and fast strain rates, respectively.

The peaks of stress paths e and f shown in Fig. 23 represent the average peak strengths of the in situ critical layer soil along the failure plane. For slow strain rates, the average in situ peak strength is about 0.75 tsf. For fast strain rates, the average in situ peak strength is about 0.85 tsf.

The test results of the monotonic tests indicated the following:

- a. In slow strain rate tests, the triggering strain was about 1.0% axial ( $\epsilon_{tr}$ ), 1.5% in shear ( $\gamma_{tr}$ ).
- b. The peak strength increased with rate of strain.
- c. The triggering strain increased with rate of strain.

The flow slide of the Lower San Fernando Dam was triggered sometime after the end of shaking, and the start of the slide itself occurred relatively slowly. Thus the appropriate triggering strain is that for slow strain rate, or  $\gamma_{tr}$  equal to about 1.5%. During the earthquake, the applicable peak strength is that appropriate for fast rates of strain.



### 5.2.2 Cyclic Load/Creep Tests

A series of cyclic load triaxial tests were performed to investigate the influence of low strain levels on the behavior of critical layer soils. The purpose of a number of these tests was to determine if samples strained to values less than  $\gamma_{tr}$  would eventually creep to failure. The details of these tests are presented in Appendix F, Section F.4.8.

Specimens of Batch Mix 7 were consolidated such that  $F_L$  was typically 0.65. Cyclic stresses were applied with a hammer, creating transient pulses which were not available to drive the failure as was the case in the field.

Ten cyclic load tests were performed, varying the magnitude of loading and the number of load cycles. After applying cyclic loads, the specimens were allowed to creep under the static consolidation loads (driving shear stress) while maintaining undrained conditions. The creep rate of the specimens was a function of the amount of strain the specimen had accumulated. A plot of creep rate vs. cumulative axial strain for the tests is shown in Fig. 24. This plot indicates that continued creep leading to complete collapse of the specimen would occur once axial strains exceeded 0.35%. An axial strain of 0.35% corresponds to a shear strain of 0.5% for Poisson's ratio = 0.5. A rapid increase in rate of strain occurred after about 1% axial strain (1.5% shear strain). The rapid increase in strain would correspond to the triggering strain as defined in Fig. 20. Thus the triggering strain for both cyclic and slow monotonic tests were comparable. The cyclic tests showed, however, that if a smaller strain were induced by cyclic loading (0.35% axial, 0.5% shear), the soil would creep until failure was triggered. Note that failure could be triggered because the driving shear stress exceeded the undrained steady state strength.

### 5.3 In situ Strains Induced by Earthquake Loading

Analyses were performed to estimate the strains that would accumulate in the critical layer on the upstream side of the dam under various earthquake load levels. A Newmark-type analysis (Newmark, 1965) was performed to estimate displacements of the potential failure mass and the corresponding strains in the critical layer.

The basic assumption in this type of analysis is that displacements are initiated only when the earthquake-induced

accelerations of the potential sliding mass exceed the yield acceleration of the mass.

The basic steps of the method, as applied for this study, are as follows:

- a. For the critical failure surface through the upstream slope, determine from a pseudostatic stability analysis the horizontal acceleration which produces a safety factor of one. This is referred to as the yield acceleration,  $k_y$ , and has units of  $g$  (acceleration due to gravity).
- b. Define a time history of average acceleration,  $k(t)$ , of the failure wedge during earthquake loading, for various earthquake levels. Values of  $k(t)$  are given in units of  $g$ . For this study, the computer program SHAKE (Schnabel et al, 1972) was used to compute  $k(t)$  by modeling the propagation of earthquake accelerations from bedrock through the critical layer.
- c. Compute the displacements which are initiated when the earthquake accelerations exceed the yield accelerations; i.e., when  $k(t) > k_y$ . Add displacements which occur each time the yield acceleration is exceeded to obtain the accumulated displacement caused by the earthquake. Do this for various  $k(t)$  developed from various earthquake levels. Convert accumulated displacement to strain of the critical layer and plot these strains vs earthquake magnitude.

Each step is discussed below as it was applied to the analysis of the upstream slope of the Lower San Fernando Dam.

#### 5.4 Determination of Yield Acceleration, $k_y$

Yield accelerations of the upstream slope,  $k_y$ , were computed using pseudostatic stability analyses as described in Appendix D. Yield accelerations of the upstream slope were computed to be in the range of 0.05  $g$  to 0.07  $g$  for the range of soil strengths assigned to the different soil layers. Details of the analysis are presented in Appendix D.

The yield strength of the critical layer (in situ) was estimated on the basis of  $\bar{R}$  tests on remolded samples of Batch Mix 7 for fast rate of loading, as presented in Section 5.2.1. The yield strength of the in situ "undisturbed" soil would likely be somewhat higher than that of remolded samples.

Therefore, the pseudostatic analysis is somewhat conservative, i.e., the computed yield accelerations will be somewhat lower than the actual value.

## 5.5 Analyses to Define Time Histories of Acceleration

Time histories of earthquake accelerations,  $k(t)$ , applied to the potential sliding mass on the upstream slope were computed using the computer program SHAKE. SHAKE consists of a one-dimensional wave propagation analysis in which the soil profile is modeled as a series of horizontal layers. Input parameters used in SHAKE analyses are presented in Appendix E. The soil profile used in the analyses is shown in Fig. 9. This soil profile represents soil layering in the approximate center of the hydraulic fill shell.

Earthquake time histories of acceleration were input at the surface of the bedrock layer. The earthquake time history was that obtained from a seismoscope located on the right abutment. The motion in the direction normal to the axis of the dam, developed by R. F. Scott (Seed et al, 1973) was used.

The maximum acceleration in the record was about 0.55 to 0.60 g. Accelerations in the record were scaled to obtain earthquake time histories with several different peak accelerations for the analyses so that the strains induced in the critical layer could be estimated as a function of maximum earthquake acceleration.

The results from SHAKE are time histories of horizontal shear stress acting at the boundaries of soil layers. The time history of acceleration of soil in the critical layer was obtained by dividing the time history of horizontal shear stress in the layer by the total vertical stress on the layer.

## 5.6 Critical Layer Strains During Earthquake Loading

Horizontal displacements of the upstream slope were computed by double integration of the quantity  $[k(t)-k_y]$ . The integration was performed assuming that movements could only occur in the downhill direction. This assumption is reasonable because the yield acceleration in the uphill direction is substantially higher than in the downhill direction.

The critical layer thickness was about 15 feet in borings performed near the central part of the shell on the downstream side of the dam. We assumed that the critical layer thickness was similar on the upstream side of the dam. Shear strains in the critical layer induced by earthquake loading were assumed to be the accumulated displacements divided by 15 feet.

A plot of calculated shear strains induced in the critical layer versus maximum base rock acceleration is presented in Fig. 25.

## 5.7 Failure Mechanism - 1971 Flow Slide

The plot shown in Fig. 25 can be used to estimate the earthquake intensity (in terms of maximum bedrock acceleration) needed to trigger a liquefaction flow slide of the upstream slope of the dam. Creep leading to a flow slide would occur if shear strains in the critical layer exceeded about 0.5% during undrained loading. Based on the Newmark-type analysis, an earthquake with a maximum acceleration of about  $0.12 \pm 0.02$  g would cause about 0.5% shear strain to accumulate in the critical layer. However, the analysis was performed using undrained peak strengths in Zone 5 that were determined from tests on remolded samples. It is likely that the peak strength of the in situ undisturbed soil is higher, and therefore, the earthquake required to cause a strain of 0.5% would have a somewhat larger peak acceleration. Therefore, a flow slide of the upstream slope would be predicted if the dam were subjected to an earthquake having a peak acceleration somewhat larger than 0.12 g, probably near 0.15 g.

The 1971 earthquake had a peak acceleration of about 0.55 to 0.60 g, which would cause accumulated strains in the critical layer to be well in excess of 0.5%. Therefore, our analysis would predict that the 1971 earthquake would cause sufficient strain to reduce the strength in the critical layer to a value close to its undrained steady state strength. Such a strength reduction would then trigger a flow slide of the upstream slope.

The actual flow slide of the upstream slope started about 26 seconds after completion of earthquake shaking (see Section 2.2). The delayed failure was most likely caused by either, or both, of the following two factors:

- a. Accumulated shear strain in some zones of the critical layer may not have been quite enough to reduce its strength to the driving shear stress, and additional creep under the static driving stress was needed to lower its strength sufficiently to cause a flow slide.
- b. The dense sandy dike at the toe of the upstream slope was dilative, and during undrained shear there was a reduction in pore pressures which caused the strength of the toe dike to be significantly greater than its drained strength. The failure occurred when the strength was gradually reduced to its drained value as water from the reservoir flowed into the soil. This mechanism of the delay in the slide was proposed by Seed, 1979.

Mechanism (a) was observed in the laboratory during triaxial testing of anisotropically consolidated, remolded samples of the critical layer (Appendix F, Section F.4.8). In a number of these tests, samples accumulated small strains under cyclic loading. The specimens resisted applied static shear stresses for a time after cyclic loading, but continued to strain slowly (creep) under static stresses. The specimens eventually collapsed under the driving stresses as the specimen strength decreased during straining.

A scenario of the failure is illustrated in Fig. 26, a plot of total shear force ( $F$ ) along the failure surface vs. the shear displacement ( $\delta$ ) across the surface. The failure surface through the upstream slope shown in Fig. D1 was used to develop Fig. 26. The plot in Fig. 26 shows the total driving force along the failure surface obtained from a static stability analysis, the resisting force contributed by each layer through which the failure surface passes, and the total available resisting force. The plot in Fig. 26 is intended to show qualitatively the shear stress transfer between the various zones.

For the upstream slope the mobilized friction angle under static conditions was approximately  $20^\circ$  for all layers, as compared with a failure friction angle of  $30$  to  $35^\circ$ . Hence the slope was stable under drained conditions. The average shear force in each layer prior to the earthquake, for drained conditions, is shown in Fig. 26 at zero displacement. Note that the total driving force is the sum of the initial shear forces under drained conditions. The total driving force remains essentially constant at the beginning of slope movements, but it eventually decreases when very large displacements cause the slope to flatten.

The resistance of the various soil layers along the failure surface will change as movements take place during and after the earthquake. The resistance depends on whether the soil responds in drained or undrained shear and on the shapes of the stress strain curves.

A brief description of the resisting forces contributed by each layer is present below.

Critical Layer - The critical layer, Zone 5 of the hydraulic fill shell, behaved undrained during the failure. Because of the relatively long section of the failure surface within Zone 5, its contribution to the total shear resistance was more significant than all of the other layers combined. The shape of the F- $\delta$  curve was based on the shape of the stress-strain curve from Test R205. The peak strength was obtained from Fig. 23 for slow strain rate conditions. The actual peak strength during an earthquake cycle would be that for fast strain rate conditions.

Clayey Core - The clayey core strained undrained during the entire failure. The peak strength of the clayey core was based on a  $S_{up}/\bar{p}$  ratio of 0.25. The F- $\delta$  curve of the core was based on the stress vs vane displacement curve from a laboratory vane test on an undisturbed core sample (Appendix F, Section F.5). Shear strains of the clayey core were estimated from vane displacements based on correlations developed from previous tests on clayey soils (Poulos et al, 1985). Very large shear strains are required to reach the steady state strength for clayey soils. Thus, during the earthquake and prior to initiation of the failure, the mobilized strength in the clay is approximately equal to the peak strength.

Embankment Cap - The embankment cap, including the ground shale layer, were assumed to act under drained conditions during the failure. The shape of the F- $\delta$  curve for the cap was based on the shape of a typical stress-strain curve of a slightly dilative sand. A steady state friction angle of 30° was used.

Toe Dike - The toe dike was assumed to be a dense sand with a steady state friction angle of 30°. The sand was probably highly dilative because of the low effective normal stresses under which it was consolidated. It was assumed to be undrained during earthquake shaking and to drain gradually after completion of shaking. The shape of the undrained F- $\delta$  curve was based on the shape of a typical stress-strain curve for a highly dilative sand. The toe dike was under a very large "back pressure," being approximately 90 feet below reservoir level. The peak undrained strength was based on the assumption that dilation occurred until cavitation of the pore water started. The undrained strength was then ten times the drained strength. After completion of earthquake shaking, the strength of the toe dike gradually decreased to the drained strength as "negative" pore pressures dissipated.

The shear displacement of the failure surface which occurred during the 14 seconds of earthquake shaking was assumed to be 1 foot, as shown in Fig. 26. This amount of displacement is consistent with the interpretation of the

seismoscope record from the dam crest which indicated a "slight tilting" of the crest immediately after shaking (Seed, 1979). One foot of displacement corresponds to a shear strain of about 7% in the critical layer which would cause the shear resistance in the critical layer to approach the undrained steady state strength.

Since the dam did not fail during the earthquake, the summation of resisting forces was still significantly greater than the total driving force during shaking, as shown in Fig. 26. As creep occurred after the earthquake, the resisting forces gradually dropped due to: a) additional loss of strength of the critical layer as it approached its undrained steady state strength and b) dissipation of negative pore pressures in the toe dike causing resisting forces in the toe dike to decrease. Eventually the total resisting force fell below the total driving force and the major slide occurred. The creep stage lasted about 26 seconds in the field based on seismoscope records (see Section 2.2). Once resisting forces fell below driving forces, the resisting forces decreased even further as soil strengths of all layers moved toward their steady state values. The actual slide duration was about 50 seconds.

The above description is a qualitative view of a rather complex process of shear stress transfer among the various zones, leading to instability and to an upstream liquefaction (flow) failure. Even though the stress-strain behavior assumed for the various layers is approximate, the process presented in Fig. 26 illustrates the importance of considering the complete stress-strain behavior rather than peak or steady state strength alone (Poulos, 1971).

The downstream slope did not develop a flow slide; however, limited movements occurred as a result of the earthquake, as described in Appendix C. Horizontal movements in excess of 0.5 feet were observed at the berm road at the maximum dam section. These movements correspond to shear strains in the critical soil in excess of 2 to 3%, which may have reduced its strength to values close to the undrained steady state strength. However, the factor of safety of the downstream slope against liquefaction susceptibility was about 1.0, and therefore, it may not have had the potential for a liquefaction flow slide. After the upstream slope failed, the downstream slope was no longer susceptible to a liquefaction flow slide due to a reduction in driving shear stress in the downstream slope.

## 5.8 Earthquake History of the Dam

Our triggering analyses indicated that an earthquake with a maximum acceleration of about 0.15 g and with a similar time history as the 1971 event would have caused a flow slide of the upstream slope of the dam. The earthquake history of the dam site prior to 1971 was reviewed to test the validity of this conclusion.

Earthquake data within a 200-kilometer radius of the dam were obtained from the National Geophysical Data Center (NGDC)/National Oceanic and Atmospheric Administration (NOAA). Richter (1973) has compiled information on pre-1971 earthquakes which appeared to be the most significant in the area affected by the 1971 San Fernando earthquake. Table 6 lists the earthquakes presented by Richter (after dam construction and prior to 1971) together with pertinent information from NGDC. Records of actual earthquake accelerations at the dam site are not available for these earthquakes. A probable range of maximum accelerations at the Lower San Fernando Dam due to each earthquake was obtained from Fig. 27 (Schnabel et al, 1973) and are presented in Table 6.

Data in Table 6 indicate that previous earthquakes at the dam site would not have caused a liquefaction flow slide of the dam because maximum accelerations were lower than the estimated value of 0.15 g needed to trigger a slide.

Generally the movements of the dam prior to 1971 occurred gradually with increased rates of movements corresponding to construction activities at the dam, such as construction of the downstream berms (see Appendix C). An exception is the movement that coincided with an earthquake on August 30, 1930. At the time of this earthquake, the geometry of the dam was the same as that shown in Fig. 2, except the 1940 berm was not in place and the reservoir was at about El. 1090. Small transverse cracks were observed in the embankment after the earthquake, near its contact with the left (east) abutment. The maximum measured movements occurred in the parapet wall located on the upstream side of the crest. The parapet wall settled about 0.15 to 0.25 foot as a result of the earthquake with maximum settlements occurring between Stas 3+00 and 9+00. Prior to the earthquake, the parapet wall was moving laterally in the downstream direction. However, the wall moved upstream an average of about 0.03 feet as a result of the earthquake, with the maximum upstream movement being about 0.06 feet.

According to a statement by the caretaker of the dam, the 1930 shock was very severe; the heaviest he had ever experienced at the dam since its construction, he having resided near the dam since it was built (Jacques, 1930). The



maximum earthquake acceleration at the dam site due to the August 30, 1930 earthquake was estimated to be only 0.02 g in Table 6 based on NOAA's epicentral location. However, Richter (1973) indicated that the epicentral location of this earthquake has been questioned and that it may have been actually closer to the Lower San Fernando Dam. The closer epicenter would result in a maximum acceleration at the dam site in the range of 0.02 to 0.09 g for the August 30, 1930 earthquake.

The Kern County earthquake of June 21, 1952 would have caused maximum accelerations at the dam site to be between 0.05 to 0.12 g according to Fig. 27, more than any other pre-1971 earthquake. However, all movement and settlement survey data of the dam indicate that the Kern County earthquake did not cause measurable movement of the embankment. It is likely that the maximum accelerations at the dam site for this earthquake were less than 0.1 g. This is consistent with measured maximum accelerations of 0.048 g and 0.058 g in the north-south direction (perpendicular to dam axis) at the two closest recording stations to the dam. These recording stations were 74 and 78 miles from the epicenter and are 18 and 22 miles further than the dam was from the epicenter.

The behavior of the dam during earthquakes prior to 1971 is consistent with the results of our triggering analysis of the dam. The most severe pre-1971 earthquake occurred in 1930 and had an estimated maximum acceleration at the dam site in the range of 0.02 to 0.09 g. Our triggering analysis indicated that an earthquake with a maximum acceleration of about 0.15 g would be required to trigger a flow slide of the upstream slope. The 1930 earthquake did not cause a flow slide but did cause small movements and some cracking of the dam.

#### 5.9 Comments on Methodology for Triggering Analysis

The methodology described in the previous sections for analyzing liquefaction triggering at the Lower San Fernando Dam involved a rather extensive series of various types of triaxial tests. Some of the tests were performed to confirm previous findings and would not be necessary in general practice. The flow chart in Fig. 21 illustrates the main items in the liquefaction triggering evaluation performed for the Lower San Fernando Dam. In practice the strain required to trigger (left branch of flow chart) can be determined using monotonic (rather than cyclic) load tests on specimens prepared to have values of  $S_{us}$  and anisotropic consolidation stresses that are representative of in situ conditions. These tests will be generally performed on remolded specimens because undisturbed specimens would have too high a value of  $S_{us}$  due to unavoidable densification during sampling and consolidation. The performance of monotonic rather than

cyclic tests is based on the finding that the triggering strain defined in Fig. 20 is the same for monotonic and for cyclic loading.

The peak undrained strength obtained from the monotonic tests described above can be used in the evaluation of the yield accelerations and the corresponding displacements and strains, as shown on the right branch of the flow chart in Fig. 21.

Note that the use of the results of tests on remolded specimens will generally underestimate the peak strengths and thus will lead to a conservative estimate of the earthquake required to trigger liquefaction. Presently there is little information available for estimating the degree of conservatism.

## 6. CONCLUSIONS

The Lower San Fernando Dam in California developed a major slide in the upstream slope and crest as a result of the 1971 San Fernando earthquake. The purpose of our re-evaluation of the slide was to test the validity of using steady state concepts and methodology to perform liquefaction analyses of the dam.

The results of the stability analyses, based on the undrained steady state strengths measured, were consistent with the observed behavior, i.e., a) the dam was susceptible to a liquefaction failure in the upstream direction, b) the dam was not susceptible to a liquefaction failure in the downstream direction once the upstream slope had failed, and c) the strains that accumulated during the 1971 earthquake were sufficient to trigger the upstream liquefaction failure.

The main conclusions are presented below:

### Composition and Strengths, $S_{us}$ , of Hydraulic Fill Shells

1. Downstream Slope. Borings performed through the downstream shell indicated similar zonation in the east-west direction (parallel to the dam centerline). The loosest zone found in the downstream section of the hydraulic fill shell was a 15-foot-thick layer of very silty fine sand located at the base of the shell. This zone corresponds to the upstream zone that experienced very large strains at the base of the hydraulic fill based on field observations in trenches and borings made on the upstream side of the dam after the 1971 failure (Seed, 1973).

Based on the results of 23 tests performed on undisturbed samples by GEI and Stanford University laboratories, the undrained steady state strength of the downstream critical layer soils was estimated to be about 0.33 tsf just prior to the 1971 failure.

2. Upstream Slope. Construction records and continuity of layers across substantial distances found in the downstream shell indicate that the hydraulic fill stratigraphy was symmetrical with respect to the centerline of the dam. Thus it was concluded that tests performed on samples from the downstream shell could be used to estimate properties of soils in the upstream shell. In particular, the zone at the base of the downstream shell was considered similar to the critical layer for the upstream failure, i.e., the layer that developed very large strains during the

slide. Considering void ratio differences between the upstream and downstream critical layer soils (due to prolonged submergence of the upstream shell and additional loading of downstream shell by berms), the undrained steady state strength of the upstream critical layer soil was estimated to be about 0.26 tsf, as compared to 0.33 tsf in the downstream shell.

### Liquefaction Susceptibility

Liquefaction is a phenomenon wherein a mass of soil loses a large percentage of its shear resistance, when subjected to undrained monotonic, cyclic, or shock loading, and flows in a manner resembling a liquid until the shear stresses acting on the mass are as low as the reduced shear resistance.

The loss in shear resistance is due to the conversion of the mass from a practically drained condition, at which it can sustain the in situ shear stresses, i.e., it is stable, to a practically undrained condition of shear under which the soil mass is unstable. Liquefaction susceptibility refers to a condition under which the soil mass can develop a liquefaction failure as defined herein.

1. Pre-earthquake Stability. The factor of safety against a slide in the upstream direction using drained strengths was about 2. The factor of safety of the downstream slope for drained conditions was slightly greater than 2. Thus, under drained (no earthquake) conditions, the dam had a factor of safety that normally would be considered ample.
2. Upstream Slope. In the upstream direction, the static driving shear stress in the critical layer was about 0.48 tsf. Therefore, the computed factor of safety against liquefaction susceptibility was about 0.54 ( $0.26/0.48$ ). Thus the results of the analysis were consistent with the fact that, even though the upstream slope was stable under drained conditions, a triggering event, such as the 1971 earthquake, could cause an undrained failure (liquefaction).
3. Downstream Slope. The static driving shear stress in the critical layer was about 0.33 tsf prior to the upstream slide and about 0.22 tsf after the slide. Therefore, the factor of safety of the downstream slope against liquefaction susceptibility was about 1.0 prior to the upstream slide and about 1.5 afterwards. The computed factors of safety are consistent with the fact that the 1971 earthquake caused high pore pressures and slight deformations in the down-

stream slope, but the earthquake did not cause the slope to fail.

### Triggering of Liquefaction

If a soil mass is susceptible to liquefaction, a triggering action is required to induce liquefaction. The triggering action is a monotonic impact or seismic type of loading that causes the mass to deform undrained. It was found that shear strains of about 0.5% in the critical soils and applied under undrained conditions were sufficient for an upstream liquefaction failure to occur in the Lower San Fernando Dam.

1. Upstream Slope. Based on our triggering analysis, an earthquake with a maximum base rock acceleration of about 0.15 g and duration similar to the 1971 earthquake would cause enough shear strain (about 0.5%) to reduce the strength in the critical layer to the point where a liquefaction failure of the upstream slope would occur. The maximum base rock acceleration at the dam site during the 1971 earthquake was about 0.55 to 0.6 g. Therefore, the results of the analysis agrees with the fact that the 1971 earthquake was severe enough to trigger the failure. In addition, an analysis of earthquake events prior to the 1971 earthquake indicated that they were not severe enough to trigger a flow slide of the upstream slope of the dam.
2. Downstream Slope. Deformation measurements of the surface of the downstream slope made by the LADWP after the 1971 earthquake indicate that shear strains in the critical layer of the downstream hydraulic fill shell were about 2 to 3%, which are sufficient to reduce its strength to values close to the undrained steady state strength. However, failure of the downstream slope did not occur. This is consistent with the fact that the downstream slope had a factor of safety against liquefaction susceptibility of about 1.0 prior to the upstream slide and about 1.5 after the slide. Once the upstream slope failed, it was not possible for the downstream slope to fail, regardless of the magnitude of pore pressure build up and of strain accumulation.

### Other Conclusions

1. The void ratio of the critical layer in the downstream shell was measured using fixed-piston sampling, hand carved "tripod" tube sampling in a deep exploration shaft, and field density testing using a sand cone in the exploration shaft. All three

methods resulted in similar measurements of in situ void ratio within the normal scatter expected for a hydraulic fill. Therefore, both the fixed piston samples from boreholes and the tripod tube samples from the exploration shaft were found to be appropriate for measuring in situ void ratio for the liquefaction analyses as well as for performing laboratory tests to obtain undrained steady state strengths.

2. In general, fixed-piston samples were more cost effective for performing the steady state analyses than tripod tube samples. This is because a) tripod tube samples required additional void ratio corrections due to swell of the exploration shaft bottom and b) construction of the exploration shaft was much costlier than performing borings.
3. Four separate laboratories performed triaxial laboratory tests to define the steady state line of the critical layer soil, Batch Mix 7. In general, the laboratories showed remarkable agreement in defining the steady state line, Fig. 16.
4. The tests performed showed that the steady state line is not a function of the following:
  - ° initial structure, i.e., method of sample preparation.
  - ° initial state, i.e., consolidation stress
  - ° stress path, i.e., test type
5. An accumulated undrained shear strain of about 1.5% in the critical layer of the upstream slope is sufficient to lower the shear resistance of the layer to the driving shear stress and trigger the flow slide. However, if a smaller shear strain of 0.5% to 1.5% is reached, the soil creeps under the driving shear stress until the failure is triggered at a strain of about 1.5%.

## REFERENCES

- Baumann, P.; Richter, C. F.; Pentegoff, V. P.; and Duke, C. M. (1966). "Lower Van Norman Reservoir - Board of Consultants' Report on Safety," 14 pp., December.
- Boutrup, E. (1977). "Computerized Slope Stability Analysis for Indiana Highways," Joint Highway Research Project, File No. 6-14-22, Vols. 1 and 2, Engineering Experiment Station, Purdue University, West Lafayette, Indiana, December.
- Castro, G. (1987). "On the Behavior of Soils During Earthquakes - Liquefaction," The Proceedings of the 3rd International Conference on Soil Dynamics and Earthquake Engineering, Princeton, New Jersey, June.
- Castro, G.; Poulos, S. J., and Leathers, F. D. (1985). "A Re-examination of the Slide of the Lower San Fernando Dam," *Journal of Geotechnical Engineering*, ASCE 111 (GT9).
- Castro, G.; Poulos, S. J.; France, J. W.; and Enos, J. L. (1982). "Liquefaction Induced by Cyclic Loading," report by Geotechnical Engineers Inc. to National Science Foundation, Washington, D.C., pp. 1-80, March.
- Castro, G. and Poulos, S. J. (1977). "Factors Affecting Liquefaction and Cyclic Mobility," *Journal of the Geotechnical Engineering Division*, ASCE, Vol. 103, No. GT6, pp. 501-516.
- Castro, G. (1968) "Laboratory Investigation on Undisturbed Samples of Subsoils for the CONOX Project," Report to Compania de Acero del Pacifico, Harvard University, Cambridge, Massachusetts.
- Earth Technology Corporation, Long Beach, California, (1985). "Cone Penetration Tests, Lower San Fernando Dam," Project No. 86-140-03 report to U.S. Army Corps of Engineers.
- Farrar, J. A. (1986). "Travel Report," Code D-1542, U.S. Bureau of Reclamation, Denver, Colorado, April 14.
- Geotechnical Engineers Inc. (1985). "Seismic Studies - Pinopolis West Dam," report submitted to U.S. Army Corps of Engineers, Savannah District, GEI Project 84351.
- Gutenberg, B. and Richter, C. F. (1956). "Earthquake Magnitude, Intensity, Energy and Acceleration (Second Paper)," *Bulletin of the Seismological Society of America*, Vol. 46, No. 2, pp. 105-146, April.

REFERENCES  
(continued)

- Ishibashi, I.; Kawamura, M., and Bhatia, S. (1985). "Effect of Initial Shear on Cyclic Behavior of Sand," *Journal of Geotechnical Engineering*, Vol. 111, No. 12, December.
- Jacques, H. L. (1930). "Report on Dams After Earthquake of August 30, 1930," Los Angeles Department of Water and Power, File No. AX-245.
- Keller, T. O. (1981). "Procedure for Undisturbed Fixed Piston Sampling of Cohesionless Soil," Geotechnical Engineers Inc. (GEI), Internal Memorandum, 23 pp., Rev. May 1982.
- Lee, K. L.; Seed, H. B.; Idriss, I. M.; and Makdisi, F. I. (1975). "Properties of Soil in the San Fernando Hydraulic Fill Dams," *Journal of the Geotechnical Engineering Division, ASCE*, Vol. 101, No. GT8, pp. 801-821.
- Marcuson, W. F. III and Franklin, A. G. (1980). "State of the Art of Undisturbed Sampling of Cohesionless Soils," *Geotechnical Engineering*, Vol. 11, pp. 31-52.
- Mayeda, S. H., Jackson, L. A., et al (1969). "Lower San Fernando Dam 1967 Core Hole Investigation," L. A. Department of Water & Power, Water Engineering Division.
- National Research Council (1985). "Liquefaction of Soils During Earthquakes," Report No. CETS-EE-001, Committee on Earthquake Engineering. National Academy Press, Washington, D.C.
- Newmark, N. M. (1965). "Effects of Earthquake on Dams and Embankments," *Geotechnique*, London, Vol. 5, No. 2, June.
- Poulos, S. J.; Robinsky, E. I.; and Keller, T. O. (1986). "Liquefaction Resistance of Thickened Tailings," *Journal of Geotechnical Engineering*, ASCE, Vol. 111, No. 12, Paper No. 20213, pp. 1380-1394.
- Poulos, S. J.; Castro, G., and France, J. W. (1985). "Liquefaction Evaluation Procedure," *Journal of Geotechnical Engineering*, ASCE, 111(6) pp. 772-791.
- Poulos, S. J. (1971). "The Stress-Strain Curves of Soils," Geotechnical Engineers Inc., Winchester, Massachusetts, pp. 1-80.



REFERENCES  
(continued)

- Reichter, C. F. (1973). "Historical Seismicity of San Fernando Earthquake Area, San Fernando, California, Earthquake of February 9, 1971, U.S. Department of Commerce, NOAA, Vol. III, U.S. Government Printing Office Stock No. 0317-0089, pp. 5-11.
- Schnabel, P. B. and Seed, H. B. (1973). "Accelerations in Rock for Earthquakes in the Western United States," *Bulletin of the Seismological Society of America*, Vol. 63, No. 2, pp. 501-516.
- Schnabel, P. B.; Lysmer, J.; and Seed, H. B. (1972). "SHAKE, A Computer Program for Earthquake Response Analysis of Horizontally Layered Sites," Report No. EERC 72-12, University of California, Berkeley.
- Seed, H. B. (1987). "Design Problems in Soil Liquefaction," *Journal of Geotechnical Engineering Division*, ASCE, Vol. 113, No. 8, August, pp. 827-845.
- Seed, H. B.; Wong, R. T.; Idriss, I. M.; and Tokimatsu, K. (1986). "Moduli and Damping Factors for Dynamic Analyses of Cohesionless Soils," *Journal of Geotechnical Engineering*, ASCE, Vol. 112, No. 12, pp. 1016-1032.
- Seed, H. B. (1985). "Influence of SPT Procedures in Soil Liquefaction Resistance Evaluations," *Journal of the Geotechnical Engineering Division*, ASCE, Vol. 111, (GT12), pp. 1425-1445.
- Seed, H. B. (1979). "Considerations in the Earthquake-Resistant Design of Earth and Rockfill Dams," *Geotechnique*, Vol. 29, No. 3, pp. 215-263.
- Seed, H. B.; Lee, K. L.; Idriss, I. M., and Makdisi, F. I. (1975a). "The Slides in the San Fernando Dams During the Earthquake of February 9, 1971," *Journal of the Geotechnical Engineering Division*, ASCE, 101, No. GT7, pp. 651-688.
- Seed, H. B.; Lee, K. L.; Idriss, I. M. and Makdisi, F. I. (1975b). "Dynamic Analyses of the Slide in the Lower San Fernando Dam During the Earthquake of February 9, 1971," *Journal of the Geotechnical Engineering Division*, ASCE, Vol. 101, No. GT9, pp. 889-911.
- Seed, H. B.; Lee, K. L.; Idriss, I. M.; and Makdisi, F. I. (1973). "Analyses of the Slides in the San Fernando Dams During the Earthquake of February 9, 1971," Report No. EERC 73-2, University of California, Berkeley, California, (NTIS No. PB 223-402).

REFERENCES  
(concluded)

Seed, H. B. and Idriss, I. M. (1970). "Soil Moduli and Damping Factors for Dynamic Response Analyses," EERC Report 70-10, College of Engineering, University of California, Berkley.

Seed, R. B.; Jong, H. and Nicholson, P. G. (1987). "Laboratory Evaluation of Undrained Cyclic and Residual Strengths of Lower San Fernando Dam Soils," Report No. SU/GT/87-01, Stanford University, Stanford, California, 168 pp.

Siegel, R. A. (1978). STABL User Manual, Joint Highway Research Project, File No. 6-14-11, Engineering Experiment Station, Purdue University, West Lafayette, Indiana, June.

Siegel, R. A. (1975). "Computer Analysis of General Slope Stability Problems," Joint Highway Research Project, File 6-14-11, Engineering Experiment Station, Purdue University, West Lafayette, Indiana, June.

Suzuki, T. (1966). "Lower San Fernando Dam Investigation of Hydraulic Fill," L. A. Department of Water and Power, Water Engineering Division, May 1966, Rev. November 1966.

U.S. Army Corps of Engineers (1970). "Engineering and Design Stability of Earth and Rock-Fill Dams," Manual No. 1110-2-1902, Office of the Chief of Engineers, Washington, D.C.

Vasquez-Herrera, A. and Dobry, R. (1988). "Evaluation of Liquefaction Triggering in Lower San Fernando Dam in 1971 Earthquake Using Torsional Cyclic Tests," Rensselaer Polytechnic Institute, Troy, N.Y., Dept. of Civil Engineering Report to U.S. Army Corps of Engineers WES, in preparation.

WES (1987). Waterways Experiment Station Laboratory Test Data. Telephone Communication.

Wilun, Z. and Starzewski, K. (1972). "Soil Mechanics in Foundation Engineering" Vol. 1 John Wiley and Sons, New York, N.Y., 252 pp.

Wright, S. G. (1974). "SSTAB2 - A General Computer Program for Slope Stability Analyses," Research Report No. GE-74-1, Department of Civil Engineering, the University of Texas at Austin, August.

## NOTATIONS

The following symbols are used in this report:

### Symbols and Abbreviations

$A_c$  = area of triaxial test specimen after consolidation

$a_{max}$  = maximum base rock acceleration

$B_c$  = Skempton's pore pressure coefficient after consolidation

$C$  = cone penetration test sounding prefix

$c$  = cohesion intercept of a strength envelope

$CR$  = clearance ratio of sampling tube =  $\frac{ID - CE}{CE}$

where  $ID$  = inside diameter of tube  
and  $CE$  = inside diameter of cutting edge

$\overline{CR}$  = consolidated undrained cyclic load triaxial test

$\overline{CRR}$  =  $\overline{CR}$  test followed by an  $\overline{R}$  phase

$D_{10}$  = diameter at which 10% of the soil is finer by weight

$E$  = east

$e_t$  = void ratio in sampling tube

$e$  = void ratio

$e_c$  = void ratio after consolidation

$ES$  = exploration shaft

$e_{1985}$  = in situ void ratio at time of sampling in 1985

$e_{1971}$  = in situ void ratio immediately prior to 1971  
San Fernando earthquake

$F$  = force

$F_a$  = maximum cyclic load applied in  $\overline{CR}$  test

NOTATIONS  
(continued)

- FD = field density test
- $F_L$  = factor of safety against liquefaction susceptibility  
(equal to ratio of  $S_{us}/\tau_d$ )
- $F_r$  = maximum load above anisotropic load felt by sample  
during cyclic loading in CR test
- ft = feet
- G = specific gravity of solids
- G = shear modulus
- g = acceleration due to gravity (32.2 feet per second)
- $G_{max}$  = shear modulus at very low strains
- $K_c$  = consolidation stress ratio =  $\bar{\sigma}_{1c}/\bar{\sigma}_{3c}$
- $K_o$  = coefficient of lateral earth pressure, equal to  
 $\bar{\sigma}_h/\bar{\sigma}_v$
- $k(t)$  = time history of average acceleration of sliding mass
- $k_{max}$  = maximum value of  $k(t)$
- $k_y$  = yield acceleration
- LV = laboratory vane shear test; undrained
- N = north
- N = standard penetration test blowcount, blows/foot
- NGVD = National Geodetic Vertical Datum; elevation
- $\bar{p}$  = mean of minor and major effective principal stresses  
or vertical effective stress when used in the form  $c/p$
- q = one half of difference between major and minor  
principal stress; shear stress on plane inclined at  
 $45^\circ$  to major principal plane;
- $q_a$  = maximum applied q during CR test; summation of  
 $q_c$  and  $F_a/A_c$

NOTATIONS  
(continued)

- $q_c$  =  $q$  at completion of consolidation
- $q_p$  =  $q$  when peak shear stress is reached during triaxial test
- $q_r$  = maximum soil stress felt by sample during  $C\bar{R}$  test; summation of  $q_c$  and  $F_r/A_c$
- $q_s$  =  $q$  during steady state deformation
- $q_{us}$  =  $q$  during steady state deformation; undrained conditions
- $\bar{R}$  = consolidated undrained, monotonically loaded triaxial test
- $S$  = south
- $S$  = degree of saturation
- $S$  = split-spoon sample boring number prefix
- $S$  = consolidated drained, monotonically loaded triaxial test
- sec = seconds
- $S_{ds}$  = drained steady state shear strength
- SSL = steady state line
- $S_{up}$  = peak undrained shear strength
- $S_{us}$  = undrained steady state shear strength
- $S_y$  = yield strength
- $t$  = time
- $t$  = tons
- tsf = tons per square foot
- TS = tripod tube sample number prefix
- U = undisturbed sample boring number prefix

NOTATIONS  
(continued)

- U = undisturbed sample number prefix for fixed piston samples from borings
- $u_c$  = backpressure in triaxial test
- V = volume
- W = west
- W = weight of sliding mass
- $\alpha_s$  = slope of line through points representing steady state of deformation on stress path plot (q versus  $\bar{p}$ )
- $\Delta V$  = change in volume
- $\Delta e$  = change in void ratio
- $\delta$  = shear deformation
- $\epsilon_a$  = axial strain
- $\epsilon_s$  = axial strain when steady state deformation is reached during triaxial test
- $\epsilon_p$  = axial strain when peak shear stress is reached during triaxial test
- $\epsilon_{ec}$  = axial strain at end of cyclic loading in  $\overline{CR}$  test (see Fig. F105)
- $\epsilon_{rf}$  = axial strain at start of rapid failure in  $\overline{CR}$  test (see Fig. 105)
- $\epsilon_{tr}$  = triggering axial strain; axial strain required to trigger liquefaction failure
- $\gamma$  = shear strain
- $\gamma_t$  = total unit weight
- $\gamma_d$  = dry unit weight
- $\gamma_{dc}$  = dry unit weight at end of consolidation
- $\gamma_{tr}$  = triggering shear strain; shear strain required to trigger liquefaction failure

NOTATIONS  
(concluded)

- $\mu$  = Poisson's ratio
- $\varphi_s$  = friction angle at steady state of deformation in terms of effective stress
- $\varphi_p$  = maximum effective stress friction angle computed from a Mohr diagram
- $\bar{\sigma}_h$  = horizontal effective stress
- $\bar{\sigma}_1$  = major principal effective stress
- $\bar{\sigma}_{1c}$  = major principal effective stress after consolidation
- $\bar{\sigma}_{3ec}$  = minor principal effective stress at end of cyclic loading in CR test (see Fig. F105)
- $\bar{\sigma}_{3s}$  = minor principal effective stress during steady state of deformation
- $\bar{\sigma}_{3rf}$  = minor principal effective stress at start of rapid failure in CR test (see Fig. F105)
- $\bar{\sigma}_3$  = minor principal effective stress
- $\bar{\sigma}_{3c}$  = minor principal effective stress after consolidation
- $\bar{\sigma}_f$  = effective normal stress on failure plane
- $\bar{\sigma}_{fs}$  = effective normal stress on failure plane during steady state of deformation
- $\bar{\sigma}_v$  = vertical effective stress
- $\bar{\sigma}_o$  = octahedral effective stress; also contact stress between soil particles
- $\tau$  = shear stress on failure plane
- $\tau_d$  = driving shear stress on failure plane

TABLE 1 - SUMMARY OF VOID RATIO AND STEADY STATE STRENGTH DATA -  
 SAMPLES FROM ZONE 5 of HYDRAULIC FILL  
 GEI TEST DATA  
 Lower San Fernando Dam

Triaxial Test No.	Boring No. or Exploration Shaft(ES)	Elev. Top of Sample (ft)	Void Ratio, e					Steady State Strength, $S_{us}$ , tsf			
			After consoli- dation in lab, $e_c$	In tube, $e_t$	1985 In situ <sup>1)</sup> $e_{1985}$	1971 In situ $e_{1971}$		In lab at $e_c$	1985 In situ at $e_{1985}$	1971 In situ at $e_{1971}$	
						Downstream <sup>2)</sup>	Upstream <sup>3)</sup>			Downstream	Upstream
R̄1	ES	1014.0	0.667	0.716	0.713	0.745	0.756	2.36	0.87	0.43	0.34
R̄5	U111A	1010.8	0.590	0.654	0.657	0.689	0.700	4.01	1.06	0.52	0.41
R̄6	ES	1014.1	0.605	0.718	0.703	0.735	0.746	3.20	0.41	0.21	0.16
R̄7	ES	1013.1	0.636	0.699	0.674	0.706	0.717	2.60	1.15	0.59	0.47
R̄8	U103	1013.0	0.626	0.723	0.724	0.769	0.780	3.46	0.43	0.17	0.13
R̄12	ES	1012.4	0.589	0.653	0.618	0.649	0.660	6.66	4.30	2.50	1.97
R̄13	ES	1013.4	0.625	0.710	0.718	0.751	0.762	3.69	0.53	0.26	0.21
R̄14	U111A	1020.6	0.635	0.723	0.715	0.748	0.759	5.33	1.13	0.55	0.43
R̄15	U111A	1016.6	0.617	0.714	0.688	0.720	0.731	4.13	1.00	0.50	0.39
R̄16	U111A	1008.6	0.568	0.662	0.667	0.699	0.710	3.53	0.44	0.22	0.17
R̄17	U111A	1008.0	0.567	0.654	0.645	0.677	0.688	4.92	1.06	0.53	0.42
R̄18	U111	1007.4	0.560	0.653	0.654	0.686	0.697	4.56	0.69	0.34	0.27
R̄19	U103	1014.7	0.563	0.654	0.655	0.698	0.709	6.98	1.30	0.51	0.40
R̄20	U111A	1011.8	0.532	0.618	0.621	0.652	0.663	4.89	0.83	0.42	0.33
CRR̄1	ES	1013.7	0.578	0.702	0.694	0.726	0.737	6.16	0.65	0.32	0.25
CRR̄2	ES	1014.0	0.588	0.701	0.681	0.713	0.724	5.40	0.90	0.44	0.35

-----  
Field Density Tests

FD301	ES	1014.0	-	-	0.676	0.708	-	-	-	-	-
FD302	ES	1013.1	-	-	0.704	0.736	-	-	-	-	-
FD303	ES	1013.1	-	-	0.679	0.711	-	-	-	-	-
FD304	ES	1013.1	-	-	0.720	0.752	-	-	-	-	-
FD305	ES	1012.3	-	-	0.639	0.670	-	-	-	-	-

Notes:

- 1) Void ratio corrected for changes during sampling. Exploration shaft samples were also corrected for swell caused by excavation of shaft.
- 2) Based on estimated void ratio changes which occurred as a result of earthquake shaking and lowering of groundwater level (see Appendix C for method).
- 3) Based on downstream void ratio corrected for difference between upstream and downstream void ratio (see Appendix C for method).



TABLE 2 - SUMMARY OF VOID RATIO AND STEADY STATE STRENGTH DATA  
 SAMPLES FROM ZONE 5 OF HYDRAULIC FILL  
 STANFORD UNIVERSITY TEST DATA  
 Lower San Fernando Dam

Triaxial Test No.; Stanford No.	Boring No. or Exploration Shaft(ES)	Sample El. (ft)	Void Ratio, e					Steady State Strength, $S_{us}$ , tsf			
			After consolidation in lab <sup>1)</sup> , $e_c$	In Tube <sup>1)</sup> $e_t$	1985 In situ <sup>2)</sup> $e_{1985}$	1971 In situ $e_{1971}$		In lab at $e_c$	1985 In situ at $e_{1985}$	1971 In situ at $e_{1971}$	
						Downstream <sup>3)</sup>	Upstream <sup>4)</sup>			Downstream	Upstream
4	U111A	1013	0.578	0.608	0.600	0.631	0.642	2.37	1.48	0.76	0.60
7	U111	1017	0.665	0.717	0.718	0.751	0.762	2.68	0.86	0.42	0.33
16	U111	1012	0.515	0.603	0.635	0.666	0.677	2.68	0.20	0.10	0.08
28	U105	1019	0.797	0.849	0.870	0.905	0.916	1.07	0.22	0.10	0.08
50	ES	1013	0.651	0.705	0.691	0.724	0.735	2.48	1.05	0.51	0.41
51	ES	1013	0.630	0.697	0.682	0.714	0.725	2.32	0.76	0.38	0.30
52	ES	1012	0.664	0.734	0.727	0.760	0.771	2.59	0.67	0.33	0.26

**Notes:**

- 1) Data obtained from R. B. Seed et al, 1987.
- 2) Void ratio corrected for changes during sampling; data obtained from R. Seed et al, 1987. The void ratio of exploration shaft samples were corrected for swell using methods described in Section 4.2.1 of this report.
- 3) Based on estimated void ratio changes which occurred as a result of earthquake shaking and lowering of groundwater level (see Appendix C for method).
- 4) Based on downstream void ratio corrected for difference between upstream and downstream void ratio (see Appendix C for method).

Geotechnical Engineers Inc.

Project 85669  
 January 15, 1988

TABLE 3 - VOID RATIO CORRECTIONS APPLIED TO  
CRITICAL LAYER TUBE SAMPLES  
Lower San Fernando Dam

Page 1 of 2

Sample Triaxial Test No. GEI Tests	Boring No. or Exploration Shaft(ES)	Void Ratio Changes Between 1971 and 1985			Upstream/ Downstream Void Ratio Difference
		$\Delta e_1$	$\Delta e_2$	$\Delta e_3$	$\Delta e_4$
		(1)	(1)	(2)	(3)
$\bar{R}1$	ES	0.0260	0.0065	-0.0248	0.011
$\bar{R}5$	U111A	0.0254	0.0063	-	0.011
$\bar{R}6$	ES	0.0259	0.0064	-0.0224	0.011
$\bar{R}7$	ES	0.0254	0.0063	-0.0309	0.011
$\bar{R}8$	U103	0.0376	0.0069	-	0.011
$\bar{R}12$	ES	0.0247	0.0061	-0.0270	0.011
$\bar{R}13$	ES	0.0261	0.0065	-0.0306	0.011
$\bar{R}14$	U111A	0.0262	0.0065	-	0.011
$\bar{R}15$	U111A	0.0258	0.0064	-	0.011
$\bar{R}16$	U111A	0.0255	0.0063	-	0.011
$\bar{R}17$	U111A	0.0252	0.0063	-	0.011
$\bar{R}18$	U111	0.0253	0.0063	-	0.011
$\bar{R}19$	U103	0.0361	0.0066	-	0.011
$\bar{R}20$	U111A	0.0248	0.0062	-	0.011
$\overline{CRR}1$	ES	0.0258	0.0064	-0.0284	0.011
$\overline{CRR}2$	ES	0.0256	0.0064	-0.0259	0.011

Notes: see page 2.

Geotechnical Engineers Inc.

Project 85669  
January 15, 1988

TABLE 3 - VOID RATIO CORRECTIONS APPLIED TO  
CRITICAL LAYER TUBE SAMPLES  
Lower San Fernando Dam

Page 2 of 2

Sample Triaxial Test No. Stanford Tests	Boring No. or Exploration Shaft(ES)	Void Ratio Changes Between 1971 and 1985			Upstream/ Downstream Void Ratio Difference
		$\Delta e_1$	$\Delta e_2$	$\Delta e_3$	$\Delta e_4$
		(1)	(1)	(2)	(3)
4	U111A	0.0246	0.0061	-	0.011
7	U111	0.0263	0.0065	-	0.011
16	U111	0.0246	0.0061	-	0.011
28	U105	0.0283	0.0070	-	0.011
50	ES	0.0261	0.0065	-0.0276	0.011
51	ES	0.0260	0.0064	-0.0262	0.011
52	ES	0.0266	0.0066	-0.0298	0.011

Notes:

1)  $\Delta e_1$  - Estimated reduction in in situ void ratio due to cyclic straining during 1971 earthquake.

$\Delta e_2$  - Estimated reduction in in situ void ratio due to lowering of groundwater level after 1971 earthquake.

See Appendix C for a description of analyses performed to estimate  $\Delta e_1$  and  $\Delta e_2$ .

2)  $\Delta e_3$  - Estimated increase in in situ void ratio immediately prior to sampling, caused by unloading at the base of the exploration shaft.

The negative values for  $\Delta e_3$  indicate swelling. See Section 4.2.1 of main text for method used to estimate  $\Delta e_3$ .

3)  $\Delta e_4$  - Estimated amount by which void ratio was higher on upstream side of dam compared to downstream side due to effect of prolonged submergence of upstream slope and additional loading of downstream slope by berms. See Section C.6 for description of analyses performed to estimated  $\Delta e_4$ .

TABLE 4 - NUMBER OF TESTS PERFORMED TO DEFINE  
STEADY STATE LINE OF CRITICAL LAYER SOIL  
Lower San Fernando Dam

	$\bar{R}$		S	
	Isotropic	Anisotropic	Isotropic	Anisotropic
COMPACTED MOIST				
Lubricated End	8	3	2	-
Conventional End	-	2	-	-
SLURRY				
Lubricated End	2	-	-	-
Conventional End	-	-	-	-

Definitions:

$\bar{R}$  - Consolidated undrained monotonically loaded triaxial test

S - Consolidated drained monotonically loaded triaxial test

Isotropic - Sample consolidated isotropically; refer to Appendix F, Section F.4.4

Anisotropic - Sample consolidated anisotropically: refer to Appendix F, Section F.4.5

Compacted Moist - Sample prepared in layers of moist soil

Slurry - Sample placed as a slurry

Lubricated End - Top and bottom platens were lubricated and height to diameter ratio of sample was typically 1.3

Conventional End - Top and bottom platens were not lubricated and height to diameter ratio of sample was typically 2.0

TABLE 5 - SUMMARY OF LIQUEFACTION SUSCEPTIBILITY ANALYSES OF  
UPSTREAM HYDRAULIC FILL ZONES 2 AND 3  
Lower San Fernando Dam

Hydraulic Fill Zone	Triaxial Test	Boring No. or Exploration Shaft(ES)	Elevation Top of Sample <sup>1)</sup> ft	In Situ $e_{1985}$ <sup>2)</sup>	In Situ $e_{1971}$ <sup>3)</sup>	SSL - Batch Mix No. <sup>4)</sup>	1971 $S_{us}$ <sup>5)</sup>	1971 $\tau_d$ <sup>6)</sup>	$F_L$ <sup>7)</sup>
							tsf	tsf	
2	R3	ES	1041.1	0.721	0.746	7	2.9	0.41	7.1
	R4	ES	1044.3	0.772	0.797	3	>0.34	0.41	>0.83
	R11	ES	1044.3	0.694	0.719	3	2.2	0.41	>5.4
	CRR3	ES	1042.4	0.569	0.593	3	>2.2	0.41	>5.4
	CRR5	U111	1036.7	0.557	0.582	3	1.5	0.42	3.6
3	R2	ES	1032.5	0.702	0.726	7	5.1	0.43	11.8
	R10	ES	1032.5	0.774	0.798	7	0.74	0.43	1.72
	CRR4 <sup>8)</sup>	U111A	1030.7	0.798	0.822	7	0.32	0.43	0.74 <sup>8)</sup>

Notes:

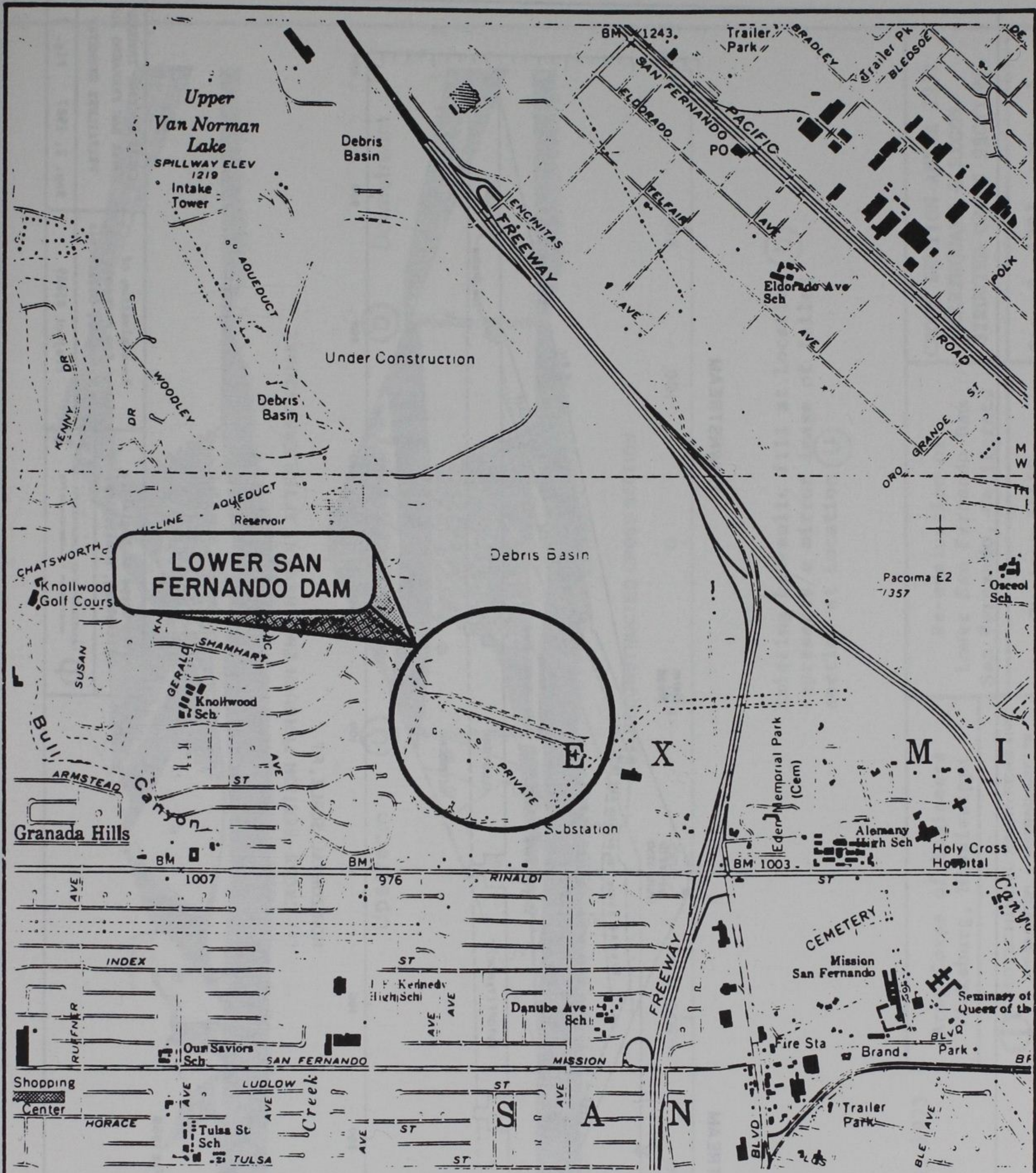
- 1) Elevation datum is NGVD.
- 2) Void ratios of tube samples obtained from Zones 2 and 3 of the exploration shaft were corrected for swelling of the base of the shaft. The method described in Section 4.2.1 was used to estimate  $\Delta e$  due to swell, except that the effective stress after excavation was computed using the following equation for partially saturated particles (Wilun et al, 1972):
 
$$\bar{\sigma}_o = \frac{\sigma_{st}}{d}$$
 where  $\bar{\sigma}_o$  = contact stress between particles caused by meniscus  
 $\sigma_{st}$  = surface tension of water (0.0050 lb/ft)  
 $d$  = diameter of particle; assumed to be  $D_{10}$  for computations
- 3) Estimated void ratio of specimen prior to 1971 failure; based on analysis of void ratio changes which took place between 1971 and 1985 and estimated difference in void ratio between upstream and downstream shells. See Appendix C for method.
- 4) Steady state line of Batch Mix number used to estimate 1971  $S_{us}$ . The steady state line of Batch Mix 3 is that in R. B. Seed et al, 1987. The selection of SSL to use was based on a similarity between grain size curves of the undisturbed sample and grain size curves of Batch Mixes 3 or 7.
- 5) Estimated undrained steady state strength of sample prior to 1971 failure based on upstream void ratio.
- 6) Computed driving shear stress in upstream hydraulic fill at elevation of sample.
- 7) Factor of safety against liquefaction susceptibility.
- 8) This specimen contained a clayey silt layer at the top and fine sand at the bottom. The specimen failed through the upper clayey silt. It is unlikely that the thin clayey silt layer extends over great lateral extent in the dam. Therefore, the  $F_L$  of the larger mass of Zone 3 is expected to be greater than 0.74.

TABLE 6 - SUMMARY OF MOST SIGNIFICANT EARTHQUAKES IN THE  
SAN FERNANDO VALLEY AREA  
Low San Fernando Dam

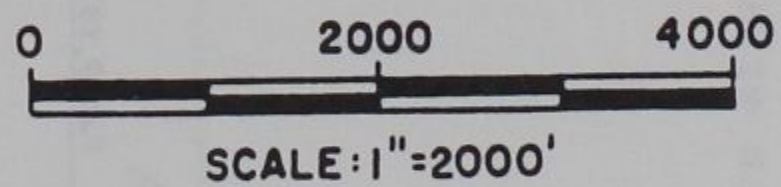
Earthquake Date <sup>1)</sup>	Data from NGDC/NOAA Records <sup>2)</sup>			
	Distance from Dam Site to Epicenter (miles)	Maximum Intensity <sup>3)</sup>	Magnitude	Estimated Maximum Acceleration at Lower San Fernando Dam <sup>4)</sup> g
1919, February 16	58	VII	N R	-
1920, June 21	22	VIII	4.9	<0.01
1925, June 29	76	X	6.25	0-0.03
1926, February 18	61	VI	N R	-
1927, November 4	>125	-	[7.5]	0-0.03
1930, August 30	27 <sup>5)</sup>	VI	5.25	0-0.02 <sup>5)</sup>
1931, April 4	[8]	-	(4)	[ 0.04]
1933, March 10	55	IX	6.3	0-0.07
1952, July 21	58	XI	7.7	0.05-0.12
1952, August 22	74	VIII	5.8	0-0.02
1952, August 23	23	VI	5.0	0-0.02
1954, January 12	58	VII	5.9	0.01-0.05
1956, February 7	22	VI	4.6	[ 0.02]
1964, February 8	[8]	-	[3.7]	[ 0.03]
1964, August 30	2.5	V	4	[ 0.05]
1965, July 16	14	VI	4	[ 0.02]
1971, February 9	9 <sup>6)</sup>	XI	6.5	0.55-0.60 <sup>7)</sup>


Notes:

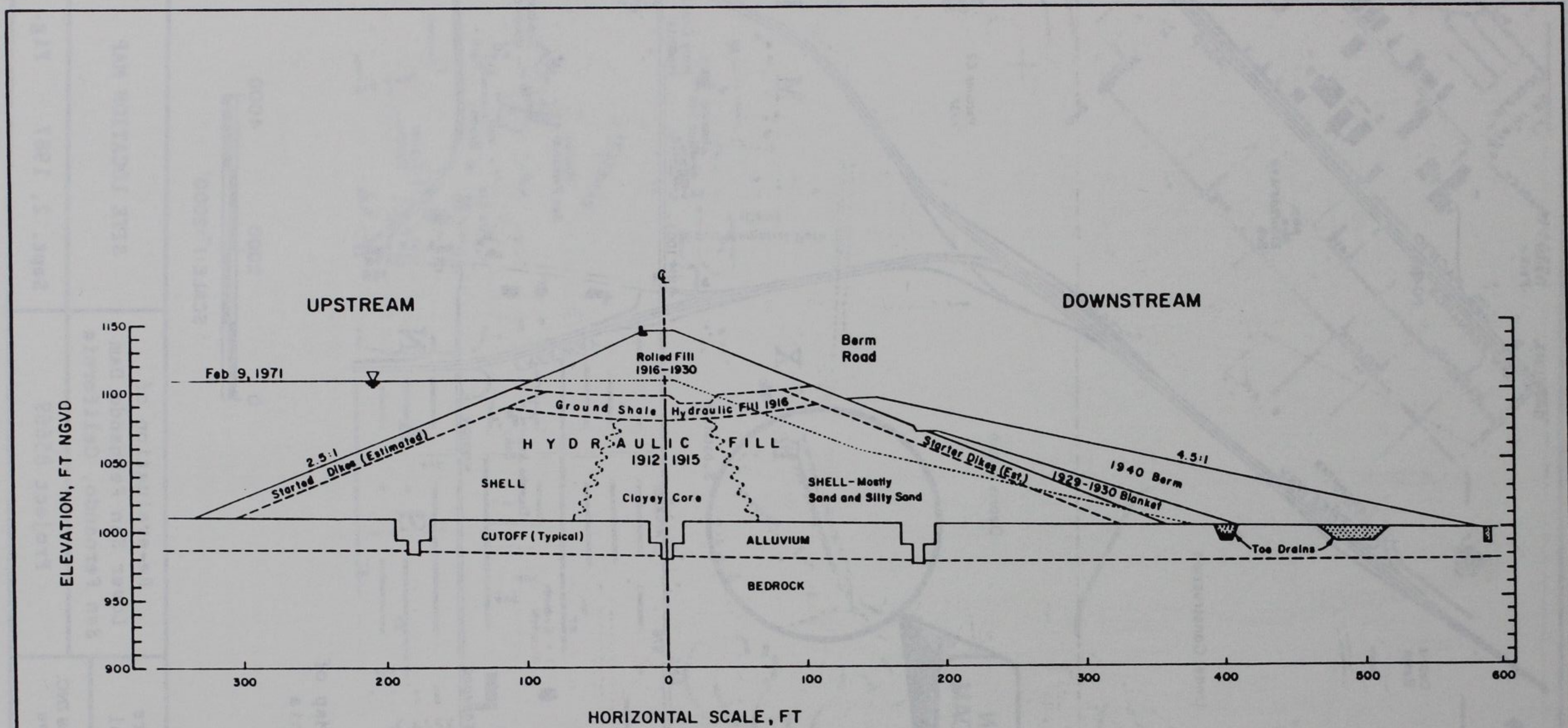
- 1) Significant pre-1971 earthquakes in the San Fernando earthquake area listed by Richter (1973), starting from the end of dam construction.
- 2) Data from the National Geophysical Data Center/National Oceanic and Atmospheric Administration earthquake data file. Values in brackets taken from Richter (1973) because information not provided by NGDC/NOAA. N R indicates no record.
- 3) Maximum Intensity is Modified Mercalli Scale of 1931.
- 4) Maximum accelerations at dam site estimated from attenuation curves presented by Schnabel, et al (1973), except for 1971 earthquake. The distance from causative fault to dam site was taken to be the distance between the epicenter location and dam site. Values in brackets for low magnitude earthquakes are based on Gutenberg and Richter (1956) relationships for California earthquakes.
- 5) Richter (1973) indicates that there are questions about the location of the epicenter for this earthquake and that it may have originated in Chatsworth (closer to the Lower San Fernando Dam). If the earthquake were located in Chatsworth, the estimated maximum acceleration at the dam site would range from 0.02 to 0.09 g.
- 6) The fault trace was closer to the dam site than the epicenter.
- 7) Maximum accelerations at the dam site based on the interpretation of seismoscope record from rock abutment (Seed, 1973).




From USGS Quadrangle Map of San Fernando, California  
 Photo revised 1972  
 (Post 1971 Failure)



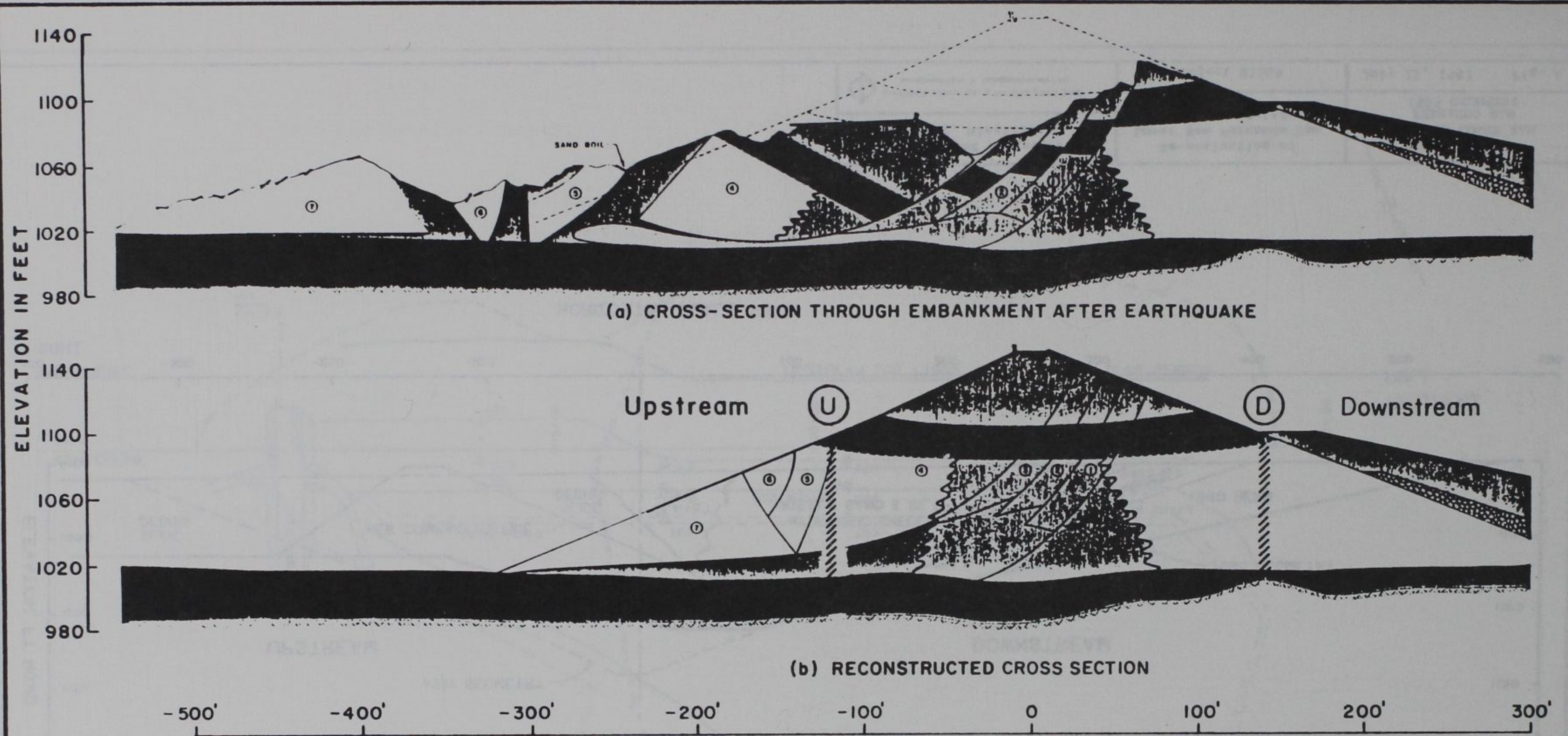
Army Corps of Engineers Vicksburg, Mississippi	Re-evaluation of Lower San Fernando Dam San Fernando, California	SITE LOCATION MAP
 GEOTECHNICAL ENGINEERS INC. WINCHESTER • MASSACHUSETTS	Project 85669	Sept. 2, 1987      Fig. 1



Based, in part, on  
LADWP Drawing, Feb 1969.

Army Corps of Engineers Vicksburg, Mississippi	Re-evaluation of Lower San Fernando Dam San Fernando, California	CROSS SECTION THROUGH LOWER SAN FERNANDO DAM PREFAILURE GEOMETRY
 GEOTECHNICAL ENGINEERS INC. WINCHESTER • MASSACHUSETTS	Project 85669	Sep. 2, 1987 Fig. 2





Existing hydraulic fill at Location (D) represents a mirror image of failed section at Location (U)

Cross section after Seed, 1973

Army Corps of Engineers  
Vicksburg, Mississippi

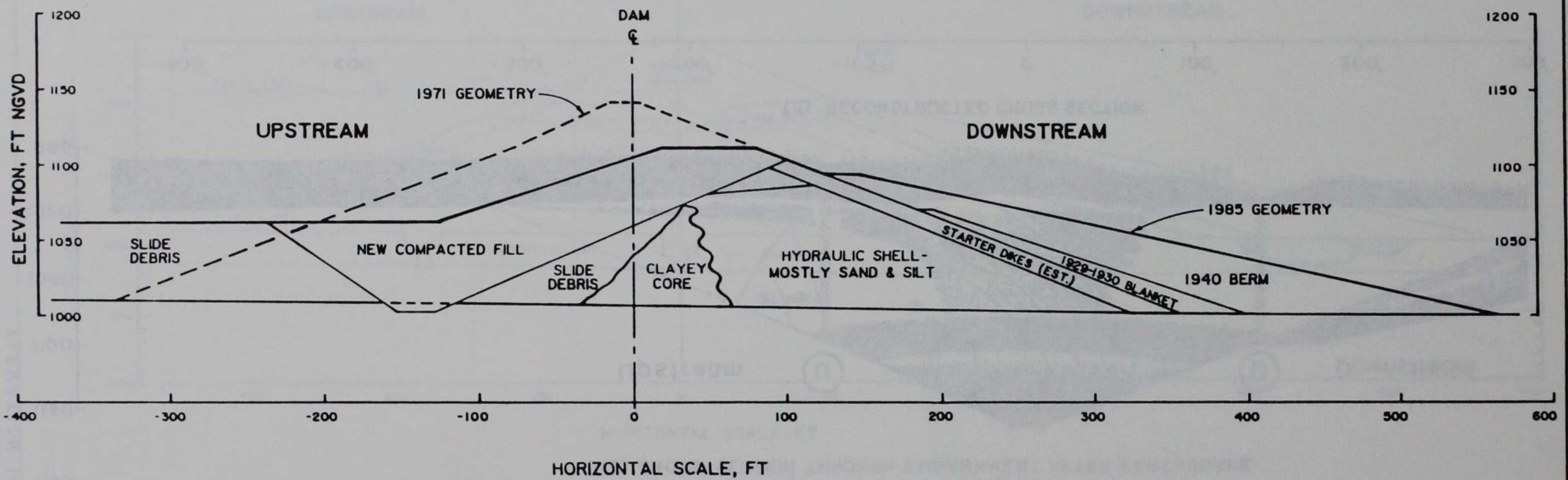
$\Phi$  GEOTECHNICAL ENGINEERS INC.  
WINDHESTER • MASSACHUSETTS


Re-evaluation of  
Lower San Fernando Dam  
San Fernando, California

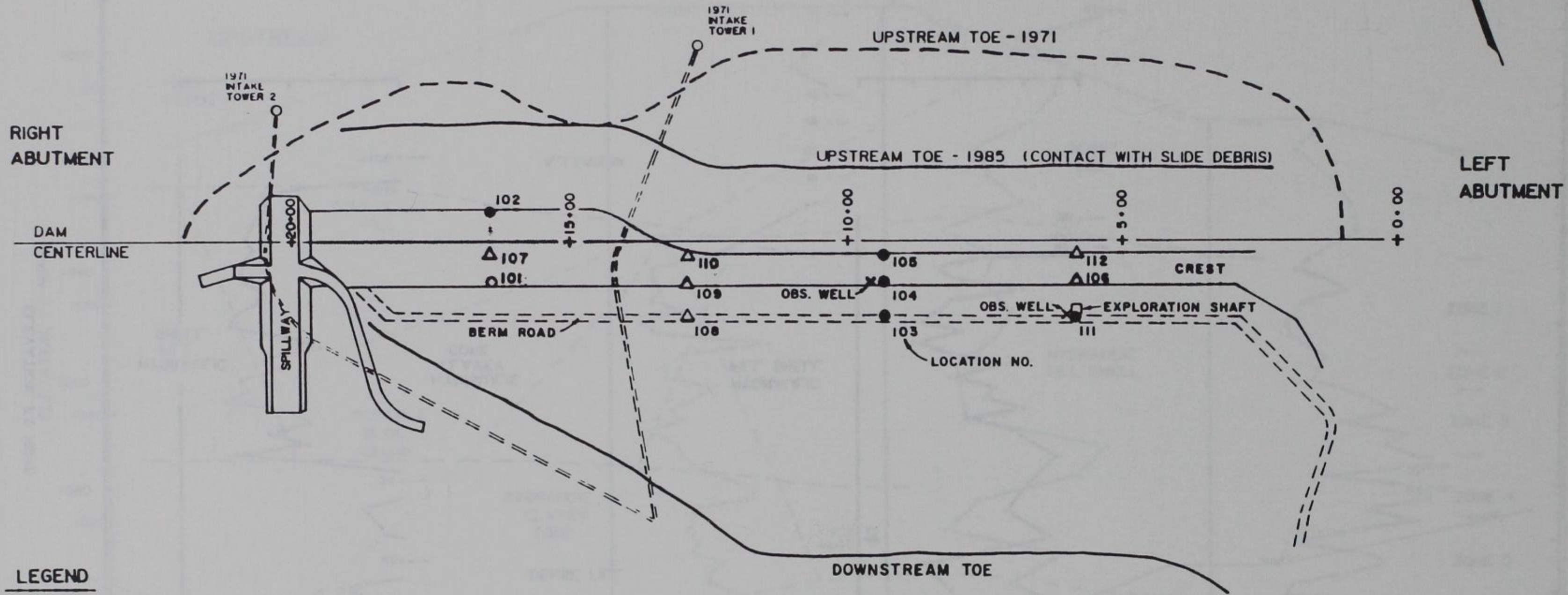
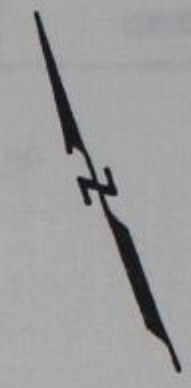
Project 85669

CROSS SECTION AFTER 1971  
EARTHQUAKE & RECON-  
STRUCTED CROSS SECTION

Sep. 2, 1987 Fig. 3



Army Corps of Engineers Vicksburg, Mississippi	Re-evaluation of Lower San Fernando Dam San Fernando, California	CROSS SECTION THROUGH LOWER SAN FERNANDO DAM 1985 GEOMETRY
 GEOTECHNICAL ENGINEERS INC. WINDHAM, MASSACHUSETTS	Project 85669	July 21, 1987 Fig. 4

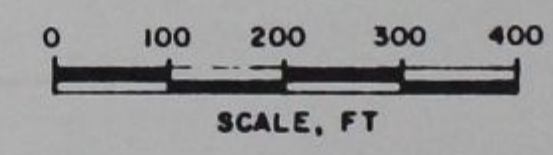



**LEGEND**

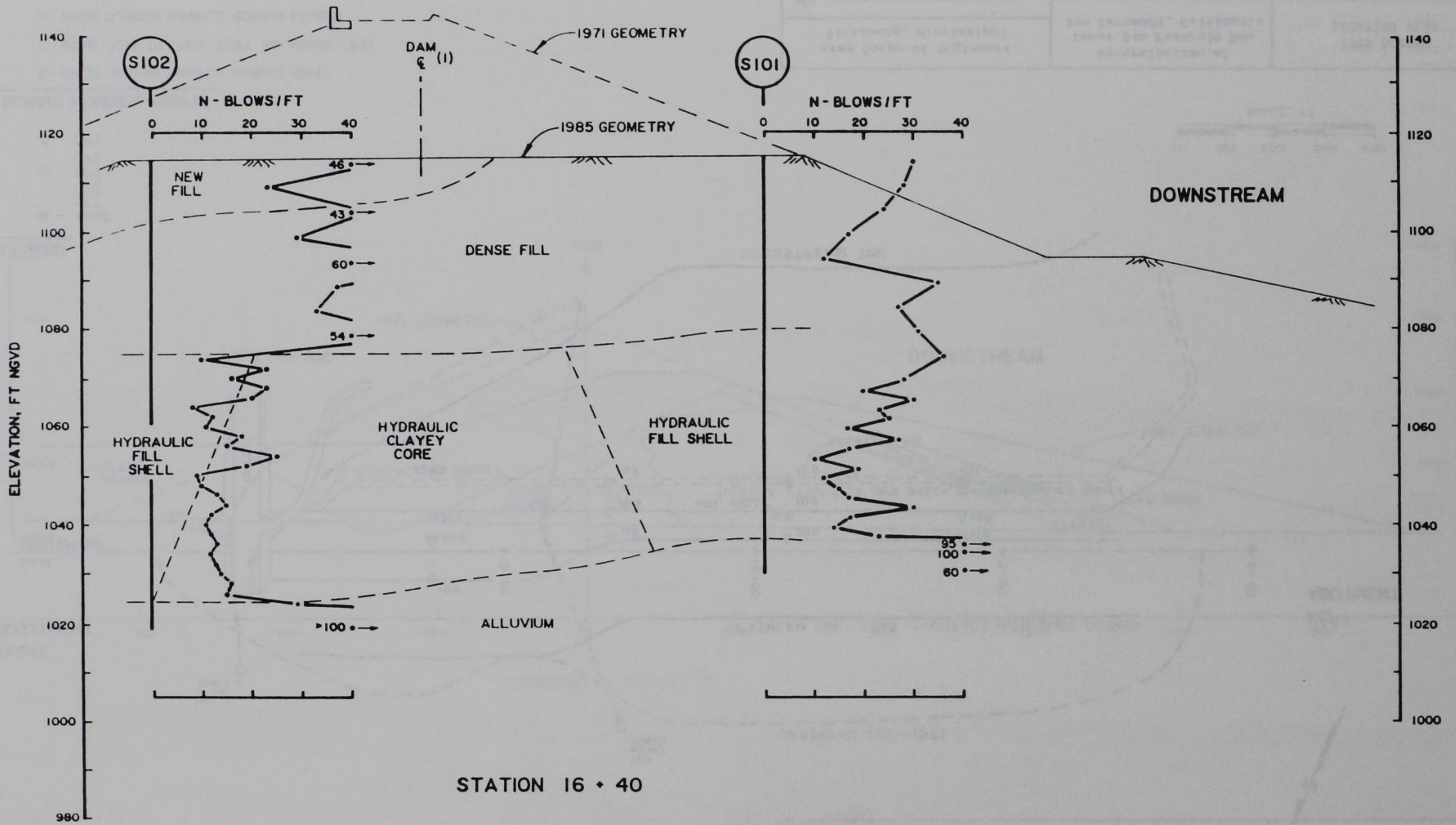
- - TUBE  
SPT  
CPT
- - SPT  
CPT
- Δ - CPT

**BORING NUMBER PREFIX**


- S - SPLIT SPOON SAMPLE BORING (SPT)
- C - CONE PENETRATION TEST SOUNDING (CPT)
- U - UNDISTURBED SAMPLE BORING (TUBE)

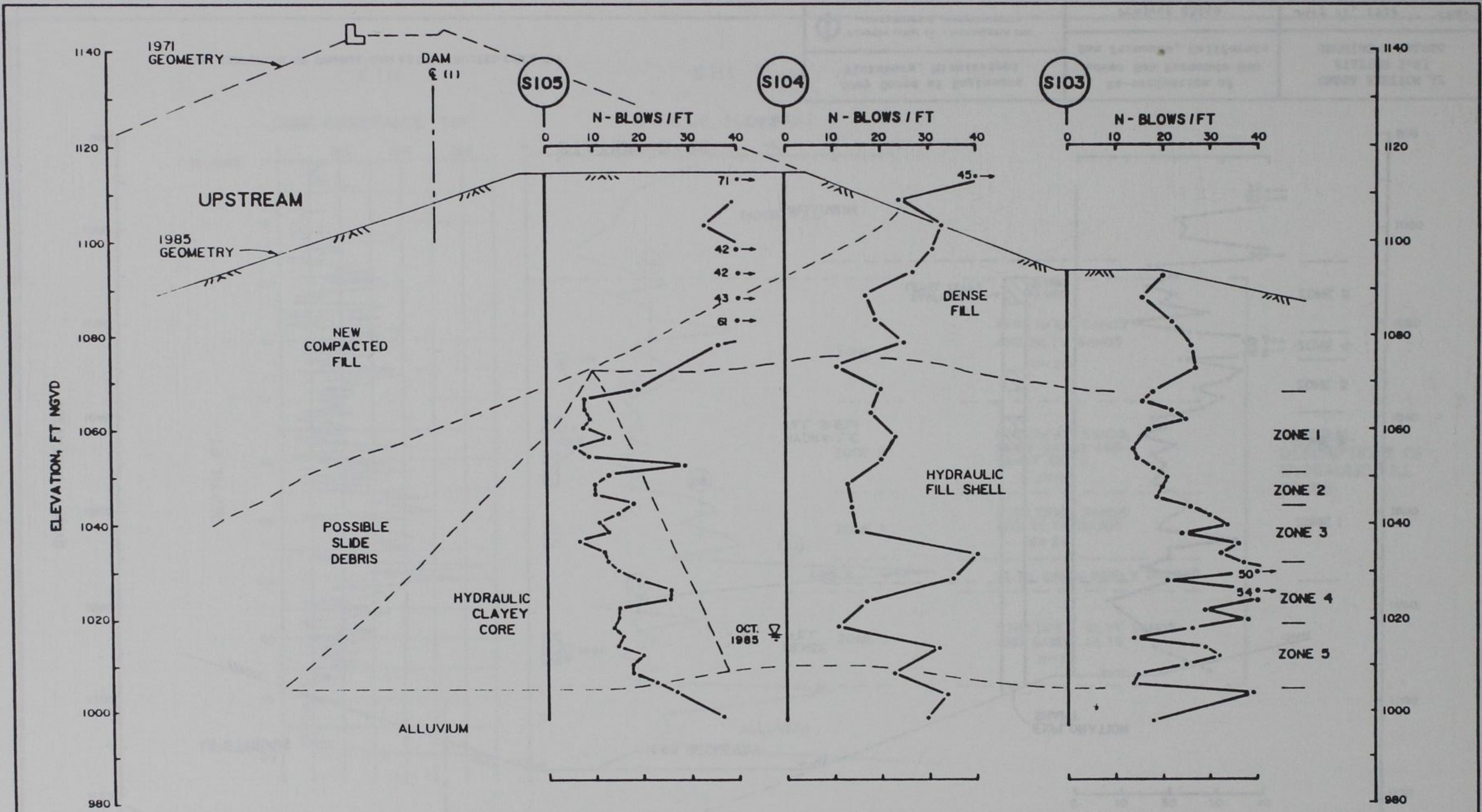


Army Corps of Engineers Vicksburg, Mississippi	Re-evaluation of Lower San Fernando Dam San Fernando, California	1985 BORING LOCATION PLAN
 GEOTECHNICAL ENGINEERS INC. WINDLESTER • MASSACHUSETTS	Project 85669	July 6, 1987      Fig. 5




(1) CENTERLINE OF ORIGINAL DAM AS CONSTRUCTED CIRCA 1917

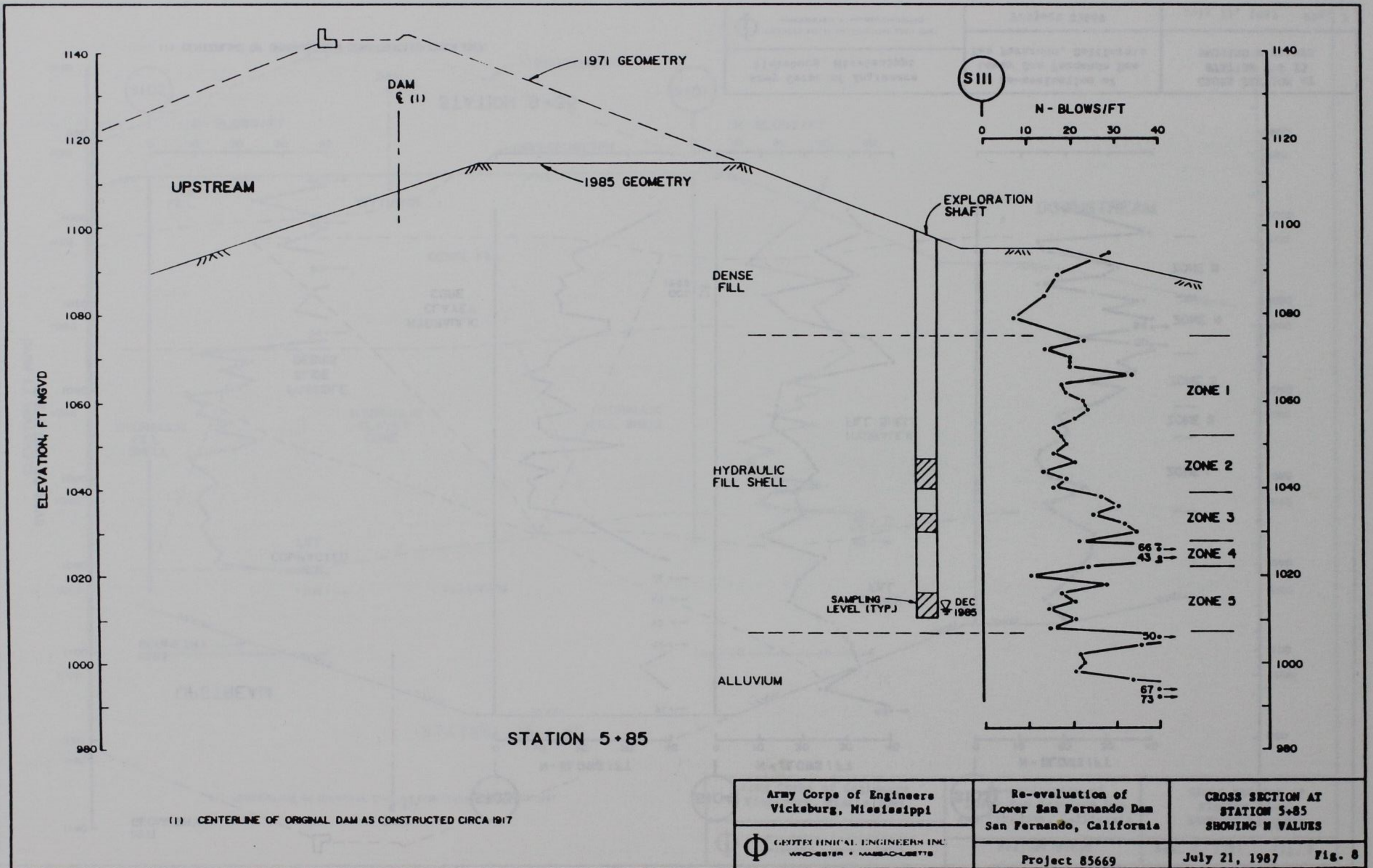
Army Corps of Engineers Vicksburg, Mississippi	Re-evaluation of Lower San Fernando Dam San Fernando, California	CROSS SECTION AT STATION 16+40 SHOWING N-VALUES
 GEOTECHNICAL ENGINEERS INC. WASHINGTON • MASSACHUSETTS	Project 85669	Sep. 2, 1987 Fig. 6

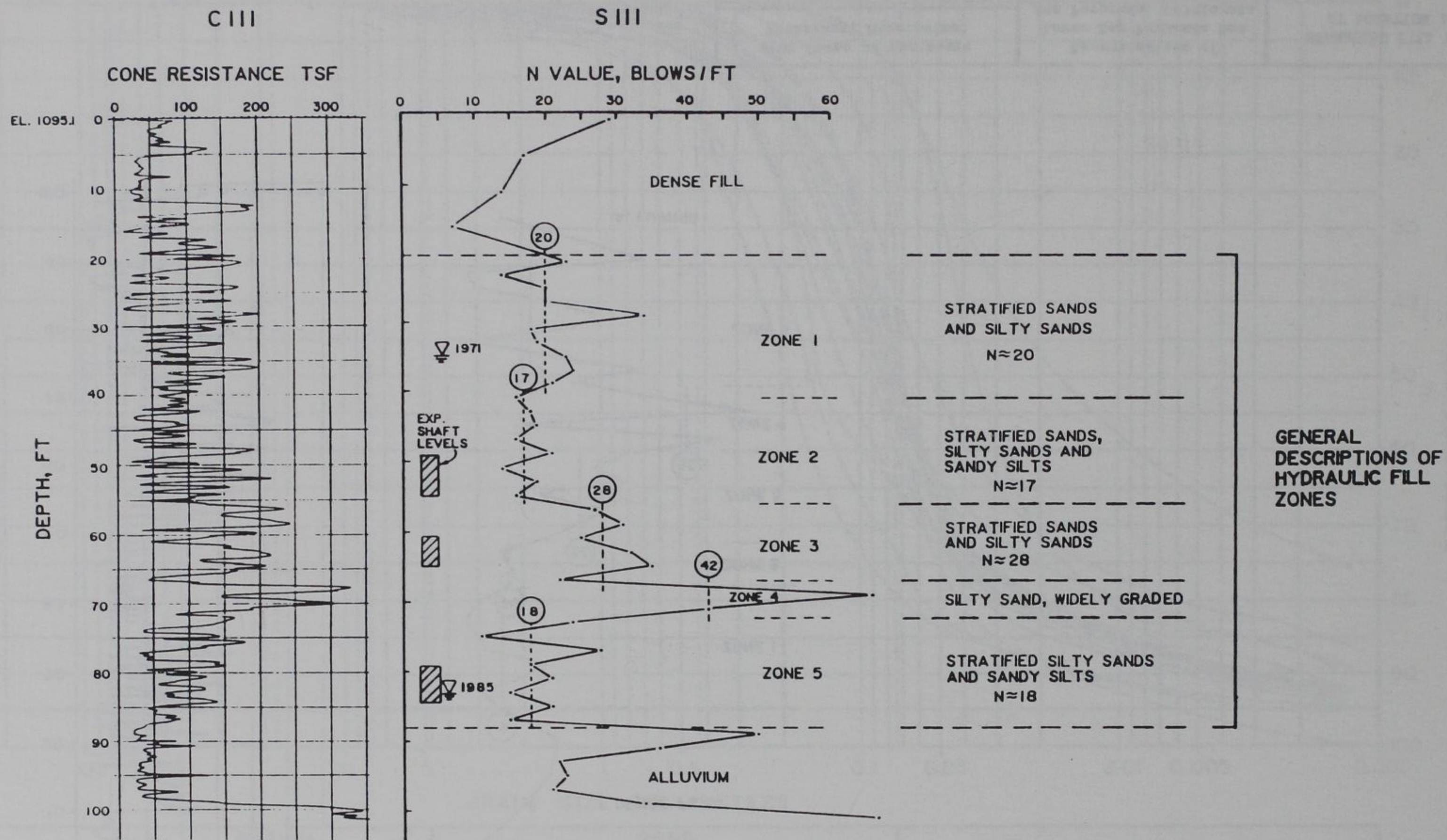


(1) CENTERLINE OF ORIGINAL DAM CONSTRUCTED CIRCA 1917.

STATION 9+35

Army Corps of Engineers Vicksburg, Mississippi	Re-evaluation of Lower San Fernando Dam San Fernando, California	CROSS SECTION AT STATION 9 + 35 SHOWING N VALUES
 GEOTECHNICAL ENGINEERS INC. WOODRIDGE • MASSACHUSETTS	Project 85669	July 21, 1987 Fig. 7





Army Corps of Engineers  
Vicksburg, Mississippi

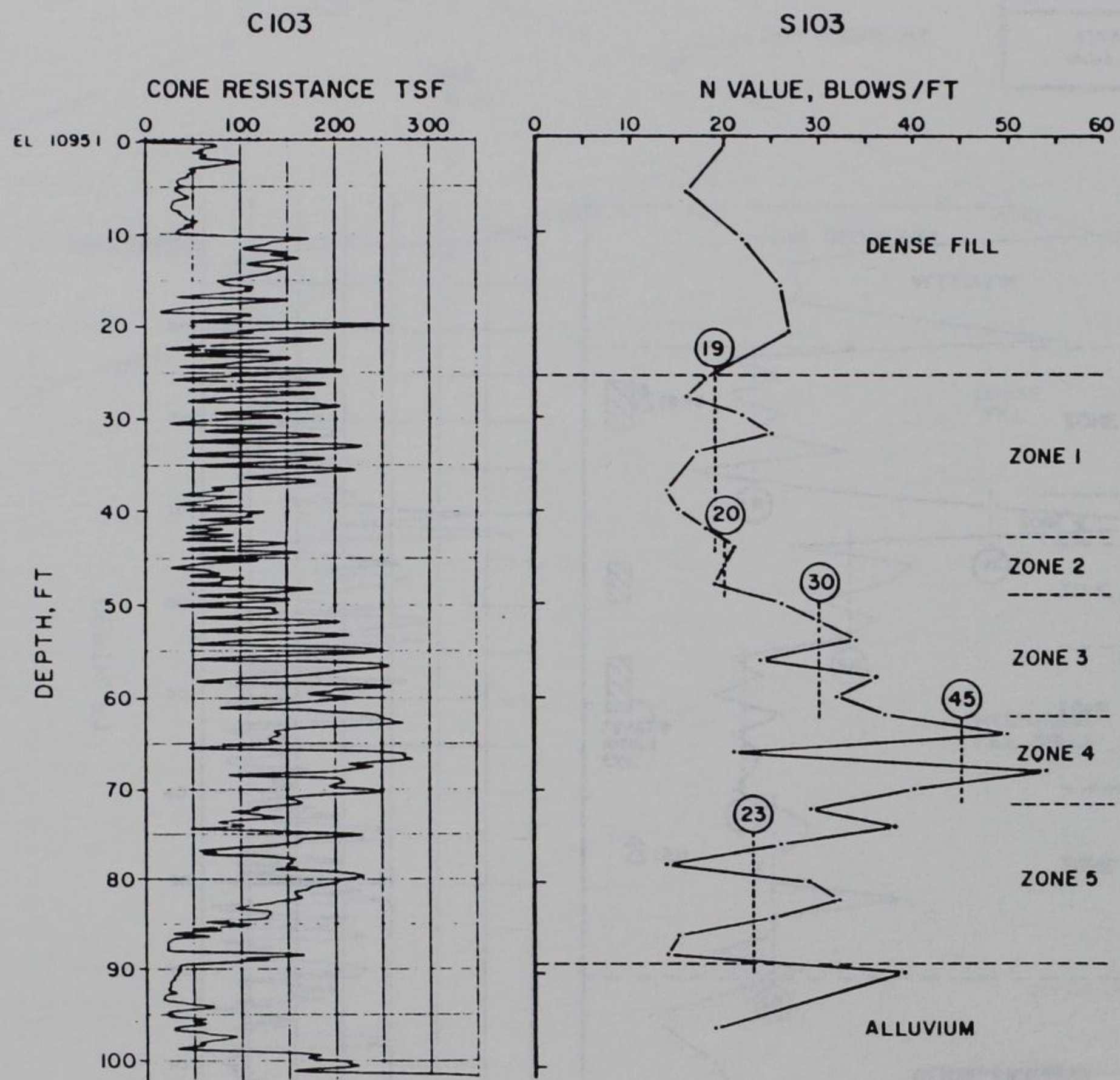
Re-evaluation of  
Lower San Fernando Dam  
San Fernando, California


HYDRAULIC FILL  
ZONES AT  
LOCATION III

GEOTECHNICAL ENGINEERS INC.  
WROXETER • MASSACHUSETTS

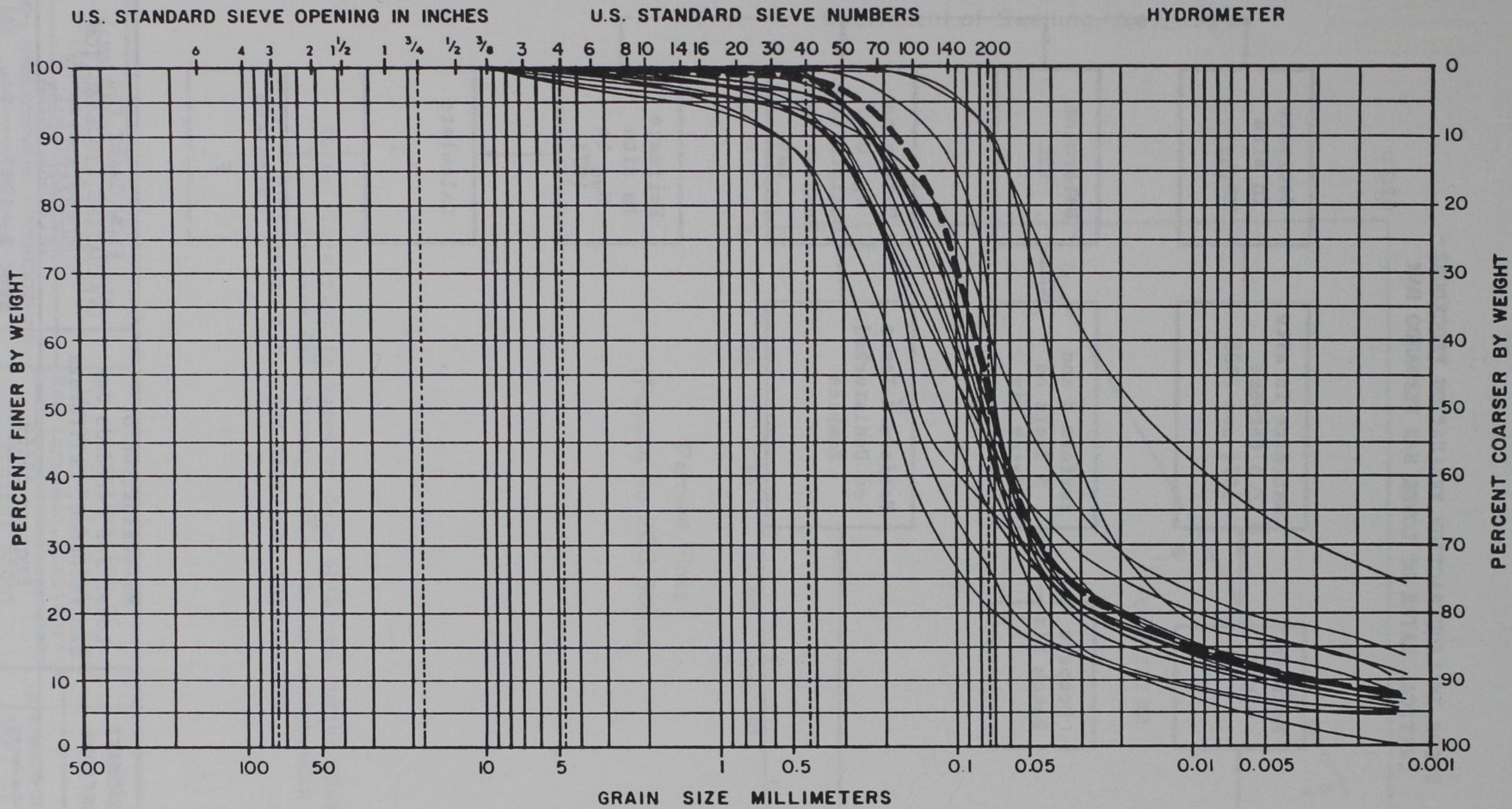
Project 85669

July 21, 1987 Fig. 9



Army Corps of Engineers Vicksburg, Mississippi	Re-evaluation of Lower San Fernando Dam San Fernando, California	HYDRAULIC FILL ZONES AT LOCATION 103
 GEOTECHNICAL ENGINEERS INC. WINDHAM, MASSACHUSETTS	Project 85669	Sep. 2, 1987 Fig. 10






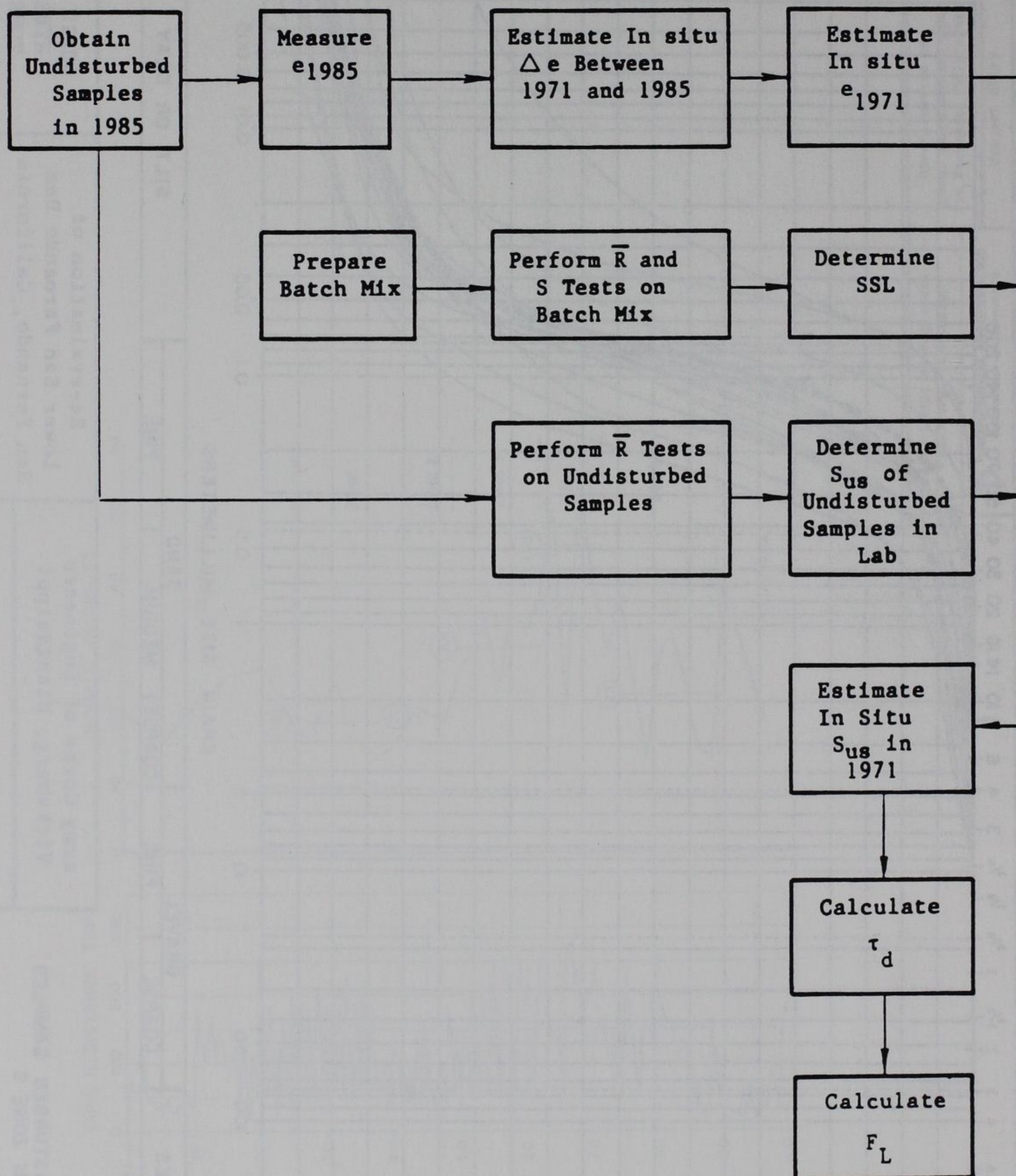
COBBLES	GRAVEL		SAND			SILT OR CLAY
	COARSE	FINE	COARSE	MEDIUM	FINE	

**LEGEND**

- UNDISTURBED SAMPLES FROM ZONE 5
- BATCH MIX NO. 7

Army Corps of Engineers Vicksburg, Mississippi	Re-evaluation of Lower San Fernando Dam San Fernando, California	GRAIN SIZE CURVES HYDRAULIC FILL ZONE 5 SAMPLES
 GEOTECHNICAL ENGINEERS INC. WINCHESTER • MASSACHUSETTS	Project 85669	Sept. 2, 1987      Fig. 11

STEPS IN LIQUEFACTION EVALUATION PROCEDURE -  
CRITICAL LAYER OF LOWER SAN FERNANDO DAM



Army Corps of Engineers  
Vicksburg, Mississippi

Re-evaluation of  
Lower San Fernando Dam  
San Fernando, California

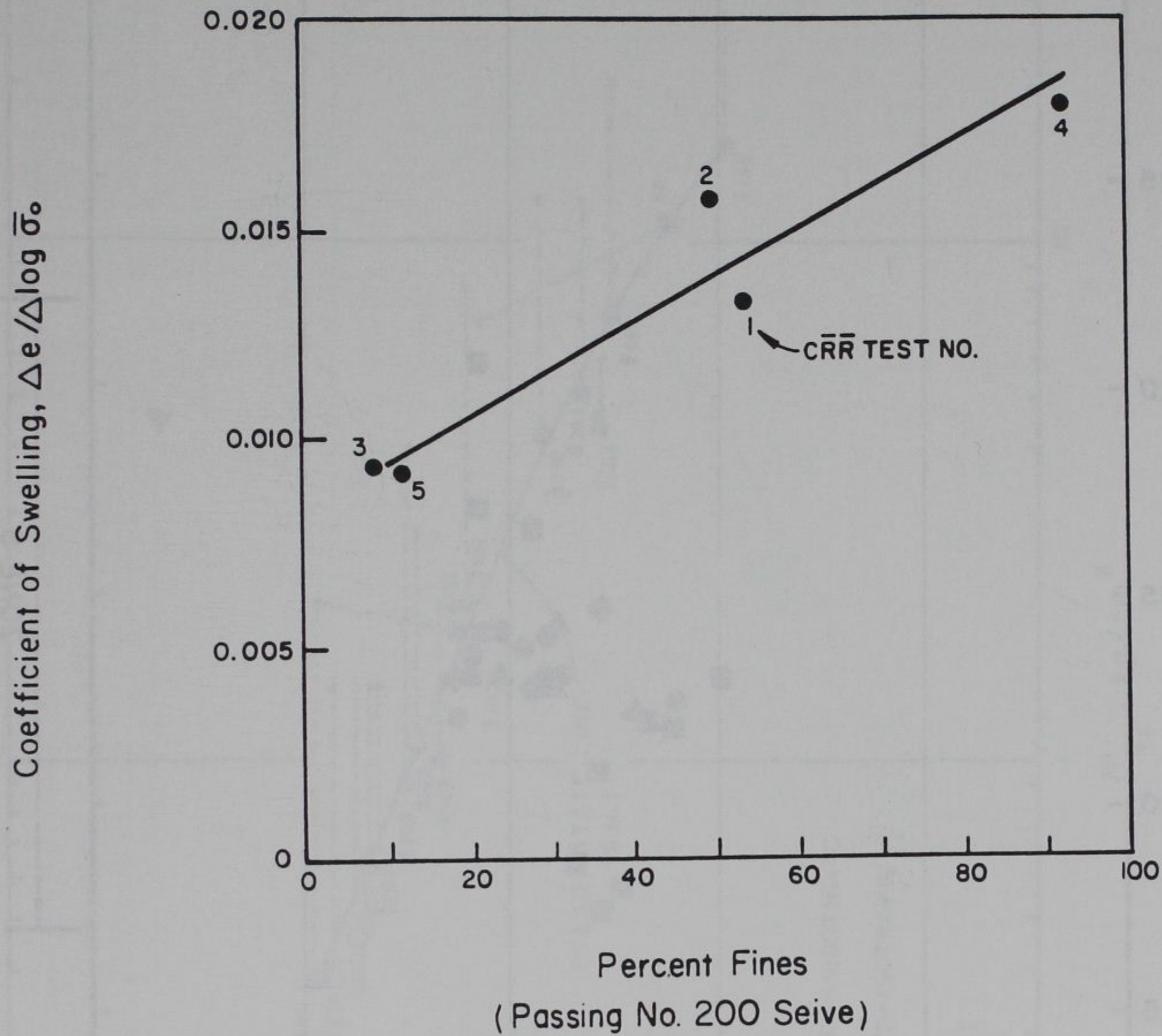
FLOW CHART FOR  
EVALUATING LIQUEFACTION  
SUSCEPTIBILITY OF  
CRITICAL LAYER



GEOTECHNICAL ENGINEERS INC.  
WINCHESTER • MASSACHUSETTS

Project 85669

Sep. 2, 1987 Fig. 12



**Note:** This plot is based on data obtained during Phase e of Tests CRR1 through CRR5. Refer to Appendix F, Section F.4.7 and Figs. F94 through F98.

Army Corps of Engineers  
Vicksburg, Mississippi

Re-evaluation of  
Lower San Fernando Dam  
San Fernando, California

COEFFICIENT OF SWELLING  
VS. INITIAL VOID RATIO

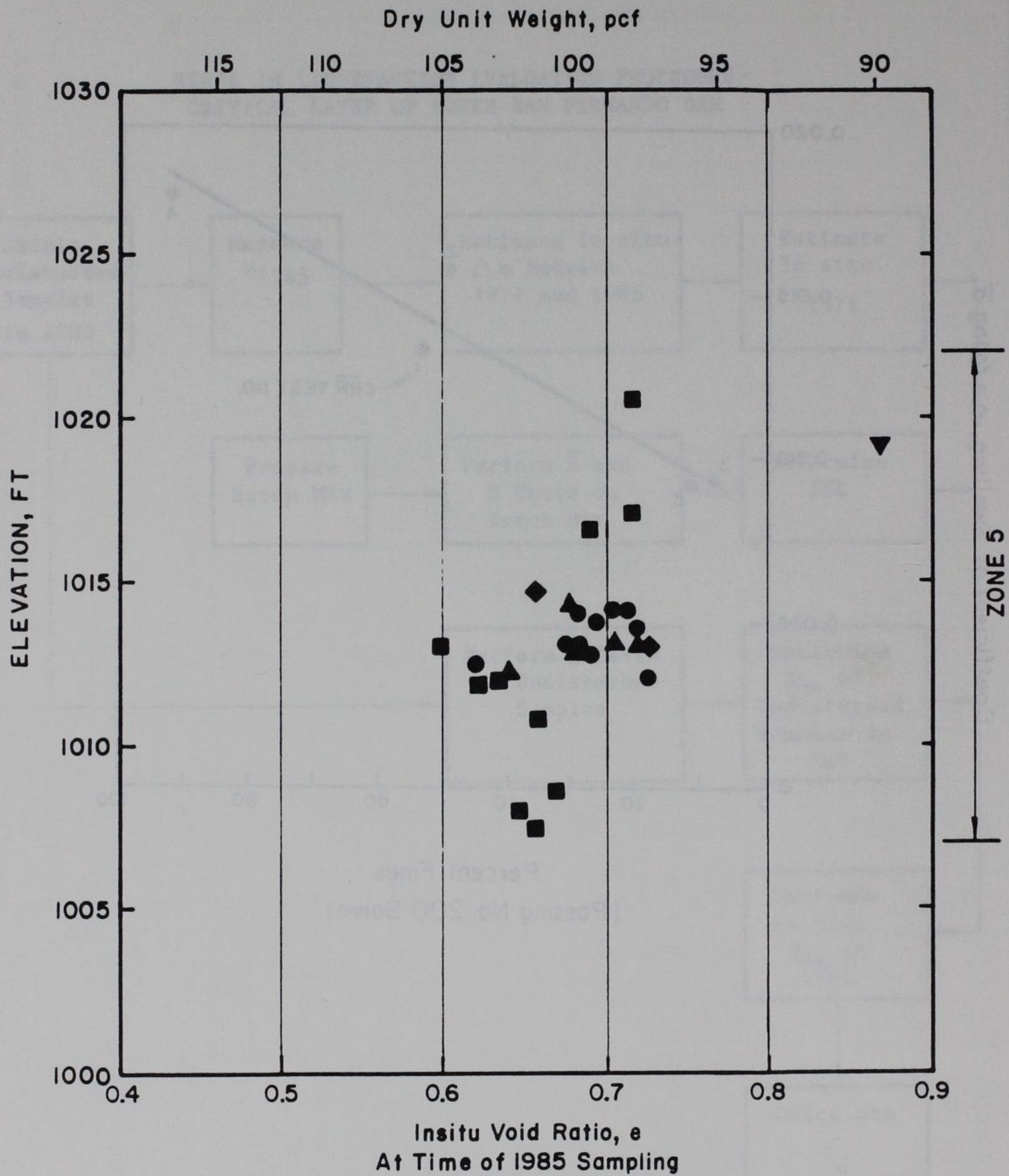


GEOTECHNICAL ENGINEERS INC.  
WINCHESTER • MASSACHUSETTS

Project 85669

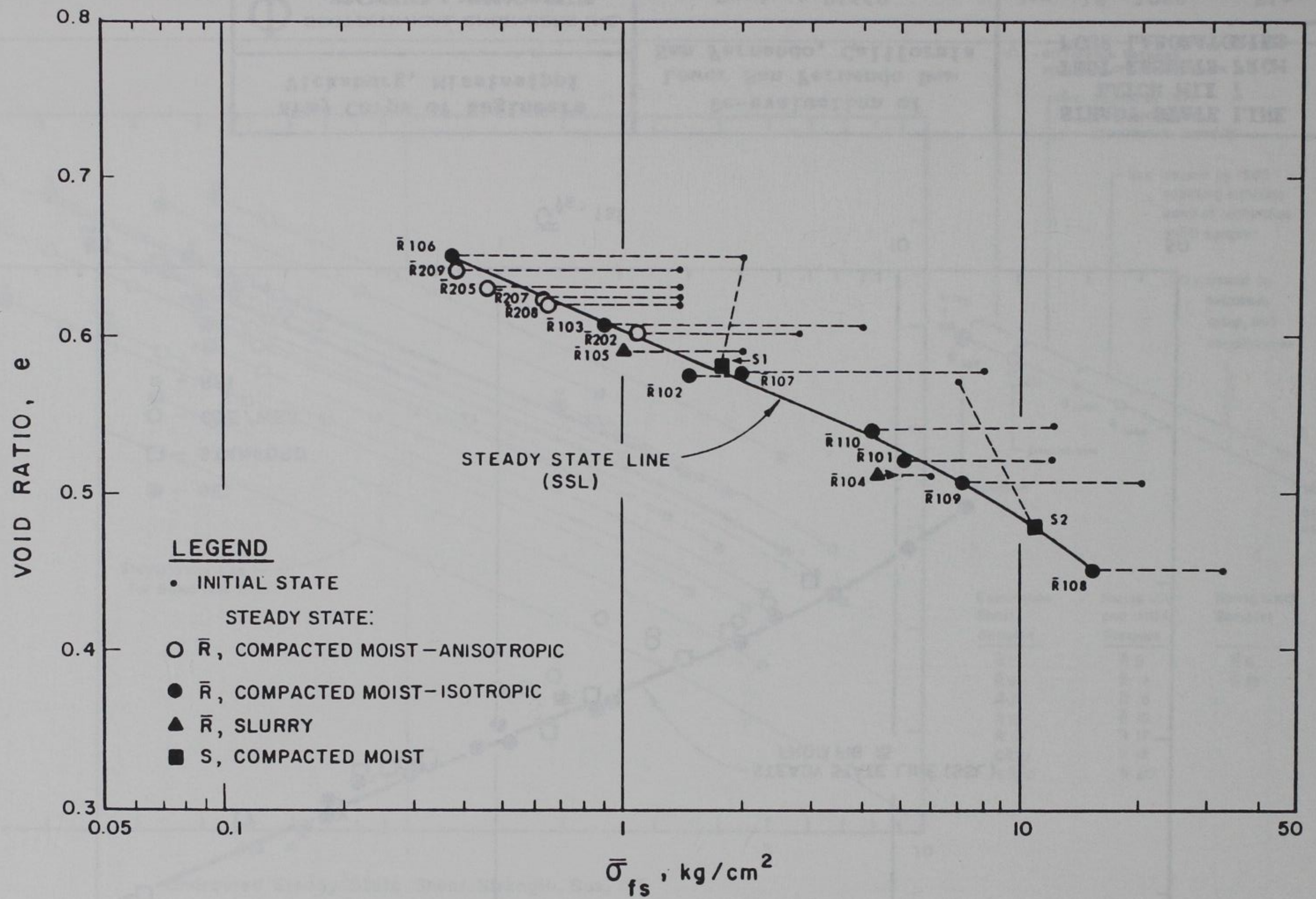
Sep. 2, 1987


Fig. 13

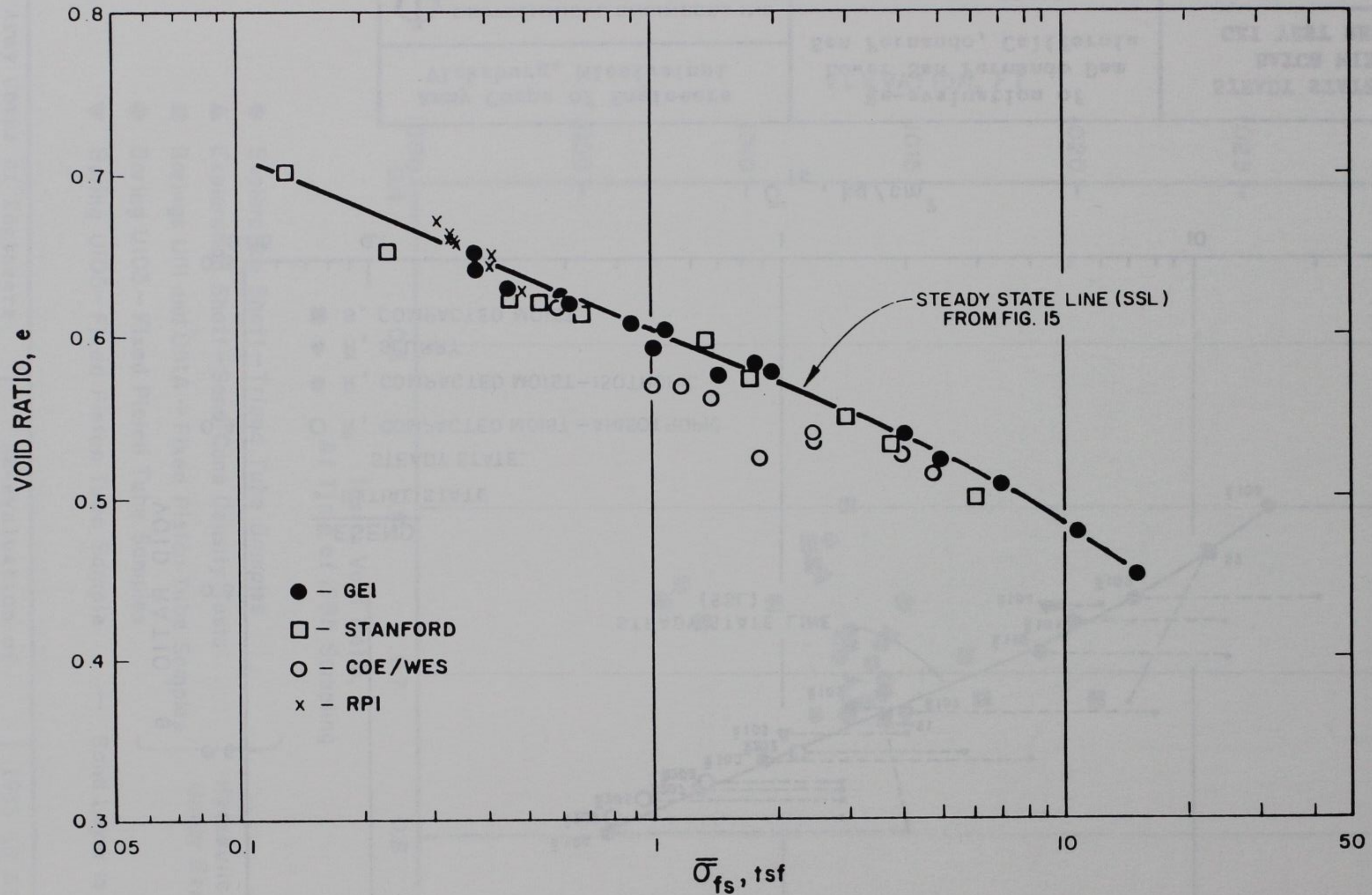


- Exploration Shaft-Tripod Tube Samples
  - ▲ Exploration Shaft-Sand Cone Density Tests
  - Borings U111 and U111A - Fixed Piston Tube Samples
  - ◆ Boring U103 - Fixed Piston Tube Samples
  - ▼ Boring U105- Fixed Piston Tube Sample
- } Hydraulic Shell Under Berm Road
- Sand Layer in Core

Army Corps of Engineers Vicksburg, Mississippi	Re-evaluation of Lower San Fernando Dam San Fernando, California	1985 IN SITU VOID RATIOS OF CRITICAL LAYER VS. DEPTH
<b>GEOTECHNICAL ENGINEERS INC.</b> WINCHESTER • MASSACHUSETTS	Project 85669	Sep. 2, 1987      Fig. 14



Army Corps of Engineers Vicksburg, Mississippi	Re-evaluation of Lower San Fernando Dam San Fernando, California	STEADY STATE LINE BATCH MIX 7 GEI TEST RESULTS
 GEOTECHNICAL ENGINEERS INC. WIND-ESTER • MASSACHUSETTS	Project 85669	Sept. 2, 1987    Fig. 15



Army Corps of Engineers  
 Vicksburg, Mississippi

**Φ** GEOTECHNICAL ENGINEERS INC.  
 WINCHESTER • MASSACHUSETTS

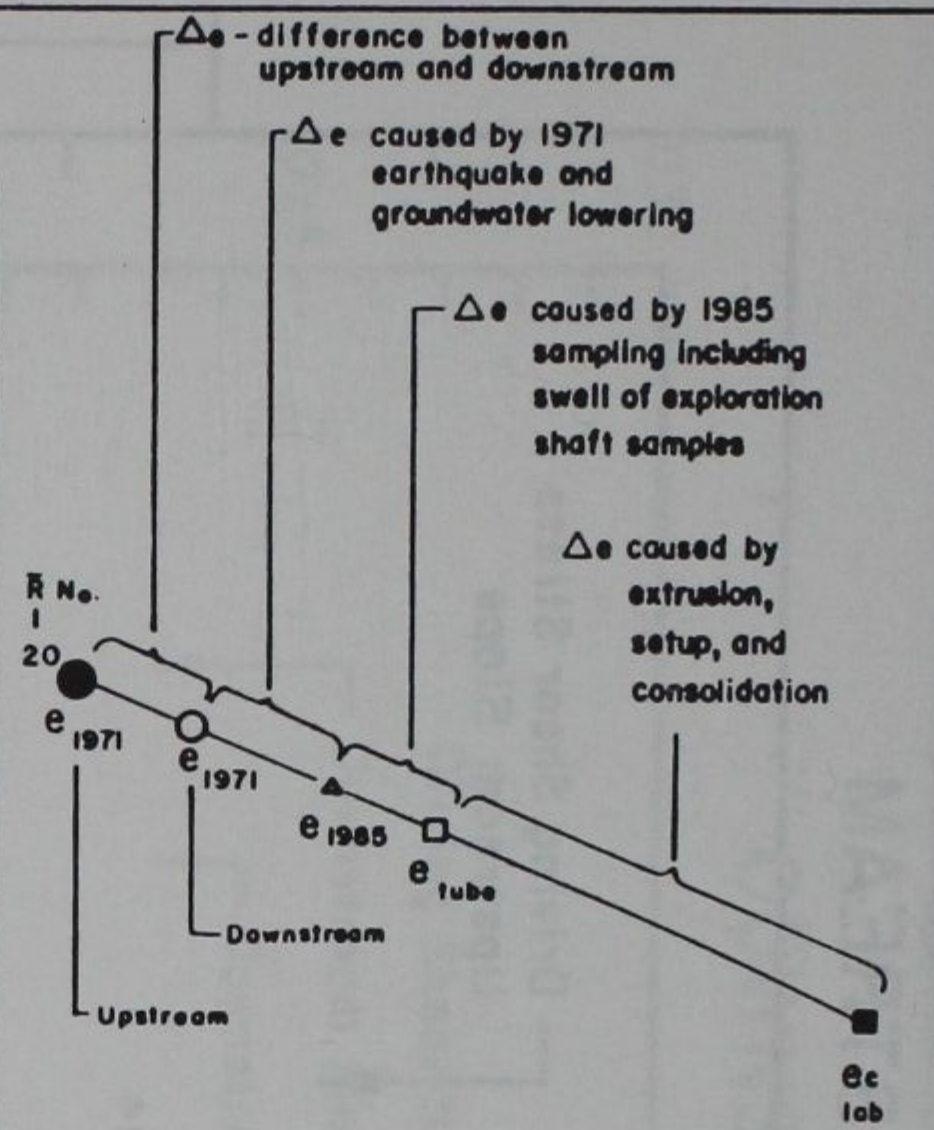
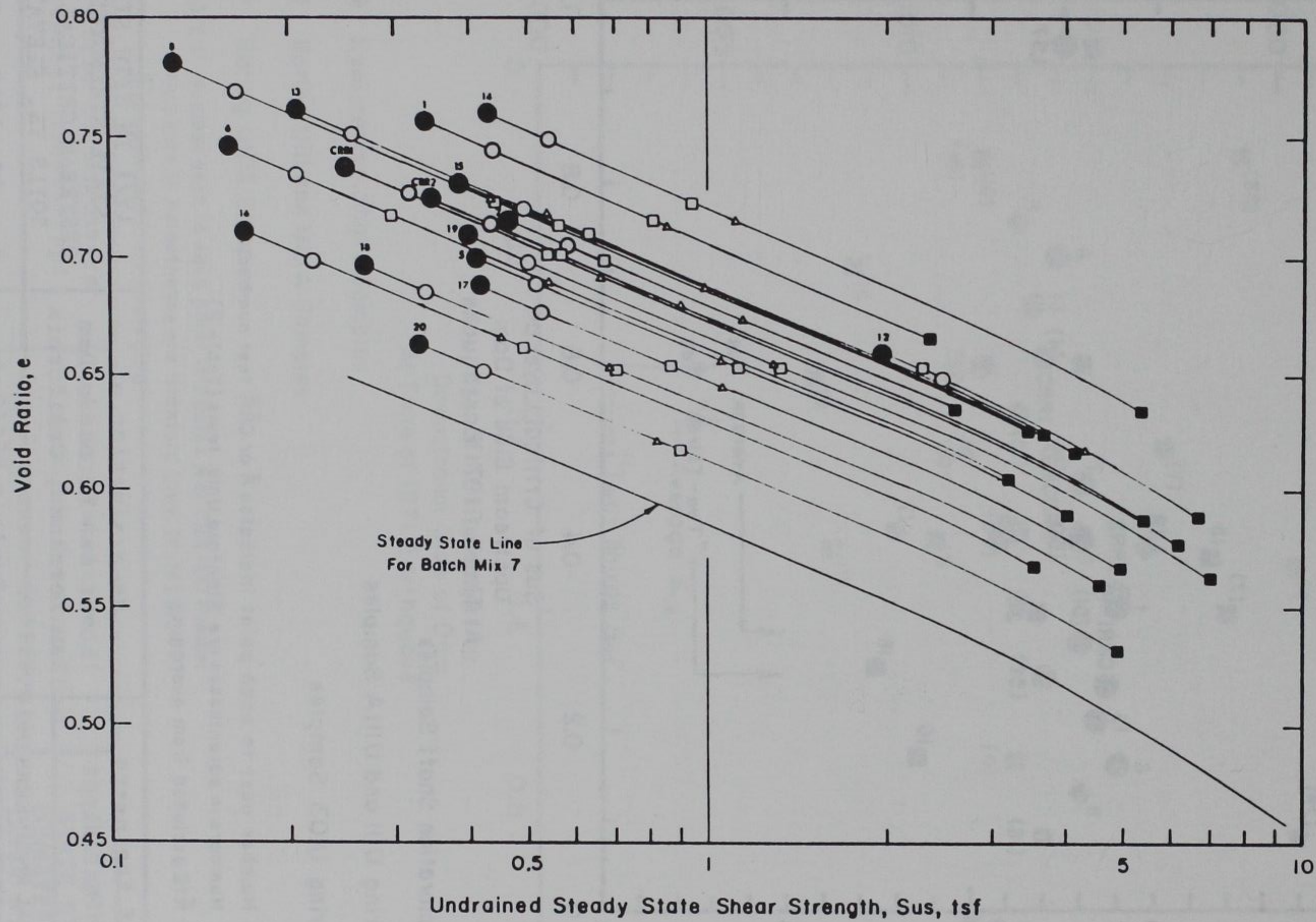
Re-evaluation of  
 Lower San Fernando Dam  
 San Fernando, California

Project 85669

STEADY STATE LINE  
 BATCH MIX 7  
 TEST RESULTS FROM  
 FOUR LABORATORIES

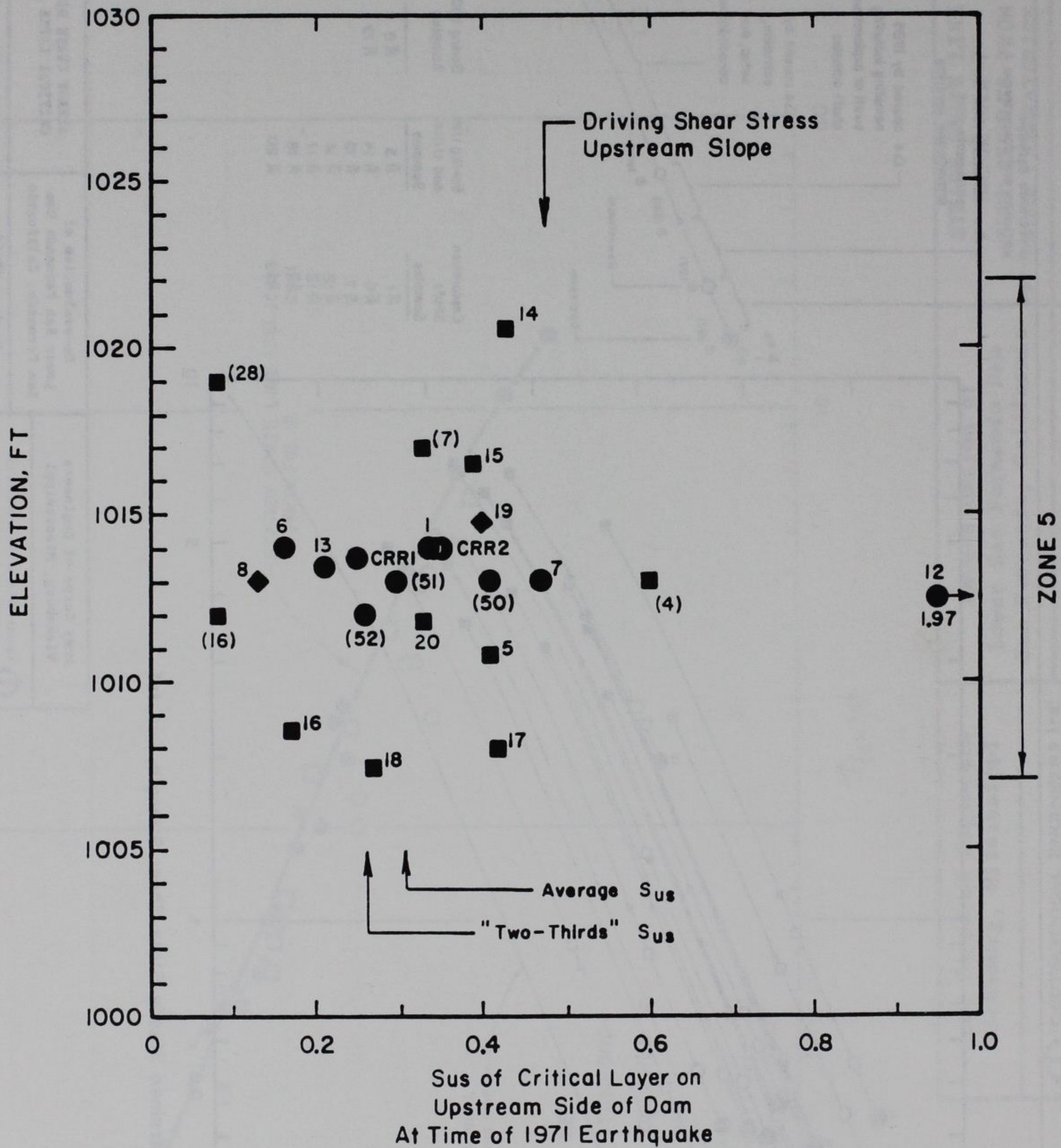
Jan. 15, 1988

Fig. 16



Exploration Shaft Samples	Boring U111 and U111A Samples	Boring U103 Samples
R 1	R 5	R 8
R 6	R 14	R 19
R 7	R 15	
R 12	R 16	
R 13	R 17	
CRR1	R 18	
CRR2	R 20	

# UPSTREAM



- Exploration Shaft Samples
- Boring U111 and U111A Samples
- ◆ Boring U103 Samples

NOTES: Number next to each point indicates  $\bar{R}$  or  $\bar{CRR}$  test number  
 Numbers in parentheses are Stanford Univ. tests (Table 2)  
 $\bar{R}12$  excluded from averaging

Army Corps of Engineers  
Vicksburg, Mississippi

Re-evaluation of  
Lower San Fernando Dam  
San Fernando, California

1971 IN SITU STEADY  
STATE STRENGTHS OF  
UPSTREAM CRITICAL LAYER  
SOILS VS. ELEVATION



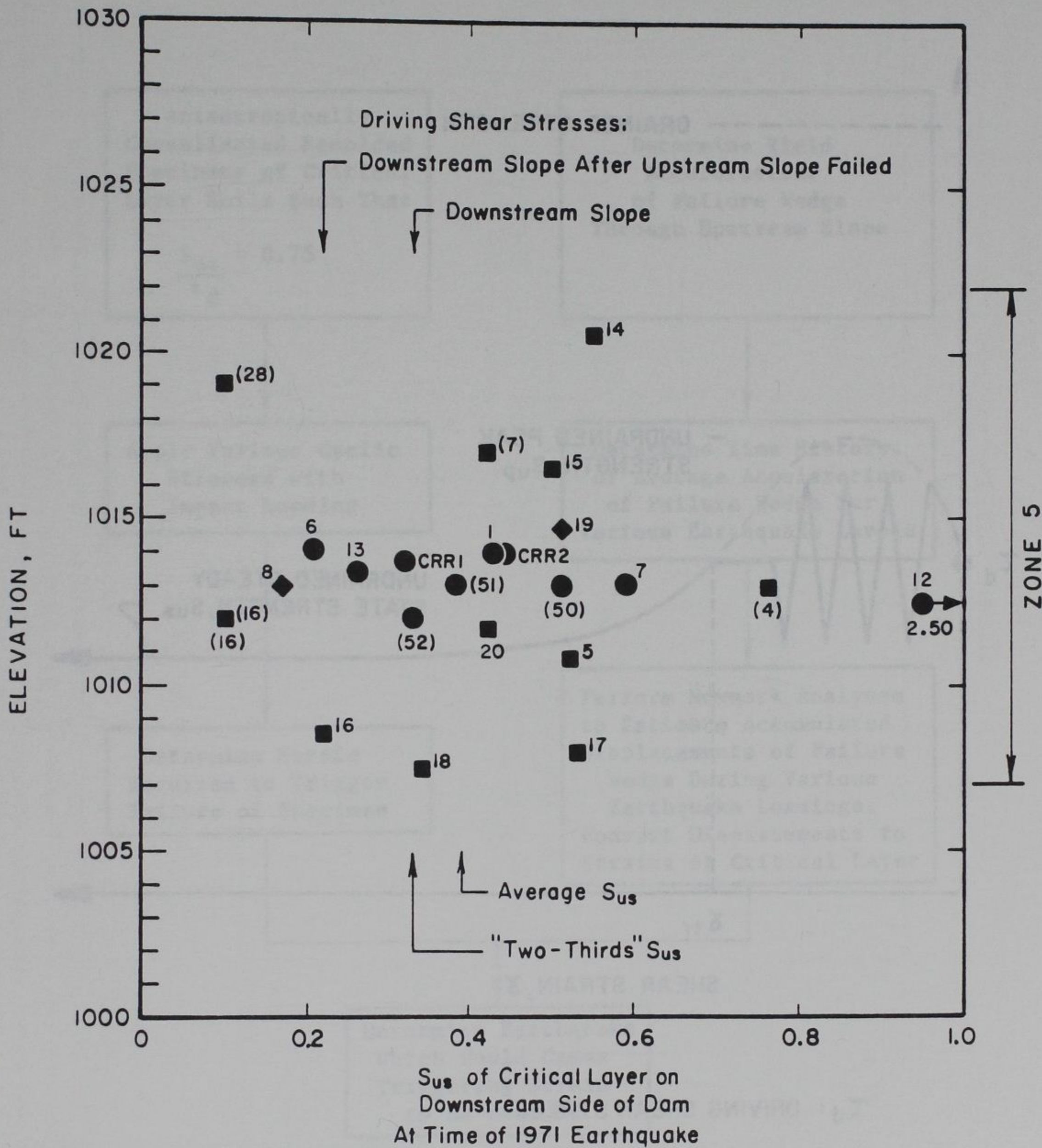
GEOTECHNICAL ENGINEERS INC.  
WINCHESTER • MASSACHUSETTS

Project 85669

Jan. 15, 1988 Fig. 18



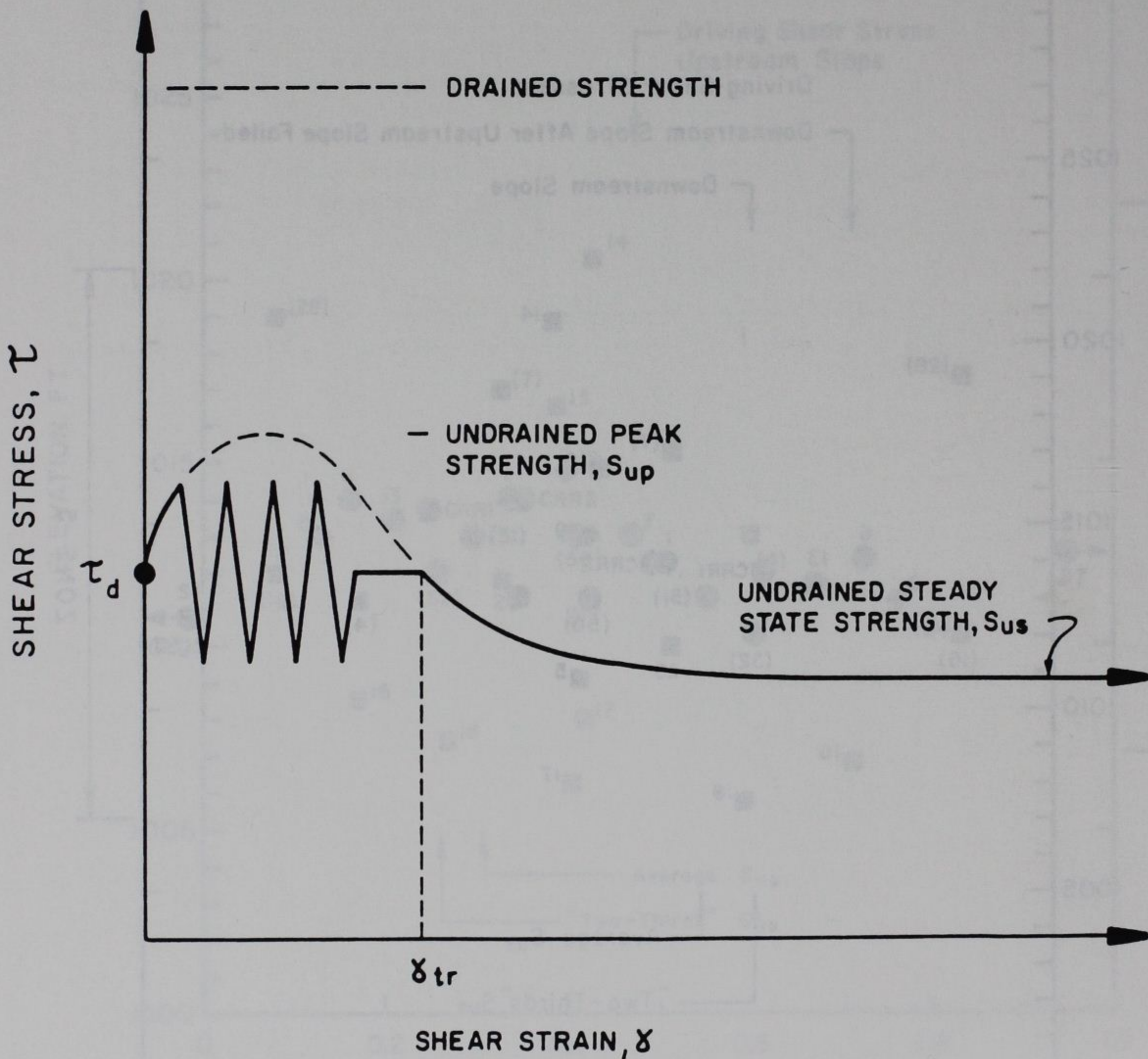
# DOWNSTREAM



- Exploration Shaft Samples
- Boring U111 and U111A Samples
- ◆ Boring U103 Samples


NOTES: Number next to each point indicates  $\bar{R}$  or  $\bar{CRR}$  test number  
 Numbers in parentheses are Stanford Univ. tests (Table 2)  
 $\bar{R}12$  excluded from averaging

Army Corps of Engineers Vicksburg, Mississippi	Re-evaluation of Lower San Fernando Dam San Fernando, California	1971 IN SITU STEADY STATE STRENGTHS OF DOWNSTREAM CRITICAL LAYER SOILS VS. EL.
GEOTECHNICAL ENGINEERS INC. WINDHAM, MASSACHUSETTS	Project 85669	Jan. 15, 1988    Fig. 19

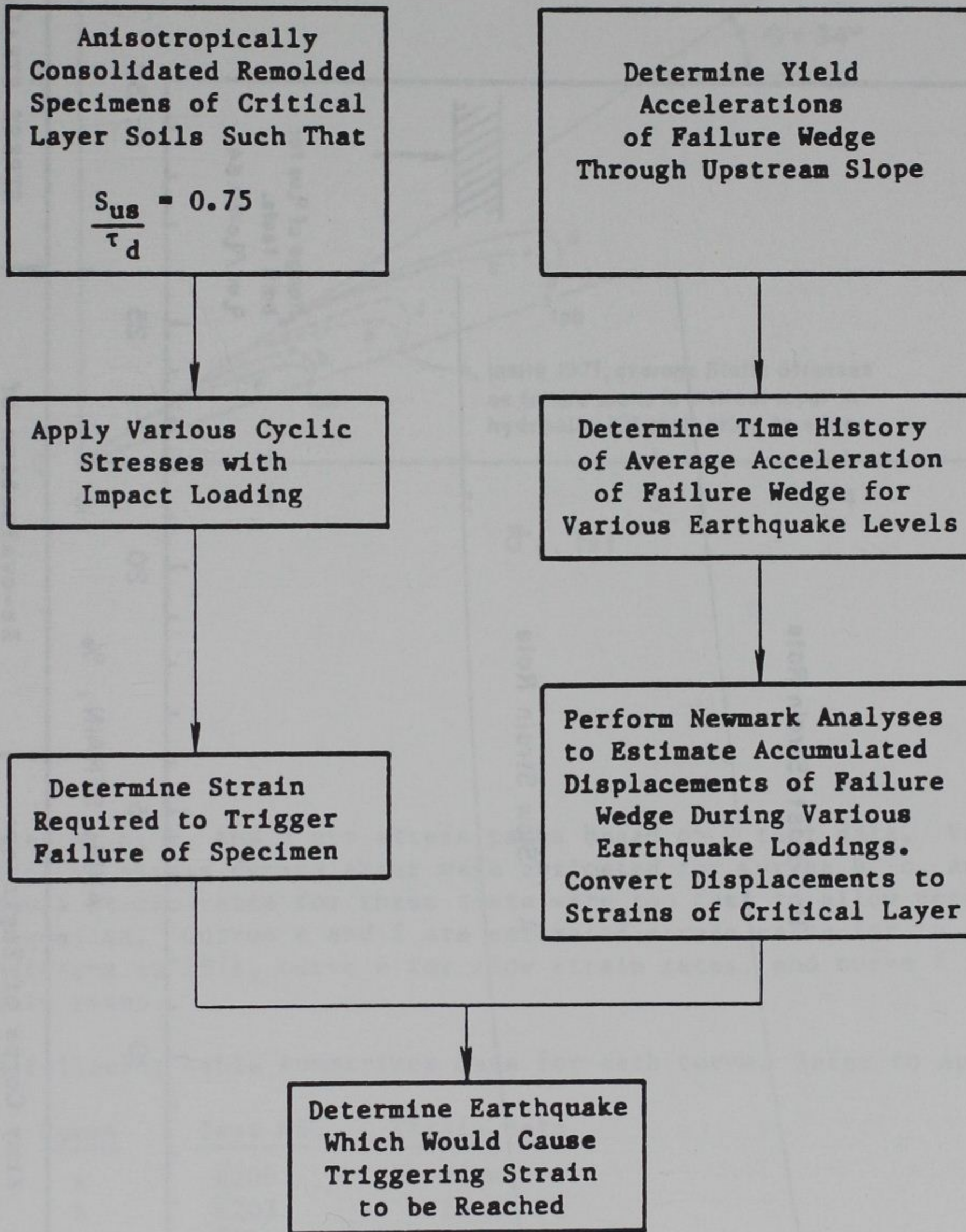


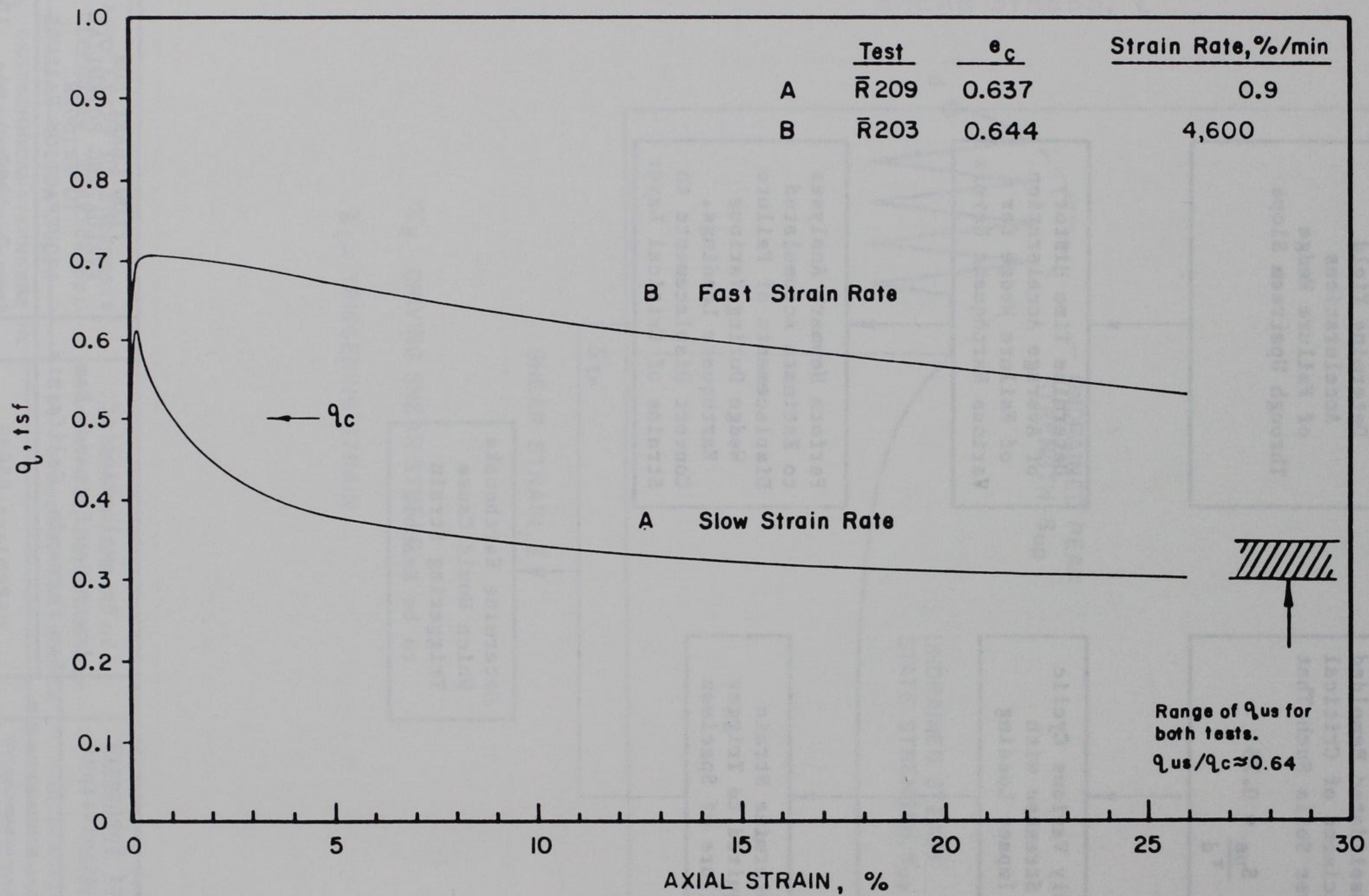
$\tau_d$ : DRIVING SHEAR STRESS


$\gamma_{tr}$ : TRIGGERING STRAIN

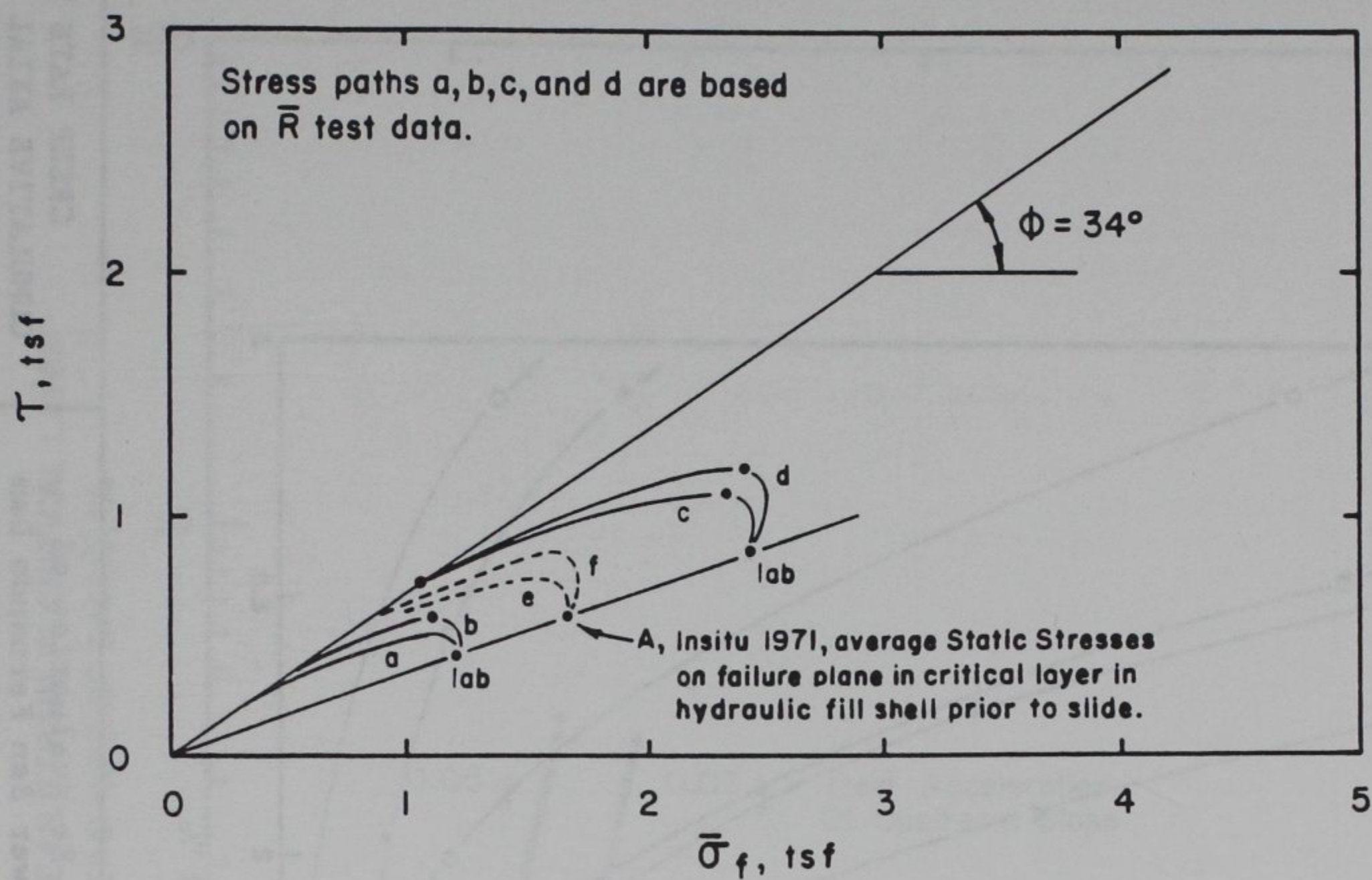
Army Corps of Engineers Vicksburg, Mississippi	Re-evaluation of Lower San Fernando Dam San Fernando, California	SCHEMATIC STRESS STRAIN CURVE FOR LIQUEFACTION FAILURE
 GEOTECHNICAL ENGINEERS INC. WINCHESTER • MASSACHUSETTS	Project 85669	Jan. 15, 1988    Fig. 20

**FLOW CHART FOR TRIGGERING ANALYSIS**





Army Corps of Engineers Vicksburg, Mississippi	Re-evaluation of Lower San Fernando Dam San Fernando, California	STRESS STRAIN CURVES OF ANISOTROPICALLY CONSOLIDATED SAMPLES OF BATCH MIX 7
 GEOTECHNICAL ENGINEERS INC. WINCHESTER • MASSACHUSETTS	Project 85669	Jan. 15, 1988 <span style="float: right;">Fig. 22</span>



Curves a, b, c, and d are stress paths based on  $\bar{R}$  test data. Values of effective stress during shear were estimated for Curves b, c, and d because strain rates for these tests were too fast to allow pore pressures to equalize. Curves e and f are estimated stress paths for in situ conditions in 1971, curve e for slow strain rates, and curve f for fast strain rates.

The following table summarizes data for each curve. Refer to Appendix F.

Curve	Test No.	Strain Rate
a	$\bar{R}209$	slow
b	$\bar{R}203$	fast
c	$\bar{R}202$	intermediate
d	$\bar{R}201$	fast
e	-	slow
f	-	fast

Army Corps of Engineers  
Vicksburg, Mississippi

Re-evaluation of  
Lower San Fernando Dam  
San Fernando, California

STRESS PATHS OF  
CRITICAL LAYER SOILS

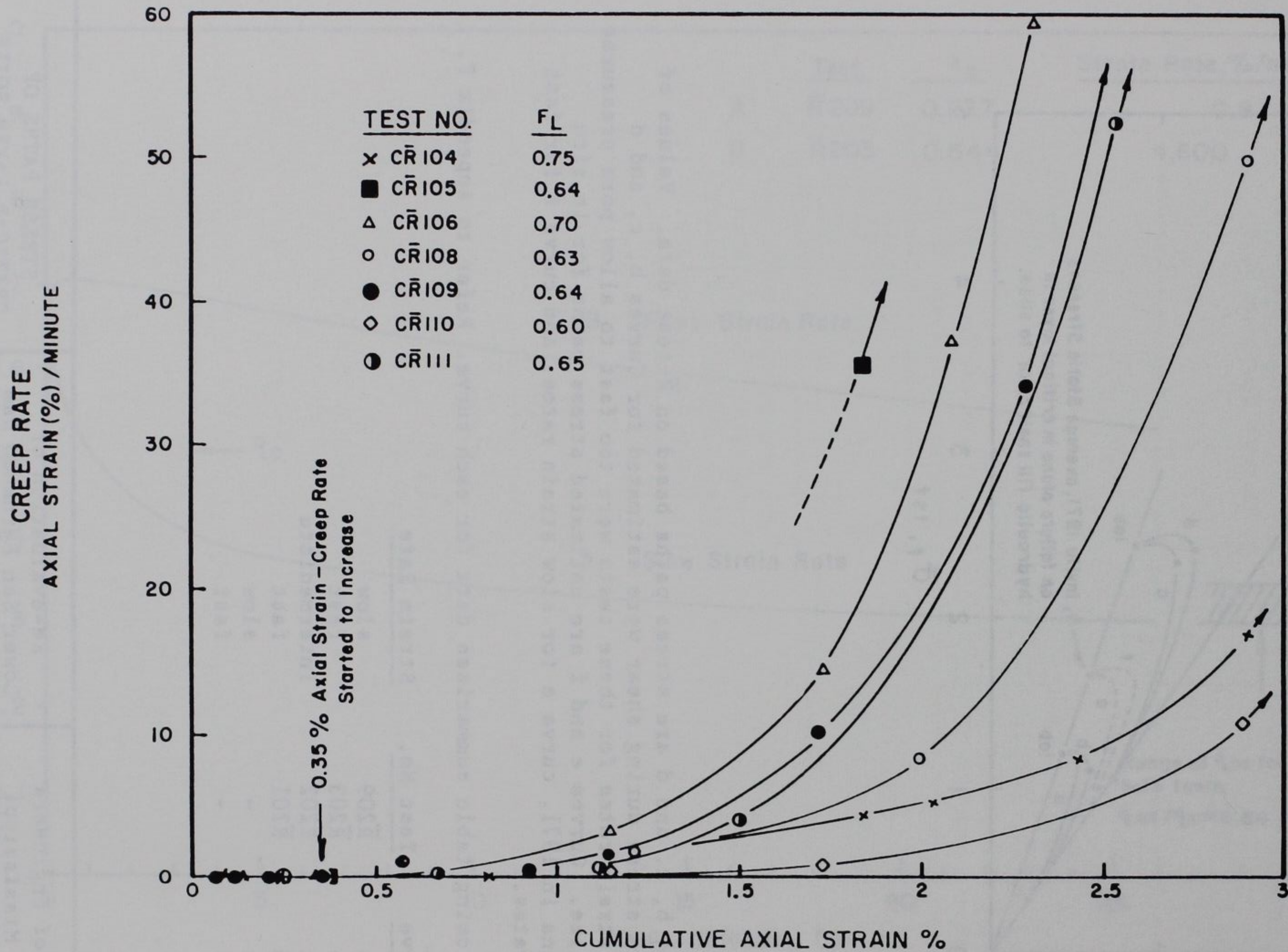


GEOTECHNICAL ENGINEERS INC.  
WINCHESTER • MASSACHUSETTS


Project 85669

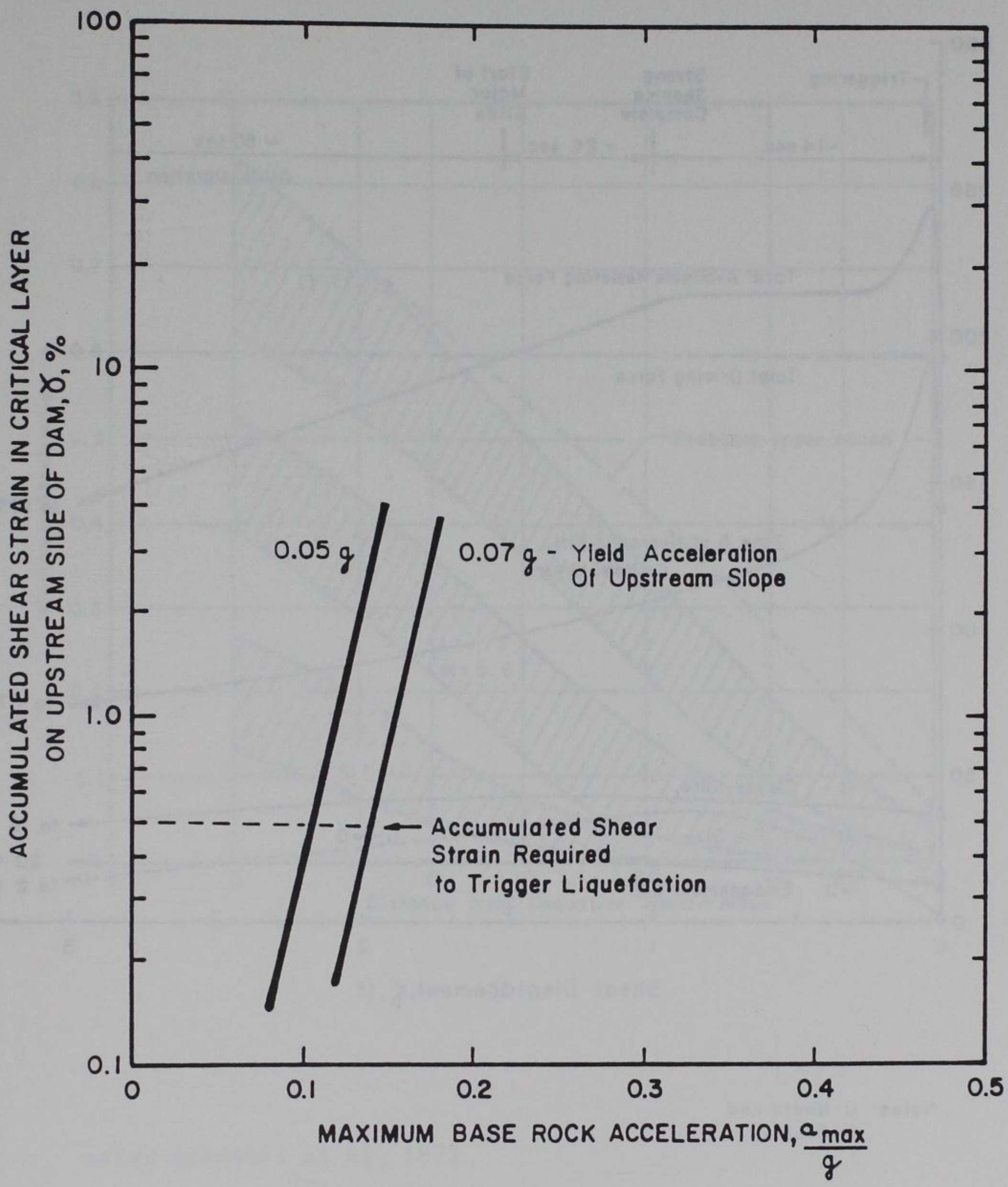
Sep. 2, 1987


Fig. 23

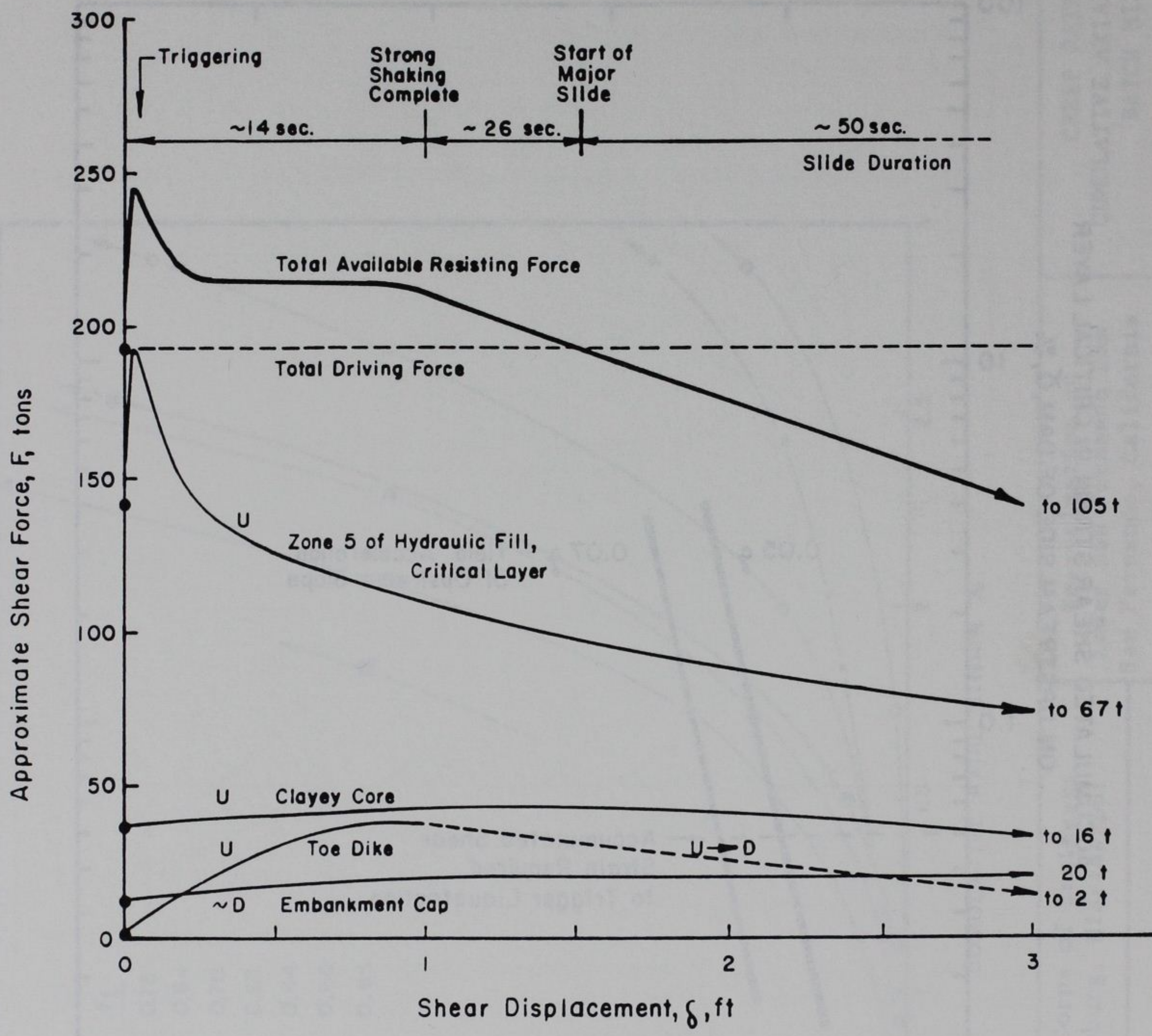


$$F_L = \frac{S_{us}}{Q_{us}}$$


Army Corps of Engineers Vicksburg, Mississippi	Re-evaluation of Lower San Fernando Dam San Fernando, California	CREEP RATE VS. CUMULATIVE AXIAL STRAIN BATCH MIX 7
 GEOTECHNICAL ENGINEERS INC. WINCHESTER • MASSACHUSETTS	Project 85669	Jan. 15, 1988      Fig. 24



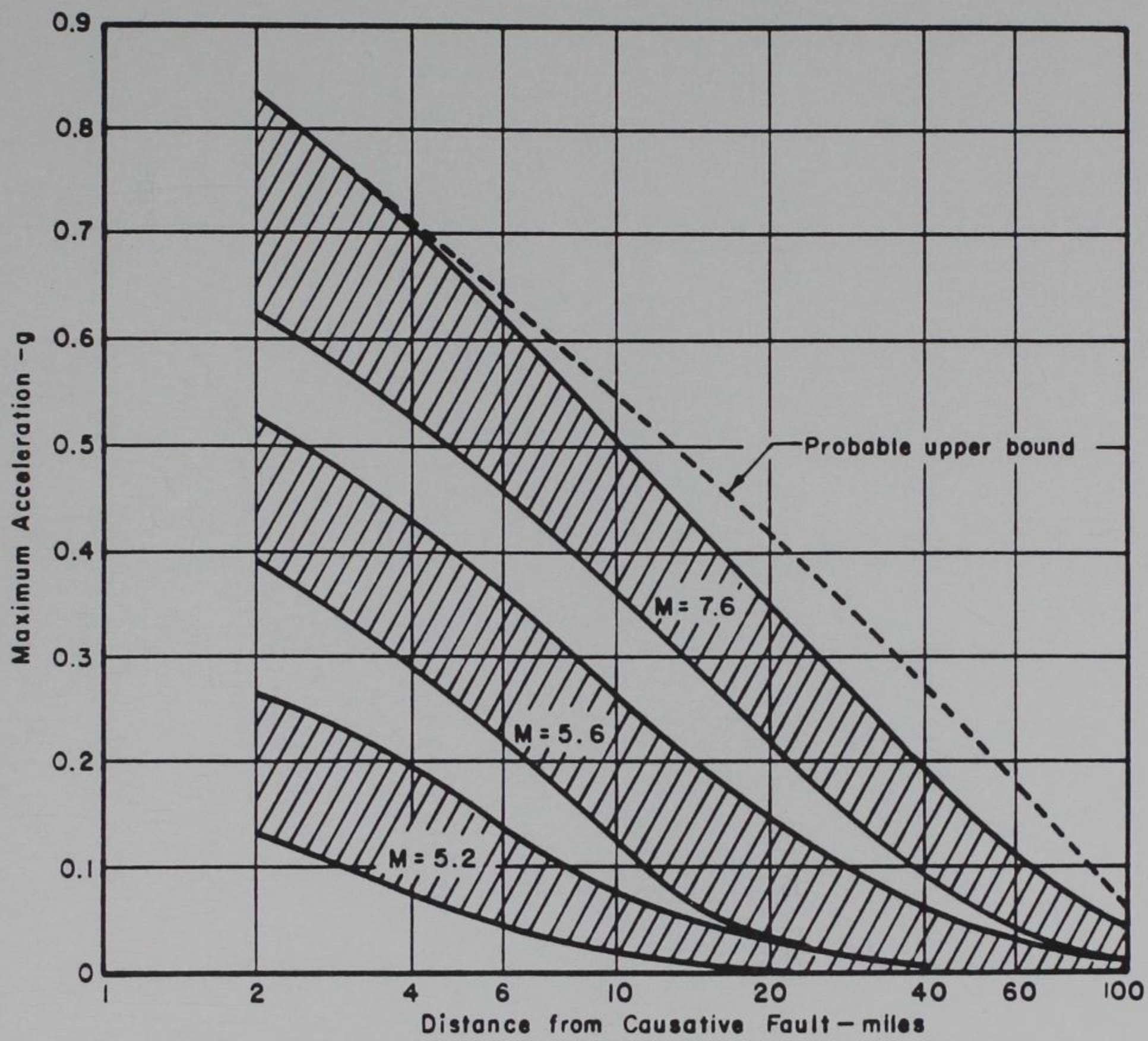
Army Corps of Engineers Vicksburg, Mississippi	Re-evaluation of Lower San Fernando Dam San Fernando, California	COMPUTED SHEAR STRAINS IN CRITICAL LAYER VS. MAX. BASE ROCK ACCELERATION
 <b>GEOTECHNICAL ENGINEERS INC.</b> WINCHESTER • MASSACHUSETTS	Project 85669	Sep. 2, 1987      Fig. 25




Notes: U-Undrained  
D-Drained

Army Corps of Engineers Vicksburg, Mississippi	Re-evaluation of Lower San Fernando Dam San Fernando, California	QUALITATIVE DRIVING & RESISTING FORCES AT INITIATION OF SLIDE
 GEOTECHNICAL ENGINEERS INC. WINCHESTER • MASSACHUSETTS	Project 85669	Jan. 15, 1988 Fig. 26





After Schnabel et al, 1973

Army Corps of Engineers Vicksburg, Mississippi	Re-evaluation of Lower San Fernando Dam San Fernando, California	RANGES OF MAXIMUM ACCELERATIONS IN ROCK
 GEOTECHNICAL ENGINEERS INC. WINCHESTER • MASSACHUSETTS	Project 85669	Sep. 2, 1987      Fig. 27